A STUDY ON HOMOGENEOUS AND HETEROGENEOUS BIMETALLIC CLUSTER CATALYSTS

BY

ATSUSHI FUKUOKA

CATALYSIS RESEARCH CENTER
HOKKAIDO UNIVERSITY
SAPPORO, JAPAN

1989

PREFACE

This is a thesis for a doctorate of The University of Tokyo on the chemistry of homogeneous and heterogeneous bimetallic cluster catalysts. The continued importance of research and development of bimetallic catalysts in homogeneous and heterogeneous catalysis, coupled with the increased interests in the cluster compounds as a model of active sites on metal surfaces and as a possible precursor for catalytic reactions, prompted the author to study the chemistry of the bimetallic cluster catalysts.

In this thesis, the catalysis of homogeneous bimetallic systems (CHAPTER 2) was studied at Department of Industrial Chemistry, Faculty of Engineering, The University of Tokyo under the guidance of Professor Masanobu Hidai and Professor Yasuzo Uchida during 1983-1985. The research work on the heterogeneous bimetallic cluster catalysts (CHAPTERS 3-5) has been performed at Research Institute for Catalysis, Hokkaido University with Professor Masaru Ichikawa since 1986.

The author wishes to express the deep appreciation to Prof. Masaru Ichikawa for his stimulative advice. He thanks Prof. Masanobu Hidai and Prof. Yasuzo Uchida for the warm encouragement and guidance. In the course of the research, aid and useful suggestions were received from many people: Mr. Takuma Kimura, Ms. Ling-Fen Rao, Mr. Toshiyuki Fujimoto, Dr. Pedro E. Hoffman, Dr. Taro Ito, Dr. Nobuhiro Kosugi, Dr. Yoshitaka Minai, Dr. Yoichi Sakai, Dr. Alessandro Fumagalli, Dr. Yukio Koyasu, Dr.

Hiroyuki Matsuzaka, and Prof. Duward F. Shriver. He thanks the members of Catalysis Research Center, Hokkaido University, particularly Ms. Atsuko Hiratsuka for skillful drafting and advice on WordStar 5.0.

Finally the author is grateful to his family, especially to his wife Tomoko.

Atsushi Fukuoka

Sapporo, Japan

June, 1989

CONTENTS

CHAPTER 1

GENERAL INTRODUCTION

CHAPTER 1

GENERAL INTRODUCTION

1. Definition and Bonding Theory of Transition Metal Clusters

A metal cluster is defined as a group of more than three metals in which there are direct bonds between the metal atoms.[1,2] This definition includes various classes of clusters[3]:

1 Polyhedral boranes

2 Transition metal clusters

3 Metal oxide and metal sulfide clusters where both the metal and the O or S atoms comprise the framework structure

4 Naked clusters without ligands, generated from metal vapors

In this thesis transition metal clusters containing carbonyl ligands are considered. Typical examples are shown in Figure 1.

Transition metal carbonyl clusters are under intensive investigation because of their potential applications, both as models for catalysis on metal surfaces and as catalyst precursors. Numerous reviews have appeared on various aspects of the clusters.[3-13]

To rationalize the bonding interactions in transition metal clusters, two main approaches have been used; *i.e.*, the simple application of the 18 electron rule (the effective atomic number rule, EAN rule) and empirical rules. The 18 electron rule accounts for the geometry of small nuclearity clusters to some extent. On the other hand, Wade developed the skeletal electron

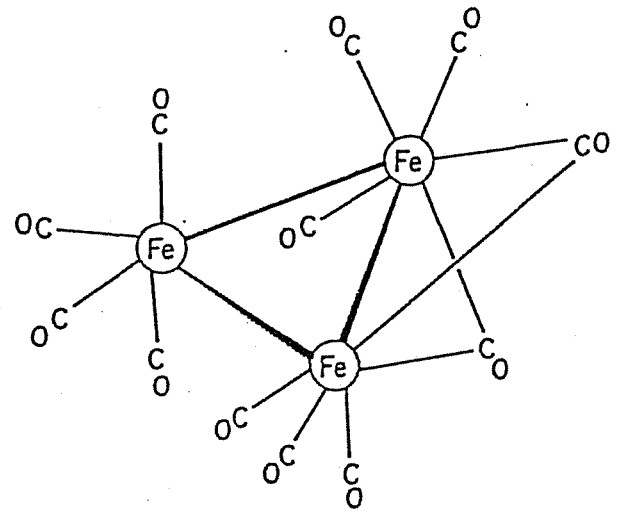

(a)

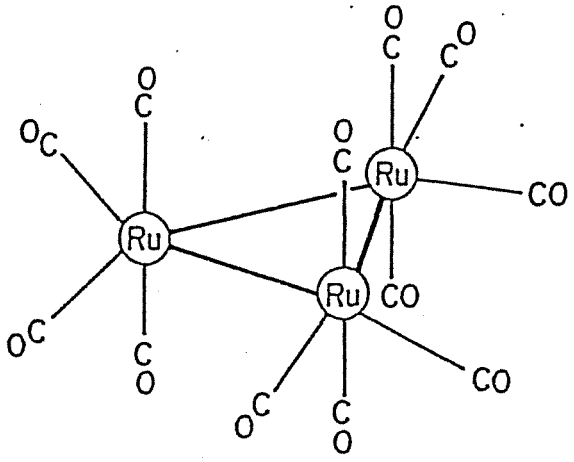

(b)

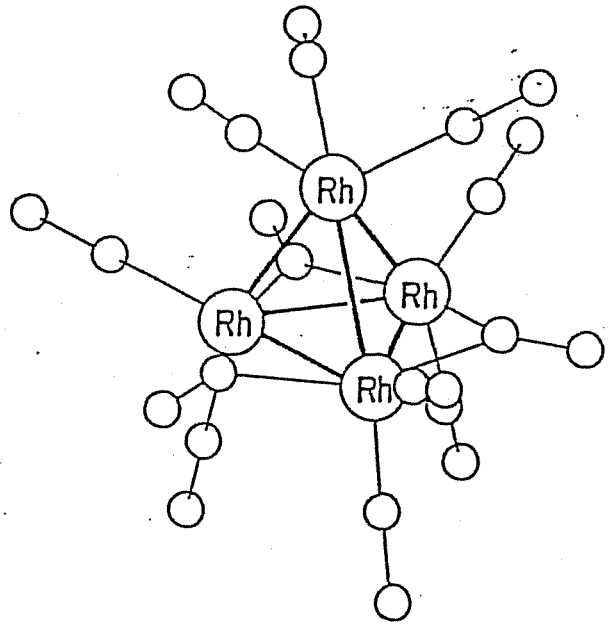

(c)

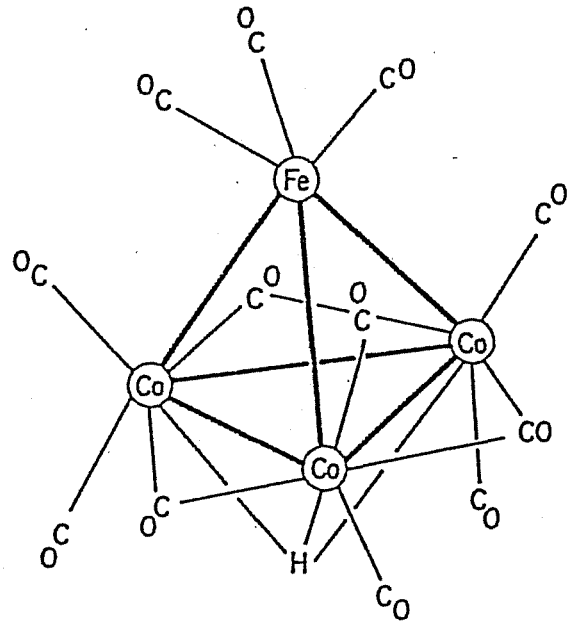

(d)

Figure 1. Typical examples of transition metal carbonyl clusters: (a) $Fe_3(CO)_{12}$, (b) $Ru_3(CO)_{12}$, (c) $Rh_4(CO)_{12}$, and (d) $HFeCo_3(CO)_{12}$.

pair theory and proposed the electron counting rule of metal carbonyl clusters correlated with boranes and carboranes.[14] Semi-empirical LCAO-MO treatments were applied to specific clusters by Mingos (the polyhedral skeletal electron pair theory).[15] Lauher made the extended Hückel calculations for bare metal clusters and explained the size and geometry of the clusters with up to 15 atoms by using a particular number of the cluster valence molecular orbitals (CVMO).[16] His table summarizing the geometry and the number of cluster valence electrons (CVE) is very useful (Table 1). Recently, Teo proposed the topological electron counting theory where he applied the Euler rule to account for the geometry of clusters.[17] Another useful approach to understand the electronic and geometric requirements of metal clusters is the isolobal concept developed by Hoffmann (Figure 2).[18]

Since the 1960's a number of classes of carbonyl clusters are known. Particularly, high nuclearity clusters containing late transition metals have been established by the pioneering work of P. Chini and his group (Figure 3).[4] $[Rh_{13}(CO)_{24}H_n]^{(5-n)-}$ has a Rh_{13} unit where the thirteen rhodium atoms form a body-centered cuboctahedron which is the smallest fragment of a hexagonal close-packed metallic array. $[Rh_{17}(CO)_{32}S_2]^{3-}$ contains encapsulated hetero atom in the skeletal structure. Remarkable structure is found in $[Pt_{19}(CO)_{22}]^{4-}$; this five-fold (D_{5h}) symmetry is not related to close-packed structures, but it is similar to that of certain microcrystalline materials such as whiskers and dendrites. $[Pt_{38}(CO)_{44}]^{2-}$ contains a fragment of

Table 1. Bonding Capabilities of Transition Metal Clusters[16]

geometry	*N*	9 x *N*	HLAO	CVMO	CVE	CVMO/*N*	example
monomer	1	9	0	9	18	9.0	$Ni(CO)_4$
dimer	2	18	1	17	34	8.5	$Fe_2(CO)_9$
trimer	3	27	3	24	48	8.0	$Os_3(CO)_{12}$
tetrahedron	4	36	6	30	60	7.5	$Rh_4(CO)_{12}$
butterfly	4	36	5	31	62	7.75	$Re_4(CO)_{16}^{2-}$
square plane	4	36	4	32	64	8.0	$Pt_4(O_2CCH_3)_8$
trigonal bipyramid	5	45	9	36	72	7.2	$Os_5(CO)_{16}$
square pyramid	5	45	8	37	74	7.4	$Fe_5(CO)_{15}C$
bicapped tetrahedron	6	54	12	42	84	7.0	$Os_6(CO)_{18}$
octahedron	6	54	11	43	86	7.17	$Ru_6(CO)_{17}C$
capped square pyramid	6	54	11	43	86	7.17	$Os_6(CO)_{18}H_2$
trigonal prism	6	54	9	45	90	7.5	$Rh_6(CO)_{15}C^{3-}$
capped octahedron	7	63	14	49	98	7.0	$Rh_7(CO)_{16}^{3-}$
square antiprism	8	72	15	57	114	7.13	$Co_8(CO)_{18}C^{2-}$
cube	8	72	12	60	120	7.5	$Ni_8(CO)_8(PPh_3)_6$
truncated hexagonal bipyramid	13	117	32	85	170	6.54	$Rh_{13}(CO)_{24}H_3^{2-}$

N is the number of atoms; 9 x *N* is the number of atomic orbitals; HLAO is the number of high lying antibonding orbitals; CVMO is the number of cluster valence molecular orbitals; CVE is the number of cluster valence electrons.

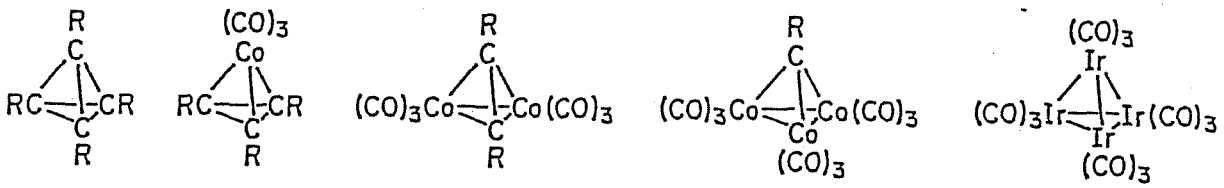

(a)

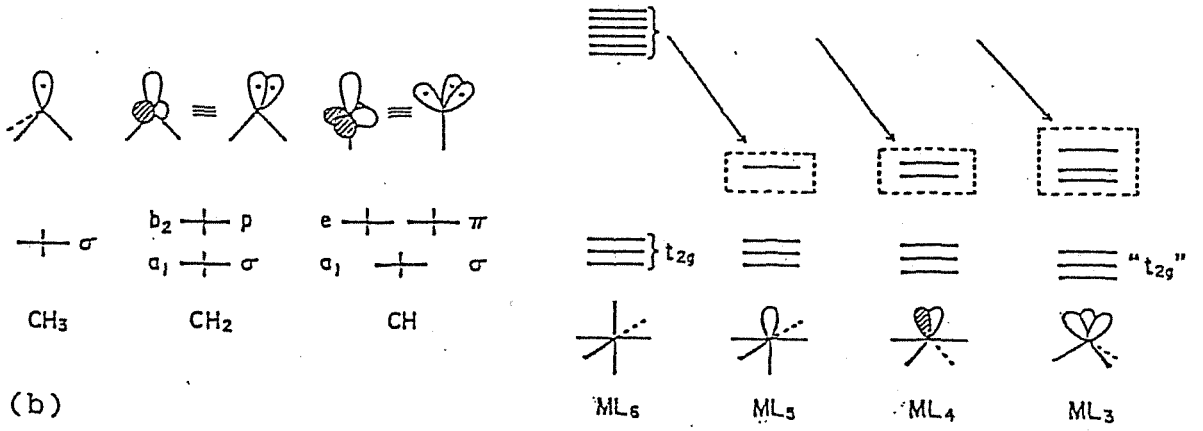

(b)

(c)

$$CH_3 \longleftrightarrow d^7\, C_{4V}\, ML_5$$

$$CH_2 \longleftrightarrow d^8\, C_{2V}\, ML_4$$

$$CH \longleftrightarrow d^9\, C_{3V}\, ML_3$$

(d)

Figure 2.
(a) A series of tetrahedrons containing RC and $M(CO)_3$ fragments;
(b) Frontier orbitals of CH_3, CH_2, and CH;
(c) Frontier orbitals of ML_6, ML_5, ML_4, and ML_3;
(d) Isolobal interactions between organic and inorganic fragments.[18]

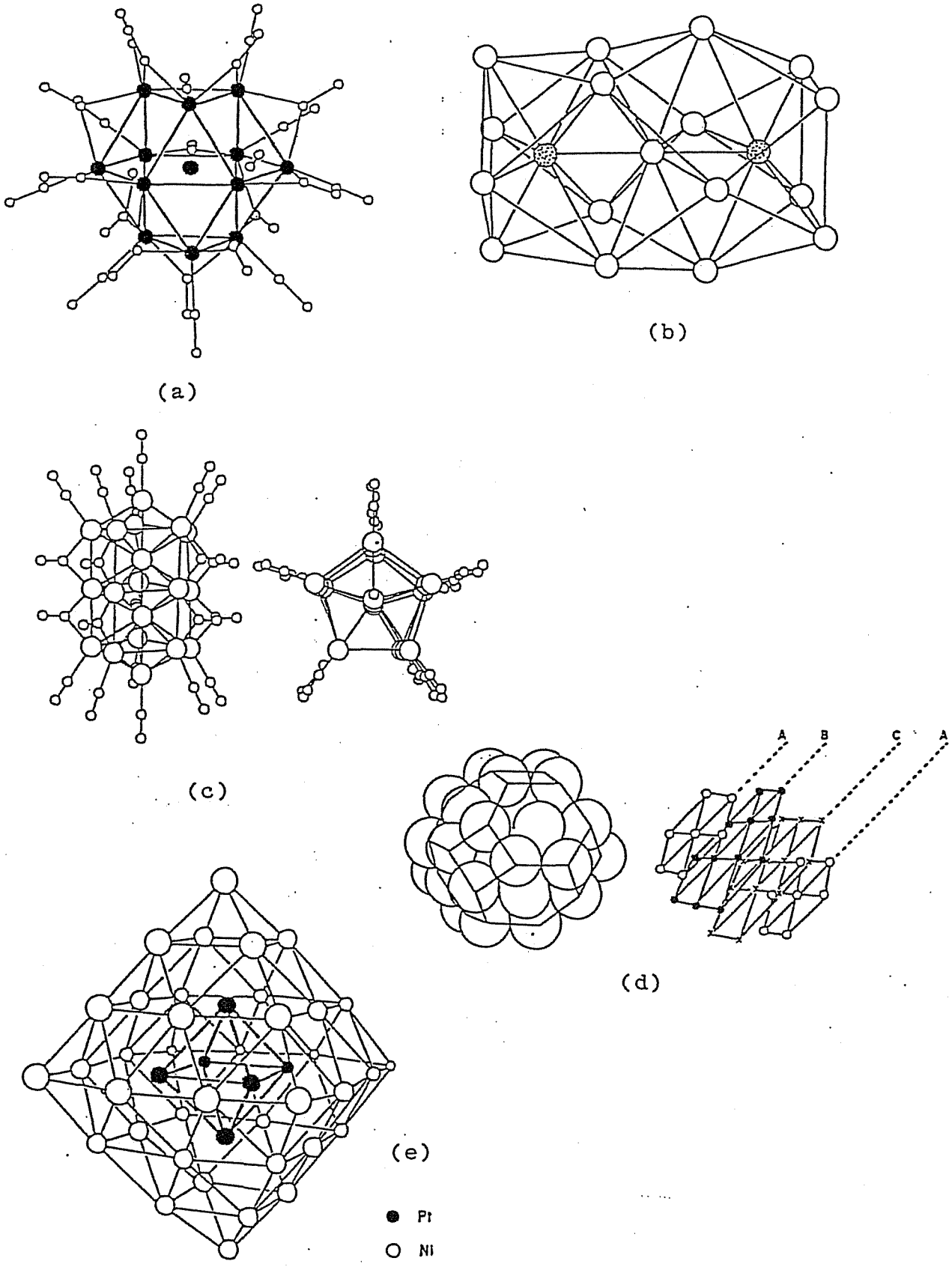

Figure 3. Typical examples of high nuclearity carbonyl clusters:[4] (a) $[Rh_{13}(CO)_{24}H_n]^{(5-n)-}$, (b) $[Rh_{17}(CO)_{32}S_2]^{3-}$, (c) $[Pt_{19}(CO)_{22}]^{4-}$, (d) $[Pt_{38}(CO)_{44}]^{2-}$, and (d) $[Ni_{38}Pt_6(CO)_{48}H_{6-n}]^{n-}$.

ccp platinum metal with a metal skeleton diameter of 11.6 Å. Finally, nickel and platinum form massive bimetallic cluster $[Ni_{38}Pt_6(CO)_{48}H_{6-n}]^{n-}$ where Pt atoms locate in the core with an octahedral structure.

2. Molecular Clusters as Models of Metal Surfaces

One of the important aspect of cluster chemistry is to regard the molecular metal clusters as models of metal surfaces, *i.e.*, the reactivity of metal frames and coordinated ligands may reflect the reactions which occur on the metal surfaces.

The catalytic conversion of carbon monoxide to hydrocarbons and oxygenates has been intensively studied since the early 1940's in the both fields of homogeneous and heterogeneous catalysis.[19,20] In these catalytic processes, transition metals of Group 8 are commonly used as catalysts or catalyst precursors. The reaction sequence of CO hydrogenation (Fischer-Tropsch reaction) appears to includes the coordination of CO to a metal atom or metal particles, followed with CO cleavage to produce surface carbide.

Shriver studied the proton-induced reduction of CO in $[Fe_4(CO)_{13}]^{2-}$ (1) as a model for production of hydrocarbons in the CO hydrogenation (Figure 4).[21] An attractive feature of this cluster is rearrangement in mild acid, which converts one CO from a metal-C-bonded geometry into an unusual η^2-geometry, where the carbonyl is both C and O bonded (2). The C-O bond in the η^2-CO is much weaker than in a terminally bound CO. The addition of strong acid to $[Fe_4(CO)_{13}]^{2-}$ leads to the cleavage of CO, as

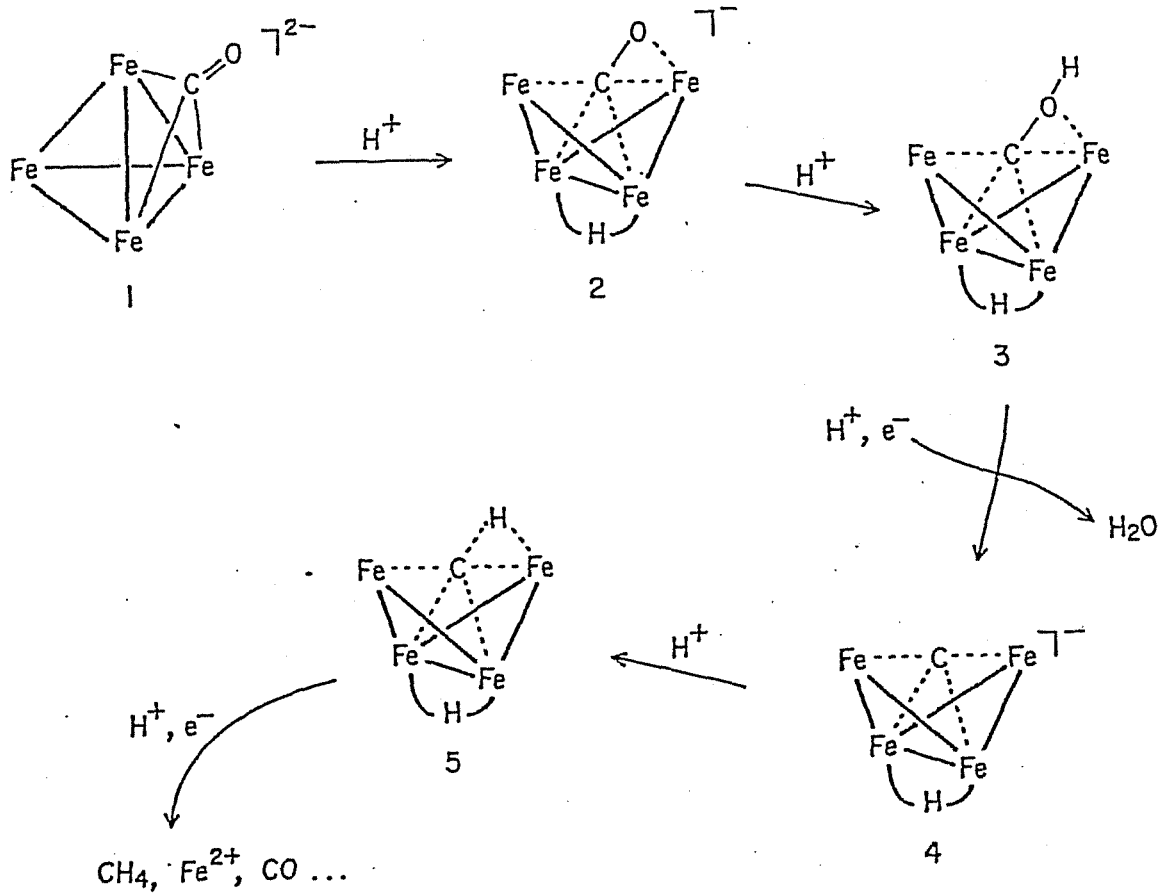

Figure 4. Proton-induced reduction of CO in $[Fe_4(CO)_{13}]^{2-}$.[21]

demonstrated by the evolution of about 0.5 mol of CH_4 per mol of cluster. In the presence of an added reducing agent, up to 1 mol of CH_4 is produced. Many of the intermediates in Figure 4 have been characterized. For example, single-crystal X-ray structural data for compounds 1, 2, 4, and 5 and a crystal structure of the methylated analogue of 3 have been obtained. Multinuclear NMR data on the reaction mixture confirm the presence of many of the intermediates shown in Figure 4.

Bradley reported another type of rearrangement of metal clusters associated with the CO hydrogenation (Figure 5).[22] $[Fe_6C(CO)_{16}]^{2-}$ (**6**) contains a internal carbide in the core, and this carbide cluster is oxidized by tropylium cation $C_7H_7^+$ to form $Fe_4C(CO)_{13}$ (**7**), where the carbide carbon is exposed. The addition of methanol to $Fe_4C(CO)_{13}$ leads to the formation of **8** which may be a intermediate for C_1- or C_2-oxygenates. The μ_4-carbomethoxy-methylidine ligand C-COOMe in **8** is suggested to form *via* the nucleophilic attack of MeO^- at the ketenylidene ligand C=C=O formed by the CO migration onto the carbide in **7**.

3. Catalysis by Molecular Clusters

The other important aspect of cluster chemistry is the catalysis by molecular clusters. Molecular clusters occupy an interdisciplinary situation between the homogeneous mononuclear complexes and the heterogeneous metal surfaces. Heterogeneous catalysis on metal surfaces is not always selective, because possible catalytic sites on the metal surfaces are poorly defined at a microscopic level: they contain terrace, step, corner, kink,

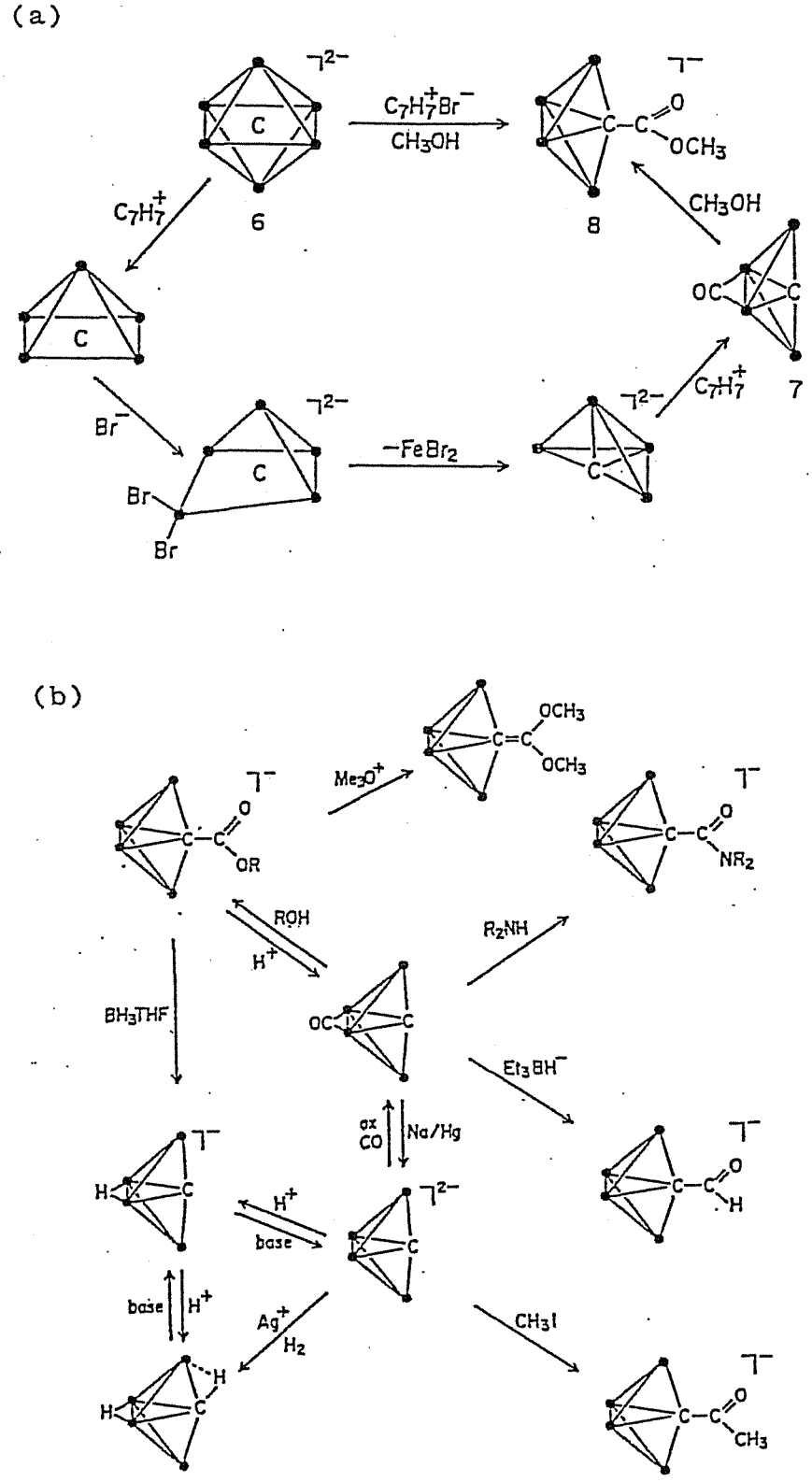

Figure 5.[22]
(a) Rearrangement of $[Fe_6C(CO)_{16}]^{2-}$ during oxidation by $[C_7H_7]Br$;
(b) Reactivity of a carbide ligand in $Fe_4C(CO)_{13}$.

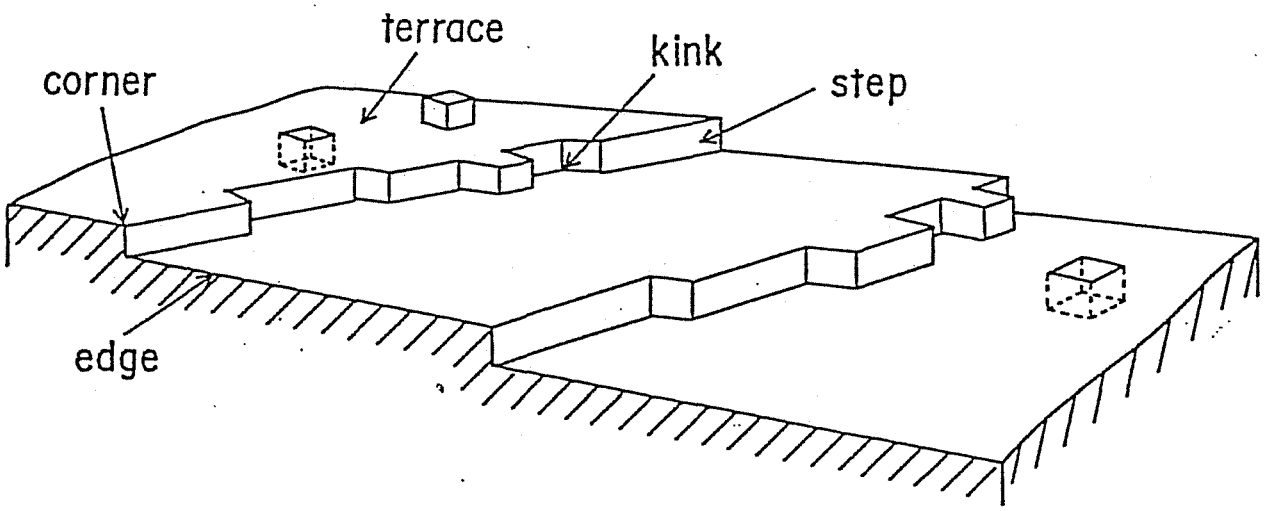

Figure 6. Microscopic view of a metal surface.

and edge (Figure 6). By contrast, the homogeneous catalysis by mononuclear complexes is considerably selective. The catalytic reactions occur in the well-defined coordination sphere of a single metal atom surrounded by a variety of ligands such as carbonyls, phosphines, and halides. The molecular clusters may offer the possibility of a cooperative effect of metal atoms for a specific activation of substrates, and thus the reactions involving two or three metals are expected to be very different from those catalyzed by mononuclear systems.

Homogeneous Catalysis by Molecular Clusters

Since Union Carbide's group claimed that Rh clusters catalyzed the synthesis of ethylene glycol from syngas at 210-250 °C and 1200-2000 atm[23] and $[Rh_5(CO)_{15}]^-$ was found to be a principal species present under the catalytic conditions,[24,25] enormous researches have been stimulated to develop the homogeneous catalytic reactions with metal clusters. A few examples are presented in this section in terms of the catalytic reactions by intact metal clusters or multinuclear metal centers.

Dombek studied the syngas conversion to ethylene glycol catalyzed by Ru complexes.[26] He found $[HRu_3(CO)_{11}]^-$ and $[Ru(CO)_3I_3]^-$ in the reaction mixture under the catalytic conditions, and proposed the reaction mechanism. In Figure 7, ethylene glycol is produced *via* formyl complex Ru-CHO formed by the reaction of two metal centers, *i.e.*, the nucleophilic attack of $[HRu(CO)_4]^-$ at the coordinated CO of $Ru(CO)_4I_2$.

Although a number of works have been attempted, the specific

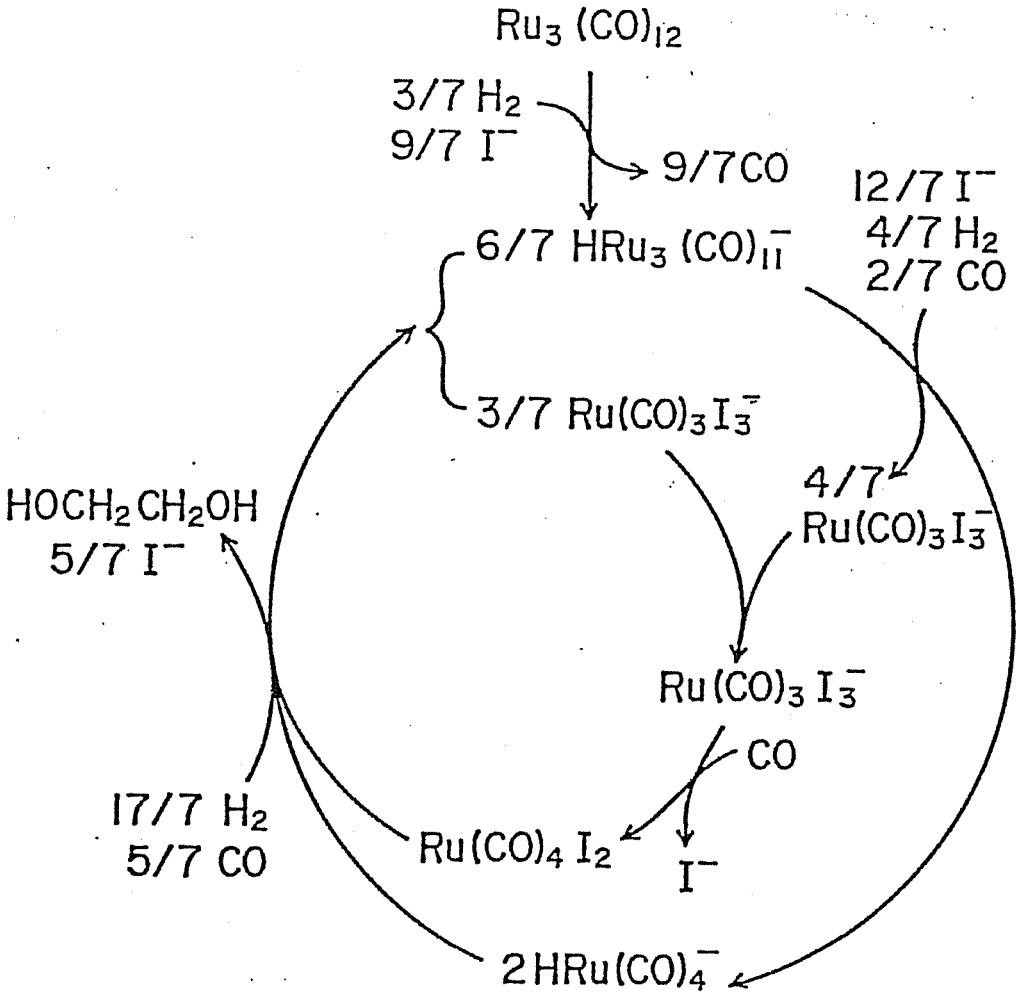

Figure 7. Proposed mechanism of syngas conversion to ethylene glycol by Ru complexes.[26]

reactions with intact metal clusters in homogeneous catalysis are still rare. Reported examples of the catalytic reactions by the monometallic clusters retaining their framework are as follows: olefin isomerization by $H_2Os_3(CO)_{10}$,[27] hydrogenation of ketones with $H_4Ru_4(CO)_{12}$,[28] water-gas shift reaction with $Ru_3(CO)_{12}$,[29] and ethylene hydroformylation with $[HRu_3(CO)_{11}]^-$.[30] In these reactions, the clusters were recovered after the catalysis.

Heterogeneous Catalysis by Supported Metal Clusters

Surface organometallic chemistry is concerned with the synthesis, structure, reactivity, and catalytic activity of surface-supported organometallic compounds. This is motivated by the opportunities to use organometallic compounds as probes of the structure and reactivity of surfaces, by opportunities offered by molecular organometallic precursors for formation of new surface structures, and by prospects that these surface structures will have new catalytic properties.

The reactions to graft the organometallic compounds on oxide surfaces are summarized as follows (Figure 8):[3]

1. reaction of a metal alkyl with OH
2. reaction of a π-allyl compound with OH
3. oxidative addition of OH into a single metal species
4. nucleophilic attack of O^{2-} of surface at a coordinated CO
5. oxidative addition of OH into a metal-metal bond
6. nucleophilic addition at a coordinated CO followed with β-H elimination

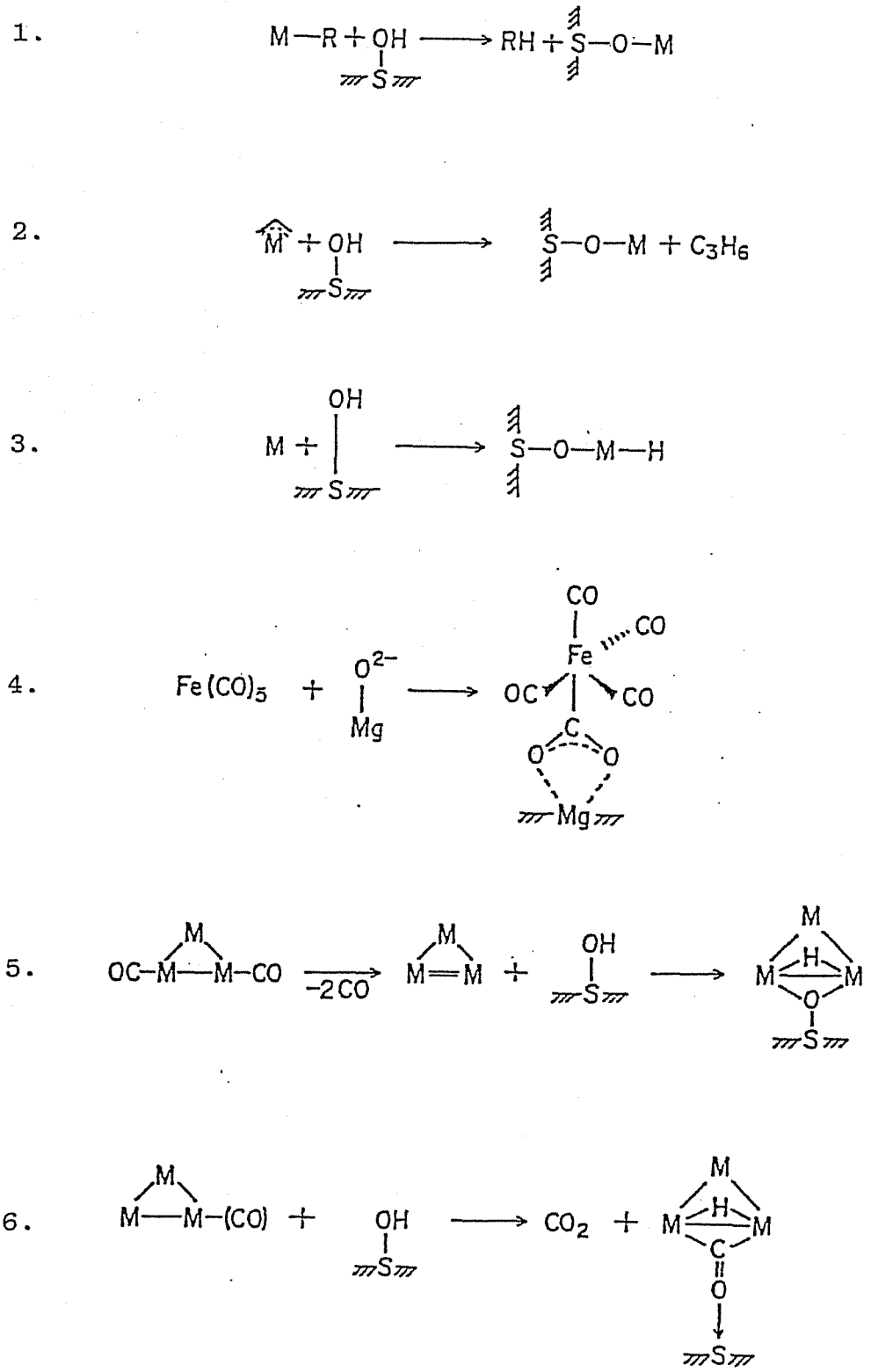

Figure 8. Reactions of organometallic compounds with oxide surfaces.[3]

Metal carbonyl clusters grafted on the solid such as SiO_2, Al_2O_3, MgO, TiO_2, and carbon have been a subject of recent interest, because they lead to the formation of well-defined multinuclear metal particles as small as 10 Å in size with high dispersion on the surface. The highly dispersed metal particles are catalytically active in many useful reactions such as hydrogenation of C-C multiple bonds, hydroformylation of olefins, and CO hydrogenation. The nature of surface-supported clusters has been studied by means of IR (Infrared), Raman, UV-Vis, EXAFS (Extended X-ray Absorption Fine Structure), XPS (X-ray Photoelectron Spectroscopy), TEM (Transmission Electron Microscopy), and *etc.*.

Basset *et al.*[31] reported that the reaction of $Os_3(CO)_{12}$ with silanol groups of silica gave the grafted cluster $HOs_3(CO)_{10}(OSi\equiv)$, which had a bridging hydride and a bridging $3e^-$ oxygen ligand. The cluster is a catalyst for the ethylene hydrogenation reactions. The proposed mechanism is shown in Figure 9. The reaction of $Os_3(CO)_{12}$ with alumina is different from that with silica (Figure 10).[32] The grafted cluster $HOs_3(CO)_{10}(OAl=)$ is unstable, it decomposes above 150 °C to give mononuclear Os(II) species with evolution of 3 moles of H_2. In contrast to the silica-supported cluster, the Os(II) dicarbonyl species are linked to alumina by two covalent bonds $Os(OAl=)_2$.

Iijima and Ichikawa succeeded in the first imaging of $Rh_6(CO)_6$ on alumina by using a high resolution transmission electron microscope (Figure 11).[33] They reported that $Rh_6(CO)_{16}$ on the Al_2O_3 appeared to be hemispherical with the size of less

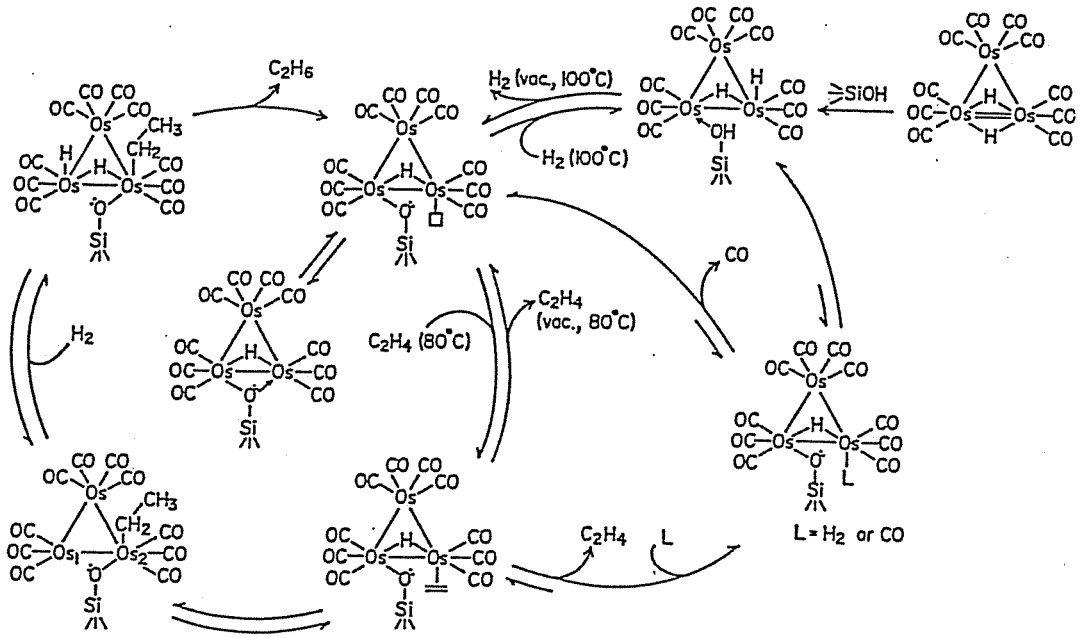

Figure 9. Proposed mechanism of ethylene hydrogenation by $HOs_3(CO)_{10}(OSi\equiv)$.[31]

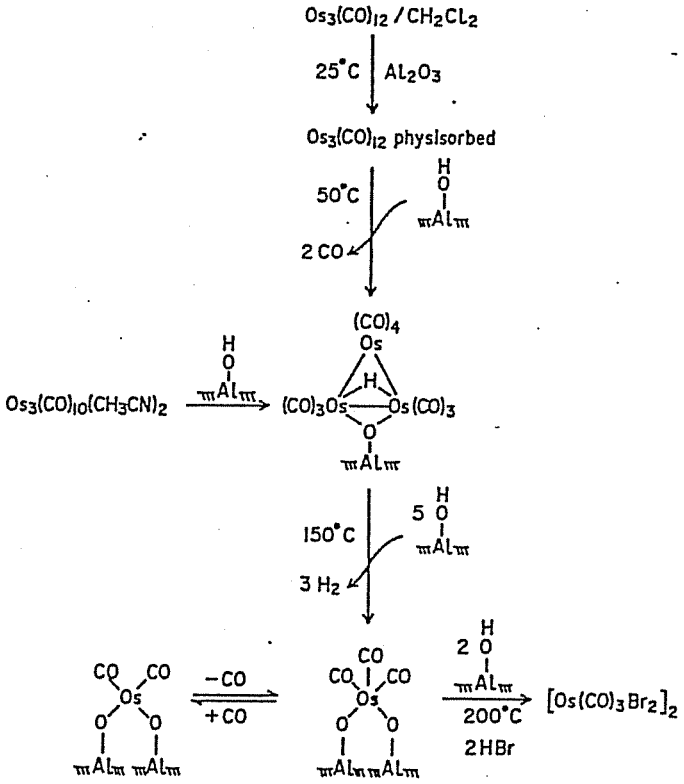

Figure 10. Reaction of $Os_3(CO)_{12}$ with Al_2O_3.[32]

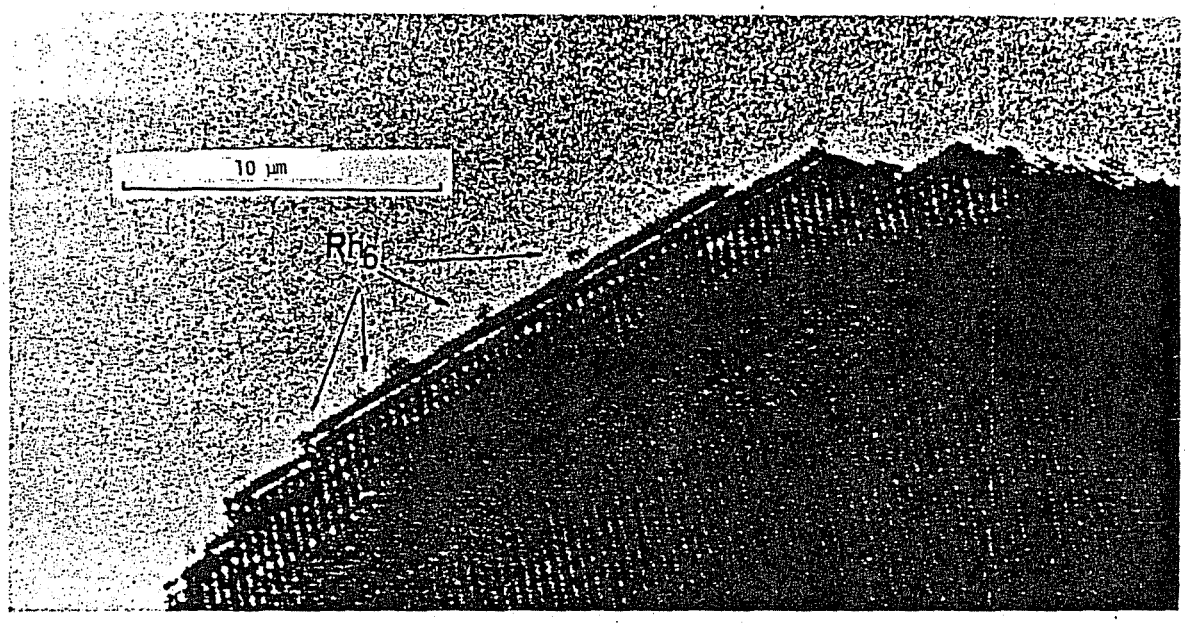

Figure 11. The image of $Rh_6(CO)_{16}$ on the (111) surface of γ-Al_2O_3 by high resolution transmission electron microscopy.[33]

than 10 Å in diameter. Recently, our group has reported that the images of $Rh_4(CO)_{12}$ and $[NEt_4]_2[Pt_{12}(CO)_{24}]$ adsorbed on graphite were observed in well-ordered structures by scanning tunneling microscopy (STM), as shown in Figure 12.[34]

Bimetallic Clusters in Homogeneous and Heterogeneous Catalysis

It is a challenge in catalysis to design multifunctional multicatalyst systems. The most promising advantage of homogeneous cluster catalysis is the potential multisite activation of a substrate leading to an unusual product. Bimetallic (or mixed metal, heterometallic) clusters have the possibility to create the effective multifunctional catalysis, because they contains more than two different metal elements.

In heterogeneous catalysis, the supported bimetallic catalysts are extensively used in technology, since the combination of metals is often more effective than the single metal. Well-known examples are the alumina-supported Pt-Re for the reforming of petroleum naphtha and the oxide-supported Pt-Rh for the abatement of automobile exhaust. These technological catalysts have highly complicated structures, incorporating metal aggregates of various sizes and shapes dispersed on high-area porous oxide supports. However, since Sinfelt *et al.* suggested the formation of alloys in the technological bimetallic catalysts by using EXAFS,[35] there has been interest in supported bimetallic clusters in order to obtain well-defined bimetallic sites on the surface of supports.

In attempts to increase the product selectivity in the

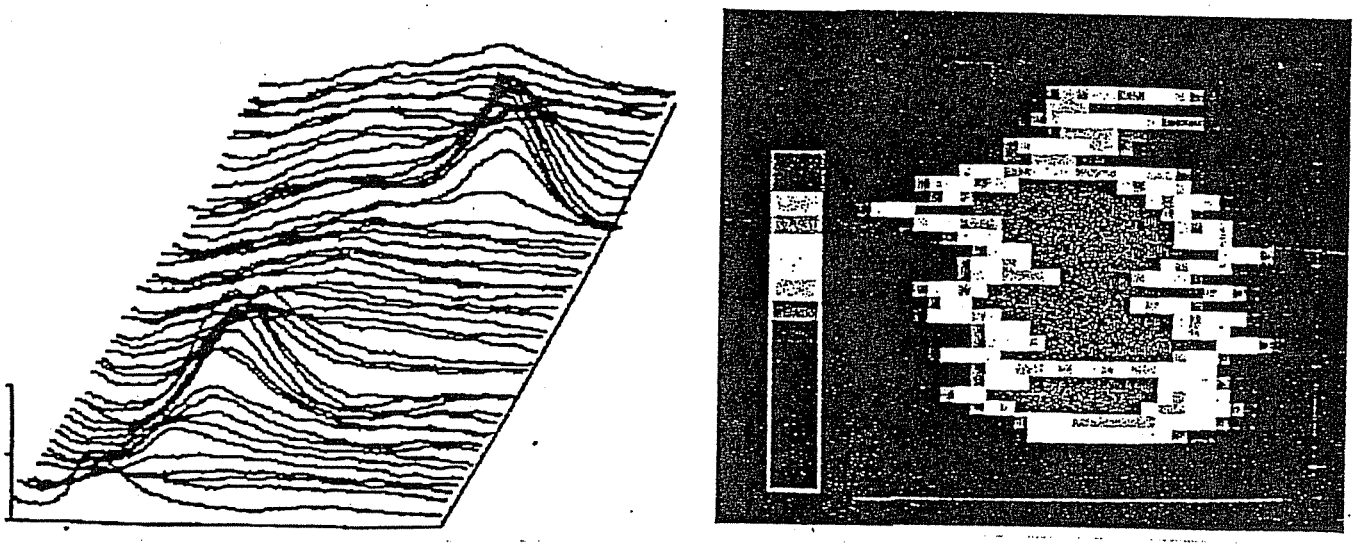

(a) (b)

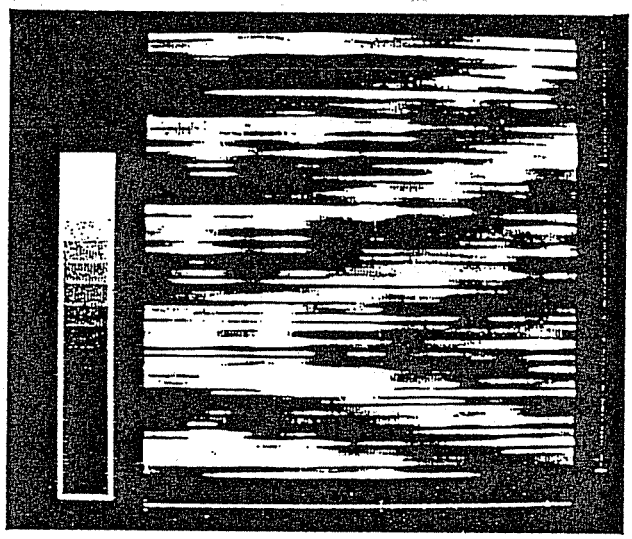

(c)

Figure 12.
(a) Line scanning STM image of $[NEt_4]_2[Pt_{12}(CO)_{24}]$ on highly oriented pyrolytic graphite (HOPG) at 25 °C: x = 210, y = 190 Å, Z = arbitrary unit;
(b) Top view of the lower hump of (a): x = y = 42 Å;
(c) Top view of $Rh_4(CO)_{12}$ on HOPG at 25 °C: x = y = 165 Å.

catalytic reactions such as CO hydrogenation and hydrocarbon hydrogenolysis, zeolites have been used as supports for the metal catalysts to impose a shape selectivity with their framework structure as well as to control the size of metal particles.[12] In the course of our research on the supported bimetallic clusters, we have studied the structural nature and the catalysis of zeolite-entrapped mono- and bimetallic clusters. The strategy for the preparation of the entrapped clusters is to introduce a small organometallic precursor into the zeolite supercages followed with reductive carbonylation to lead the *"ship-in-a-bottle"* formation[36-38] of carbonyl clusters in the supercages (Figure 13).

In this thesis, homogeneous and heterogeneous catalysts derived from bimetallic carbonyl systems and/or clusters are studied to achieve the multifunctional catalysis. CHAPTER 2 describes the catalysis of homogeneous Co and Ru mixed metal catalysts in olefin hydroformylation and hydroesterification. The synergistic effect of Co and Ru is discussed. Supported RuCo bimetallic clusters are applied to the olefin hydroformylation in heterogeneous catalysis (CHAPTER 3). In section 4-1 of CHAPTER 4, the synthesis, characterization, and catalysis of RhFe, PtFe, PdFe, and IrFe bimetallic clusters supported on SiO_2 are presented. The bimetallic catalysts show high activity and selectivity for alcohol synthesis in CO-based reactions. $M\text{-}Fe^{3+}$ (M = Rh, Pt, Pd, and Ir) sites are proposed to activate CO and to enhance migratory CO insertion. The activation of CO on

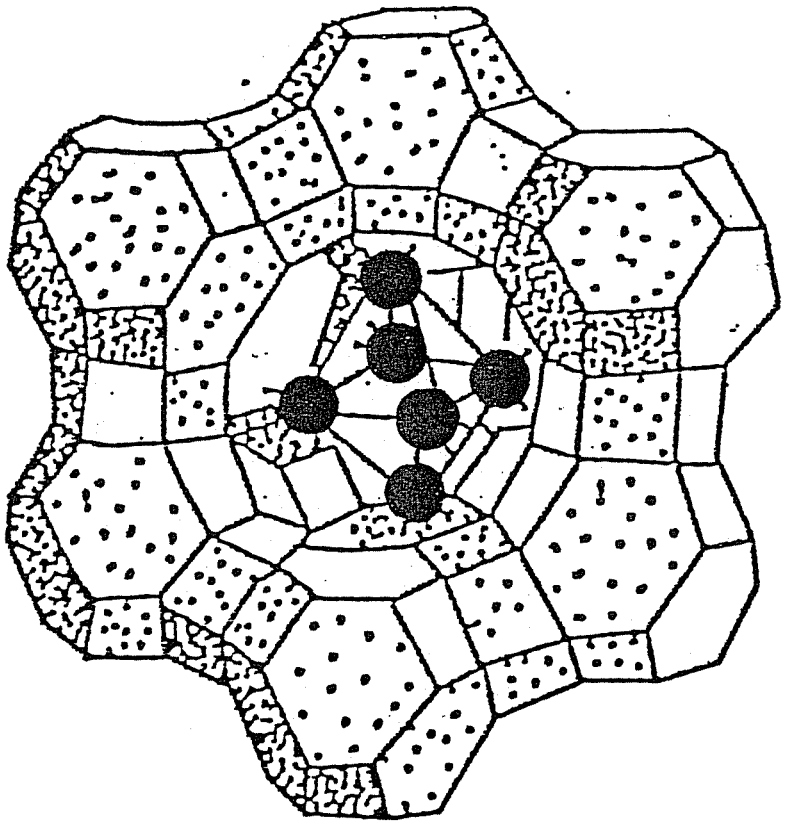

Figure 13. *"Ship-in-a-bottle"* synthesis of $Rh_6(CO)_{16}$ in NaY supercage.

bimetallic sites is verified on Rh-Mn/SiO_2 catalyst (section 4-2). Finally, *"ship-in-a-bottle"* synthesis of Rh_6, RhFe, RhIr, and Ir_6 carbonyl clusters and their catalysis are described in CHAPTER 5.

References

1 J.P. Collman, L.S. Hegedus, J.R. Norton, R.G. Finke, *"Principles and Applications of Organotransition Metal Chemistry"*, 2nd ed., University Science Book, Mill Valey, 1987.

2 F.A. Cotton and G. Wilkinson, *"Advanced Inorganic Chemistry"*, 5th ed., A Wiley-Interscience, 1988.

3 J.M. Basset, in *"Industrial Applications of Homogeneous Catalysis"*, A. Mortreux and F. Petit eds., D. Reidel Pub., Dordrecht, 1988, p. 293.

4 P. Chini, G. Longoni, and V.G. Albano, *Adv. Organomet. Chem.*, 14, 285(1976).

5 E.L. Muetterties, T.N. Rhoudui, E. Band, C.F. Brucker, W.R. Pretzer, *Chem. Rev.*, 79, 9(1979).

6 B.F.G. Johnson ed., *"Transition Metal Clusters"*, A Wiley-Interscience, Chichester, 1980.

7 W.L. Gladfelter and G.L. Geoffroy, *Adv. Organomet. Chem.*, 18, 207(1980).

8 H. Vahrenkamp, *Adv. Organomet. Chem.*, 22, 169(1983).

9 R.D. Adams and I.T. Horvath, *Prog. Inorg. Chem*, 33, 127 (1985).

10 M.D. Vargas and J.N. Nicholls, *Adv. Inorg. Chem. Radiochem.*, **30**, 123(1986).

11 M. Ichikawa, in *"Tailored Metal Catalysts"*, Y. Iwasawa ed., D. Reidel Pub., Dordrecht, 1986, p. 183.

12 B.C. Gates, L. Guczi, and H. Knözinger eds., *"Metal Clusters in Catalysis"*, Elsevier, Amsterdam, 1986.

13 P. Braunstein and J. Rose, in *"Stereochemistry of Organometallic and Inorganic Compounds"*, I. Bernal ed., Elsevier, Amsterdam, 1988.

14 K. Wade, *Adv. Inorg. Chem. Radiochem.*, **18**, 1(1976).

15 D.M.P. Mingos, *Acc. Chem. Res.*, **17**, 311(1984).

16 J.W. Lauher, *J. Am. Chem. Soc.*, **100**, 5305(1978).

17 B.K. Teo, *Inorg. Chem.*, **23**, 1251, 1257(1984).

18 R. Hoffmann, *Angew. Chem. Int. Ed. Eng.*, **21**, 711(1982).

19 J. Falbe ed., *New Syntheses with Carbon Monoxide*, Springer, Berlin, 1980, and references therein.

20 R.A. Sheldon, *Chemicals from Synthesis Gas, Catalytic Reactions of CO and H_2*, D. Reidel Pub., Dordrecht, 1983, and references therein.

21 D.F. Shriver and M.J, Sailor, *Acc. Chem. Res.*, **21**, 374(1988), and references therein.

22 J.S. Bradley, E.W. Hill, G.B. Ansell, M.A. Modrick, *Organometallics*, 1, 1634(1982).

23 R.L. Pruett, *Ann. N. Y. Acad. Sci.*, **295**, 239(1977).

24 J.L. Vidal and W.E. Walker, *Inorg. Chem.*, **19**, 896(1980).

25 B.T. Heaton, J. Jonas, T. Eguchi, and G.A. Hoffman, *J. Chem. Soc., Chem. Commun.*, 709(1981).

26 B.D. Dombek, *J. Organomet. Chem.*, **250**, 467(1983).

27 J.B. Keister and J.R. Shapley, *J. Am. Chem. Soc.*, **98**, 1056(1976).

28 P. Frediani, U. Matteoli, M. Bianchi, F. Piacenti, and G. Menchi, *J. Organomet. Chem.*, **150**, 273(1978).

29 P.C. Ford, *Acc. Chem. Res.*, **14**, 31(1981).

30 G. Süss-Fink and G. Herrman, *J. Chem. Soc., Chem. Commun.*, 735(1985).

31 B. Besson, A. Choplin, L. D'Ornelas, and J.M. Basset, *J. Chem. Soc., Chem. Commun.*, 842(1982); A. Choplin, B. Besson, L. D'Ornelas, R. Sanchez-Delgado, J.M. Basset, *J. Am. Chem. Soc.*, **110**, 2783(1988).

32 R. Psaro, R. Ugo, G.M. Zandelighi, B. Besson, A.K. Smith, and J.M. Basset, *J. Organomet. Chem.*, **213**, 215(1981).

33 S. Iijima and M. Ichikawa, *J. Catal.*, **94**, 313(1985).

34 T. Fujimoto, A. Fukuoka, J. Nakamura, and M. Ichikawa, *J. Chem. Soc., Chem. Commun.*, in press.

35 J.H. Sinfelt, *Acc. Chem. Res.*, **10**, 15(1977); **20**, 134(1987).

36 P. Gelin, F. Lefebvre, B. Elleuch, C. Naccache, Y. Ben Taarit, *ACS Symp. Ser.*, **218**, 469(1983).

37 P. Zhou and B.C. Gates, *J. Chem. Soc., Chem. Commun.*, 347(1989).

38 L.L. Sheu, H. Knözinger, and W.M.H. Sachtler, *Catal. Lett.*, **2**, 129(1989).

CHAPTER 2

HOMOGENEOUS CATALYSIS BY COBALT-RUTHENIUM BIMETALLIC SYSTEMS

CHAPTER 2

2-1

HYDROFORMYLATION AND HYDROESTERIFICATION OF OLEFINS CATALYZED BY HOMOGENEOUS COBALT-RUTHENIUM BIMETALLIC CARBONYL COMPLEXES

Summary

Bimetallic systems $Co_2(CO)_8+Ru_3(CO)_{12}$ and bimetallic cluster $HRuCo_3(CO)_{12}$ showed high catalytic activity for hydroformylation of olefins such as cyclohexene, 1-hexene, and styrene, compared with $Co_2(CO)_8$ or $Ru_3(CO)_{12}$ alone. The rates of hydroformylation by the bimetallic catalysts were substantially influenced by the nature of solvents used, and alcohols such as methanol and ethanol gave higher rates. Thus the initial rate of the hydroformylation of cyclohexene with the $Co_2(CO)_8+Ru_3(CO)_{12}$ catalyst (Ru/Co = 1 atomic ratio) in methanol was nineteen times faster than that with $Co_2(CO)_8$ under the reaction conditions of 110 °C and $CO+H_2$ = 40+40 kg/cm^2 (initial pressure at room temperature). The cobalt-ruthenium bimetallic catalysts also active for the hydroesterification of cyclohexene. The synergistic effect of Co and Ru on hydroformylation and hydroesterification is discussed.

Introduction

Homogeneous multimetallic catalysts have been recently received much attention because it is hoped that the cooperativity of different metals during chemical transformations might lead to more selective and efficient reactions and, in some cases, to new type of reactions which are inaccessible through homometallic systems. Many examples using bimetallic catalysts have appeared in recent years, including the hydroformylation and aminomethylation of 1-pentene under the conditions of water-gas shift reaction with Fe-Ru bimetallic carbonyl complexes,[1] hydroformylation of olefins using Co-Rh clusters as catalyst precursors,[2] homologation reactions of MeOH[3-6] and carboxylic acid methyl esters[7,8] by Co-Ru mixed metal catalysts, CO hydrogenation to ethylene glycol and its derivatives by Rh-Ru catalysts,[9] synthesis of γ-keto acids from alkynes, methyl iodide, and CO by Co-Ru phase-transfer catalysts,[10] and the reduction of nitro compounds by Co-Rh phase-transfer catalysts.[11]

In the study of homogeneous multimetallic catalysis, our group found that Co-Ru bimetallic catalysts were very effective for the homologation of methanol to ethanol, and Ru not only was involved in the hydrogenation of acetaldehyde to ethanol but also slightly but notably enhanced acetaldehyde formation. These observations led us to discover that $Co_2(CO)_8$+$Ru_3(CO)_{12}$ bimetallic catalysts show higher activity for the hydroformylation of olefins than $Co_2(CO)_8$ or $Ru_3(CO)_{12}$ alone, since both homologation and hydroformylation involve alkyl and

acyl complexes as common intermediates.

The rate enhancement of the olefin hydroformylation and hydroesterification by the synergistic effect of Co and Ru complexes is discussed in this section 2-1.

Experimental

All olefins and solvents were dried by appropriate agents and distilled under N_2 atmosphere. $Co_2(CO)_8$ was obtained commercially and used without further purification. $Ru_3(CO)_{12}$,[12] $Ru(CO)_3(PPh_3)_2$,[13] $Ru(CO)_4(PPh_3)$,[14] tris(diphenylphosphino)methane $HC(PPh_2)_3$,[15] and $HRuCo_3(CO)_{12}$[4] were prepared according to published procedures (see Figure 1).

High Pressure Reactions

A 100 ml stainless-steel autoclave (Figure 2) was used as the reactor. In a typical run (Table 1, Run 4), $Co_2(CO)_8$ (Co atom 0.20 mmol), $Ru_3(CO)_{12}$ (Ru atom 0.19 mmol), cyclohexene (8 ml, 80 mmol) and THF (10 ml) as a solvent were charged into the reactor under N_2 atmosphere. The autoclave was closed and then pressurized to 80 kg/cm^2 with CO/H_2 = 1 at room temperature. Agitation was begun and the autoclave was heated to 110 °C within 20 min. The reaction was allowed to proceed at that temperature for 4 h, and the initial rate was determined by measuring the pressure drop at the early stage of the reaction, the time-dependence curve of which is shown in Figure 3. After the reaction, the autoclave was rapidly cooled to room temperature,

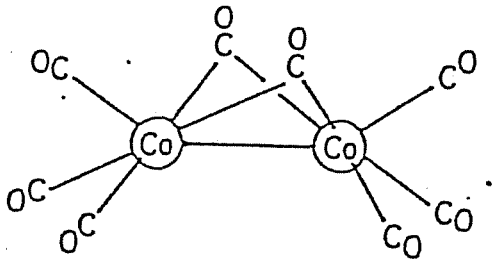

(a)

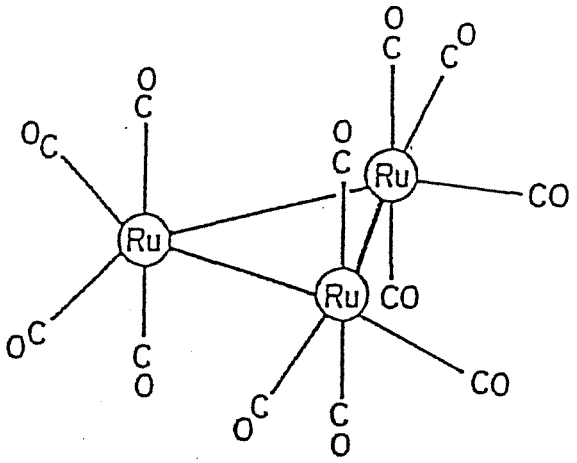

(b)

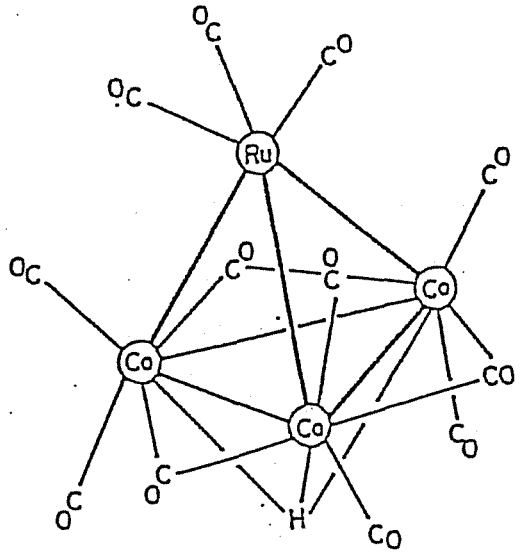

(c)

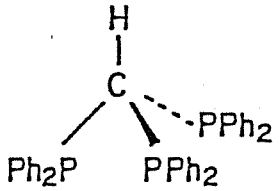

(d)

Figure 1. Metal carbonyl compounds (a) $Co_2(CO)_8$, (b) $Ru_3(CO)_{12}$, (c) $HRuCo_3(CO)_{12}$, and a triphosphine (d) $HC(PPh_2)_3$.

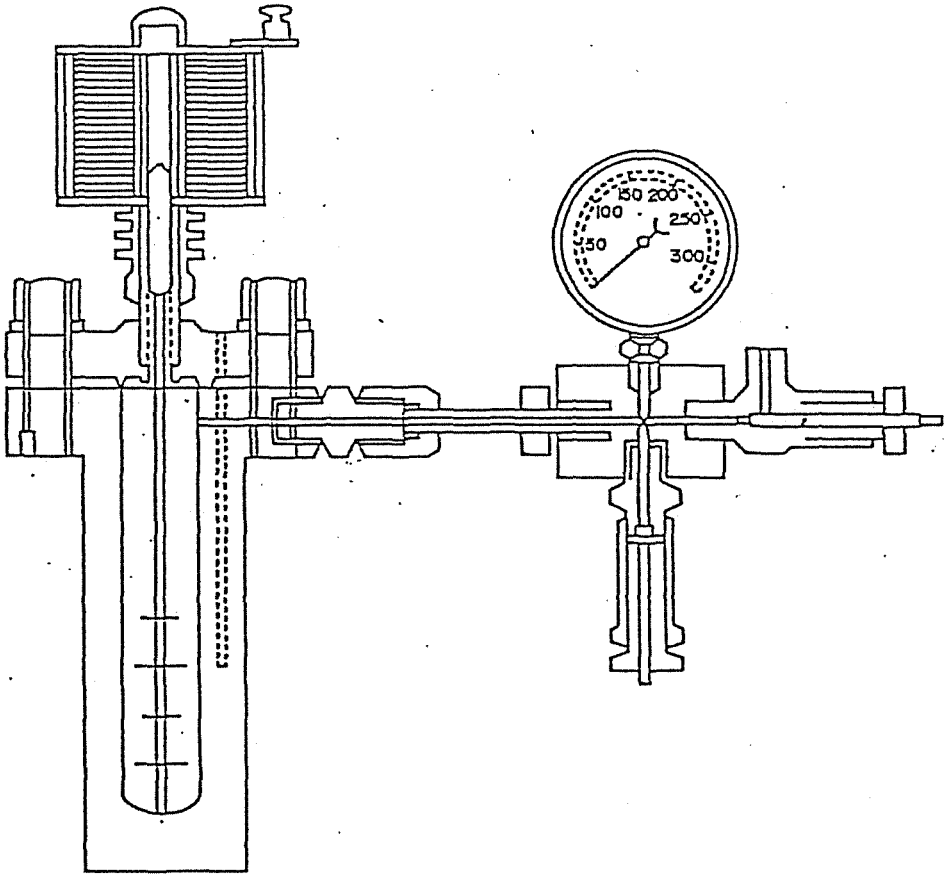

Figure 2. A stainless-steel autoclave used as a high pressure reactor.

and the pressure was slowly released. The autoclave was opened, 5 mmol of toluene was added as an internal standard, and the liquid phase was analyzed by gas chromatography. The conversion of cyclohexene was 55 % and cyclohexanecarbaldehyde (1) was formed in 52 % yield based on the cyclohexene initially added. The yields of cyclohexane and cyclohexanemethanol were less than 1 %.

Gas Chromatographic Analyses

Gas chromatographic analyses were performed on a Hitachi 163 instrument with a flame ionization detector using a 3 mmϕ x 3 m PEG-20M column (PEG-20M (20 %) on Chromosorb W, 60-80 mesh, N_2 gas 20 ml/min). The analytical conditions were as follows:

Reaction	Internal standard	Temperature range (°C) (Rate of temperature increase)
Hydroformylation of cyclohexene	Toluene (5 mmol)	70-200 (5 °C/min)
Hydroformylation of 1-hexene	Toluene (5 mmol)	60-200 (5 °C/min)
Hydroformylation of styrene	Butylbenzene (5 mmol)	100-200 (10 °C/min)
Hydroesterification of cyclohexene	Toluene (5 mmol)	70-200 (5 °C/min)

Kinetic Measurements

Effect of Cobalt Concentration The effect of cobalt concentration on the rate of hydroformylation of cyclohexene was studied over the range 5.4×10^{-3} to 2.2×10^{-2} M (Co/Ru = 0.48-2.0) under the following conditions: 110 °C, Ru 1.1×10^{-2} M, cyclohexene 4.4 M, $CO+H_2$ = 40+40 kg/cm^2 (initial pressure at room temp.).

Effect of Ruthenium Concentration The effect of ruthenium concentration on the rate was studied over the range 3.6×10^{-3} to 1.1×10^{-1} M (Ru/Co = 0.34-9.9) under the following conditions: 110 °C, Co 1.1×10^{-2} M, cyclohexene 4.4 M, $CO+H_2$ = 40+40 kg/cm^2 (initial pressure at room temp.).

Effect of Cyclohexene Concentration The influence of cyclohexene concentration on the rate was studied over the range 5.3×10^{-1} to 4.7 M under the following conditions: 110 °C, Co 1.1×10^{-2} M, Ru 1.1×10^{-2} M, $CO+H_2$ = 40+40 kg/cm^2 (initial pressure at room temp.).

Effect of Hydrogen Pressure The rates were measured for different initial pressures of hydrogen over the range 20 to 80 kg/cm^2 under the following conditions: 110 °C, Co 1.1×10^{-2} M, Ru 1.1×10^{-2} M, cyclohexene 4.4 M, CO 40 kg/cm^2 (initial pressure at room temp.).

Effect of Carbon Monoxide Pressure The rates were measured for different initial pressures of carbon monoxide over the range 20 to 60 kg/cm^2 under the following conditions: 110 °C, Co 1.1×10^{-2} M, Ru 1.1×10^{-2} M, cyclohexene 4.4 M, H_2 40 kg/cm^2 (initial pressure at room temp.).

Results

Hydroformylation of Cyclohexene

Table 1 summarizes the results of the hydroformylation of cyclohexene in THF using $Co_2(CO)_8$+$Ru_3(CO)_{12}$ mixed metal catalysts (eq 1).

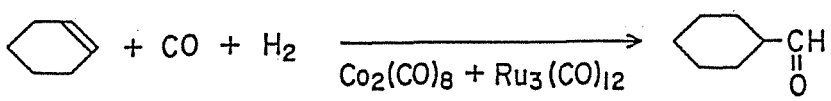

(1)

(1)

The yield of cyclohexanecarbaldehyde (1) with the bimetallic catalyst is considerably higher than would be expected by a simple additive effect based on the values observed for $Co_2(CO)_8$ and $Ru_3(CO)_{12}$, respectively. Thus, the yield of (1) in Run 5 was much higher than the sum of the yields of (1) from Runs 1 and 2. Furthermore, as more $Ru_3(CO)_{12}$ was added to $Co_2(CO)_8$, the initial rate increased. At Ru/Co = 9.9, the initial rate was twenty-seven times faster than that with $Co_2(CO)_8$ alone. When the conversion of cyclohexene increased above *ca.* 50 %, 2,4,6-tricyclohexyl-1,3,5-trioxane (Figure 4) was formed together with the aldehyde (1), but neither cyclohexanemethanol nor cyclohexane was formed under the conditions employed, although a small amount of cyclohexanemethanol was formed at very high conversion of cyclohexene. The time-dependence curve of the reaction pressure, illustrated in Figure 3, clearly shows that the cobalt-ruthenium bimetallic systems provide high catalytic activities for the hydroformylation of cyclohexene. With $Ru_3(CO)_{12}$ alone, the pressure hardly changed throughout the reaction, whereas with

Table 1. Hydroformylation of Cyclohexene by Co and/or Ru Catalysts.[a]

Run	Catalyst	Ru/Co	Yield of (1) (%)[b]	Initial rate (V_0)[c]
1	$Co_2(CO)_8$	-	14	1.0
2[d]	$Ru_3(CO)_{12}$	-	3	0.3
3	$Co_2(CO)_8$ + $Ru_3(CO)_{12}$	0.34	32	3.6
4	$Co_2(CO)_8$ + $Ru_3(CO)_{12}$	0.95	52	5.9
5	$Co_2(CO)_8$ + $Ru_3(CO)_{12}$	3.2	62	8.4
6	$Co_2(CO)_8$ + $Ru_3(CO)_{12}$	9.9	100[e]	27
7	$Co_2(CO)_8$ + $Ru(CO)_3(PPh_3)_2$	0.96	0	0
8[f]	$Co_2(CO)_8$ + $Ru(CO)_3(PPh_3)_2$	0.89	10	1.1
9[g]	$Co_2(CO)_8$ + $Ru(CO)_4(PPh_3)$	0.99	35	3.3
10	$HRuCo_3(CO)_{12}$ + $HC(PPh_2)_3$	0.33	37	3.0

[a] Reaction conditions: Co atom 0.2 mmol; cyclohexene 80 mmol; THF as solvent 10 ml; reaction temperature 110 °C; reaction time 4 h; $CO+H_2$ = 40+40 kg/cm^2 (initial pressure at room temp.).
[b] The yield of (1) is based on the starting cyclohexene. It includes the 2,4,6-tricyclohexyl-1,3,5-trioxane formed, because the latter quantitatively decomposes to (1) under the conditions of our direct GC analysis.
[c] Relative to $Co_2(CO)_8$ alone (Run 1).
[d] Ru atom 0.6 mmol.
[e] Small amount of cyclohexanemethanol formed.
[f] Reaction temp. 130 °C.
[g] Benzene as solvent 10 ml.

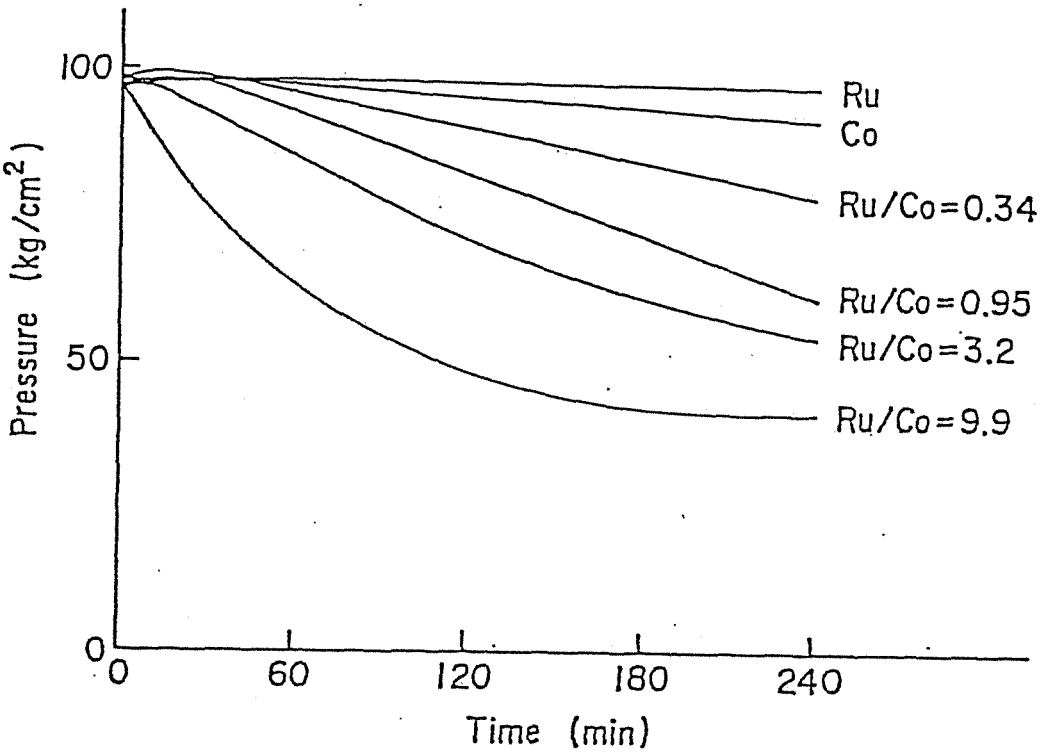

Figure 3. Time-dependence curve of the reaction pressure in hydroformylation of cyclohexene with $Co_2(CO)_8$ and/or $Ru_3(CO)_{12}$ catalysts. Reaction conditions: see Table 1.

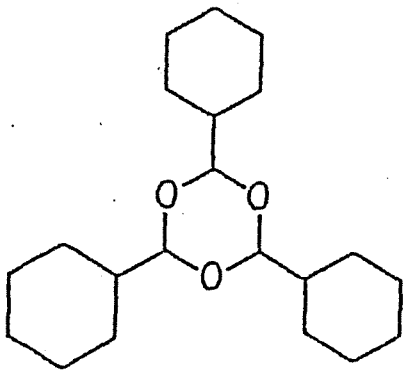

Figure 4. 2,4,6-Tricyclohexyl-1,3,5-trioxane, a trimer of (1).

$Co_2(CO)_8$ alone, the pressure decreased linearly but slowly after an induction period of *ca.* 40 min. However, at Ru/Co = 0.95, the pressure drop was much greater than that with the $Co_2(CO)_8$ system, although a similar induction period was observed. At Ru/Co = 9.9, no induction period was observed and the reaction was completed after *ca.* 180 min. Kinetic studies on the hydroformylation of cyclohexene with the $Co_2(CO)_8+Ru_3(CO)_{12}$ catalysts in THF showed that the rate is expressed by eq 2:

$$V_0 = k_{obs}[Co]^{1.0}[Ru]^{0.6}[\text{cyclohexene}]^{0.5}P(H_2)^{0.9}P(CO)^{-1.0} \quad (2)$$

If phosphine-substituted ruthenium carbonyls such as $Ru(CO)_3(PPh_3)_2$ and $Ru(CO)_4(PPh_3)$ were used instead of $Ru_3(CO)_{12}$ as the catalyst component, the catalytic activity was decreased (Table 1, Runs 7-9). A triphosphine, tris(diphenylphosphino)-methane (Figure 1) was also added to the cobalt-ruthenium bimetallic cluster $HRuCo_3(CO)_{12}$ in order to maintain the metals in close proximity under the reaction conditions (Table 1, Run 10). The yield of (1) and the initial rate were almost the same as those by the $Co_2(CO)_8+Ru_3(CO)_{12}$ (Ru/Co = 0.34) catalyst (Table 1, Run 3). After the catalytic reaction, the cluster $HRuCo_3(CO)_{12}$ was not recovered but the peaks of cobalt carbonyls and ruthenium carbonyls such as $HCo(CO)_4$ and $Ru(CO)_5$ were observed in the IR spectrum of the reaction solution. The IR spectrum was very similar to that with the $Co_2(CO)_8+Ru_3(CO)_{12}$ catalyst.[16] Thus the $HRuCo_3(CO)_{12}$ seems to be decomposed to its fragments under the catalytic conditions even in the presence of

Table 2. Solvent Effect on the Hydroformylation of Cyclohexene by Co-Ru Bimetallic Catalysts.[a]

Run	Solvent	Initial rate (V_0)[b]	Yields of products[c] (%)			
			CyCHO[d]	$CyCH_2OH$	Acetal	Ester
1	pyridine	1.4(0.1)	19 (0)	0(0)		
2	hexane	5.4(1.1)	58(12)	1(0)		
3	dioxane	5.8(0.9)	61(11)	1(0)		
4	THF	5.9(1.0)	52(14)	1(0)		
5	benzene	9.1(1.1)	73(12)	2(0)		
6	ethanol	15 (1.1)	39 (2)	2(0)	$CyCH(OEt)_2$ 54(14)	CyCOOEt 2(1)
7	methanol	19 (1.1)	19 (0)	1(0)	$CyCH(OMe)_2$ 68(15)	CyCOOMe 5(1)
8[e]	Benzene	14	91	4		
9[e]	THF	27	93	6		
10[e]	methanol	32	16	2	$CyCH(OMe)_2$ 76	CyCOOMe 4

[a] Reaction conditions: $Co_2(CO)_8$ 0.10 mmol, $Ru_3(CO)_{12}$ 0.067 mmol, Ru/Co = 1 atomic ratio; cyclohexene 80 mmol; solvent 10 ml; reaction temperature 110 °C; reaction time 4 h; $CO+H_2$ = 40+40 kg/cm^2 (initial pressure at room temp.). Values in parentheses are those catalyzed by $Co_2(CO)_8$ (0.10 mmol) alone.

[b] Relative to $Co_2(CO)_8$ in THF.

[c] Yields are based on the starting cyclohexene.

[d] Cy = cyclohexyl, C_6H_{11}-

[e] $Co_2(CO)_8$ 0.10 mmol; $Ru_3(CO)_{12}$ 0.67 mmol (Ru/Co = 10 atomic ratio).

$HC(PPh_2)_3$.

Solvent effect is shown in Table 2, where the initial rate is expressed as the relative value compared with that using $Co_2(CO)_8$ in THF. The initial rate of the hydroformylation of cyclohexene with $Co_2(CO)_8$ was almost independent of the nature of the solvent employed, except for pyridine. In contrast, the initial rate of the same reaction with the $Co_2(CO)_8+Ru_3(CO)_{12}$ catalysts was largely influenced by the nature of the solvent. Interestingly, alcohols such as methanol and ethanol were the best among the solvents investigated. The rate of the hydroformylation using a Ru/Co atomic ratio of 1 or 10 in methanol was nineteen or thirty-two times faster, respectively, than that with $Co_2(CO)_8$ alone in THF. In this case, the aldehyde initially formed is mostly converted into its dimethyl acetal.

Hydroformylation of Other Olefins

A synergistic effect for cobalt and ruthenium was also observed for hydroformylation of other olefins such as 1-hexene and styrene (eqs 3 and 4).

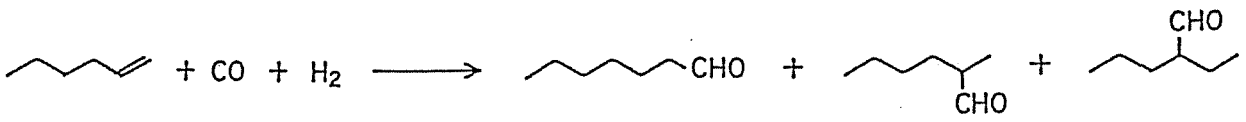

(3)

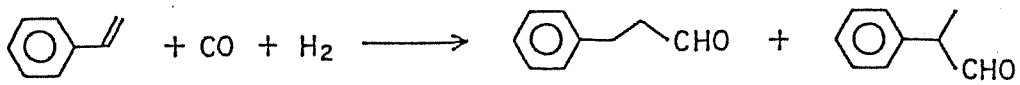

(4)

Table 3. Hydroformylation of 1-Hexene and Styrene by Co and/or Ru Catalysts.[a]

Run	Olefin	Catalyst	Ru:Co ratio	Reaction time (h)	Yield of aldehyde[b] (%)	n/iso ratio	Initial rate[c] (V_0)
1	1-hexene	$Co_2(CO)_8$	-	1.5	22	3.2	1.0
2	1-hexene	$Ru_3(CO)_{12}$	-	1.5	1	5.0	0.2
3	1-hexene	$Co_2(CO)_8$ + $Ru_3(CO)_{12}$	0.99	1.5	50	3.1	3.1
4	styrene	$Co_2(CO)_8$	-	4.0	12(1)	1.3	1.0
5	styrene	$Ru_3(CO)_{12}$	-	4.0	3(1)	0.7	0.3
6	styrene	$Co_2(CO)_8$ + $Ru_3(CO)_{12}$	1.0	4.0	20(4)	1.2	2.0

[a] Reaction conditions: $Co_2(CO)_8$ 0.10 mmol; $Ru_3(CO)_{12}$ 0.067 mmol; olefin 80 mmol; benzene as solvent 10 ml; reaction temp. 110 °C; $CO+H_2$ = 40+40 kg/cm^2 (initial pressure at room temp.).

[b] Yields are based on the starting olefin. Values in parentheses represent the yields of ethylbenzene.

[c] Relative to $Co_2(CO)_8$ for each olefin (Run 1, Run 4).

As shown in Table 3, the initial rate of the hydroformylation of 1-hexene in benzene by the bimetallic catalyst with a Ru/Co molar ratio of 1 was about three times faster than that with $Co_2(CO)_8$ alone. However, the normal/iso ratio of the aldehydes formed was essentially the same as in the case of $Co_2(CO)_8$. It is noteworthy that the initial rate is not improved more greatly than that in the hydroformylation of cyclohexene, because in the latter case the relative rate increase was about nine-fold under the same reaction conditions (Table 2, Run 5). On the other hand, the initial rate of the hydroformylation of styrene was roughly doubled if the bimetallic catalyst was used instead of $Co_2(CO)_8$. The normal/iso ratios in the styrene hydroformylation were not affected by the addition of $Ru_3(CO)_{12}$ to the $Co_2(CO)_8$ catalyst system.

The rate of hydroformylation of olefins with $Co_2(CO)_8$ decreases in the following order: 1-hexene >> styrene ~ cyclohexene (Table 4). 1-Hexene is rapidly hydroformylated, whereas cyclohexene and styrene are much less reactive. However, if the $Co_2(CO)_8$+$Ru(CO)_{12}$ bimetallic catalyst is used, cyclohexene as well as 1-hexene are much more readily converted into the corresponding aldehydes than is styrene. The magnitude of the synergistic effect for cobalt and ruthenium on hydroformylation of the three olefins decreases in the following order: cyclohexene > 1-hexene > styrene. It is of great interest that cyclohexene, which is the least reactive substrate in the $Co_2(CO)_8$-catalyzed hydroformylation,[17] is the most effectively hydroformylated if the $Co_2(CO)_8$+$Ru_3(CO)_{12}$ bimetallic catalyst is

Table 4. Comparison of Initial Rates in Hydroformylation of Olefins.[a]

Catalyst	Initial rate[b] (V_0)		
	1-Hexene	Cyclohexene	Styrene
$Co_2(CO)_8$	0.13	0.03	0.03
$Co_2(CO)_8$ + $Ru_3(CO)_{12}$ (Ru/Co = 1)	0.40	0.27	0.06

[a] Reaction conditions: $Co_2(CO)_8$ 0.10 mmol; $Ru_3(CO)_{12}$ 0.067 mmol; olefin 80 mmol; benzene as solvent 10 ml; reaction temp. 110 °C; $CO+H_2$ = 40+40 kg/cm^2 (initial pressure at room temp.).
[b] Described as the pressure drop ($kg \cdot cm^{-2} \cdot min^{-1}$) at the early stage of the reaction.

Table 5. Hydroesterification of Cyclohexene by Co and/or Ru Catalysts.[a]

Run	Catalyst	Ru/Co	Yields of products[b] (%)	
			CyCOOMe[c]	$CyCH(OMe)_2$
1	$Co_2(CO)_8$	-	16	0
2	$Ru_3(CO)_{12}$	-	6	0
3	$Co_2(CO)_8$ + $Ru_3(CO)_{12}$	1.0	53	2

[a] Reaction conditions: $Co_2(CO)_8$ 0.10 mmol; $Ru_3(CO)_{12}$ 0.067 mmol; cyclohexene 80 mmol; MeOH 10 ml; reaction temp. 150 °C; reaction time 24 h; CO 50 kg/cm^2 (initial pressure at room temp.).
[b] Yields are based on the starting cyclohexene.
[c] Cy = cyclohexyl, C_6H_{11}-

used.

Hydroesterification of Cyclohexene

The $Co_2(CO)_8$+$Ru_3(CO)_{12}$ catalyst is also effective for the hydroesterification of cyclohexene (eq 5). As is shown in Table 5, the yield of the methyl ester CyCOOMe was notably improved by using the mixed metal catalyst.

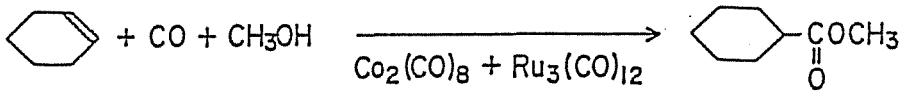

(5)

Discussion

Although the mechanism of the hydroformylation reaction with $Co_2(CO)_8$ proposed by Heck and Breslow is widely accepted,[18,19] the hydrogenolysis step of a metal acyl intermediate forming aldehydes is still the subject of controversy. Certain evidence has indicated that the dinuclear reductive elimination of aldehydes from metal acyls and metal hydrides occurs in the hydroformylation by the cobalt[20] and the rhodium[21] catalysts (eq 6). This led us to expect that the synergistic effect for cobalt and ruthenium might be explained by such a dinuclear reductive elimination between a cobalt acyl and a ruthenium hydride (eq 7).

$$RCOCo(CO)_3 + HCo(CO)_4 \rightarrow RCHO + Co_2(CO)_7 \quad (6)$$

$$RCOCo(CO)_3 + H_xRu_y(CO)_z \rightarrow RCHO + \text{"Co carbonyl"} + \text{"Ru carbonyl"} \quad (7)$$

We have recently investigated the reactions between hexanoyl cobalt tetracarbonyl and several kinds of metal carbonyl hydrides, including $HCo(CO)_4$, $[Et_4N][HRu_3(CO)_{11}]$, and $[PPN][HRu(CO)_4]$ (PPN = bis(triphenylphosphine)iminium, $(Ph_3P)_2N$) as the model reactions. Interestingly, the hydride $[PPN][HRu(CO)_4]$ reacts much more readily with the acyl cobalt complex to form hexenal than does $HCo(CO)_4$. This finding indicates that ruthenium is probably involved in the aldehyde-forming step in the hydroformylation with the cobalt-ruthenium bimetallic catalysts. Details of this reaction is described in section 2-2.

Whyman reported that in the hydroformylation of internal olefins catalyzed by $Co_2(CO)_8$, initial interaction of the olefins with the hydride species $HCo(CO)_4$ might be the rate-determining step.[22] As described above, the synergistic effect for cobalt and ruthenium is most effectively observed if cyclohexene is hydroformylated with the cobalt-ruthenium bimetallic systems. This indicates that ruthenium might also be involved in the olefin insertion step. This is compatible with the fact that a synergistic effect for cobalt and ruthenium also appears in the hydroesterification of olefins which does not involve the hydrogenolysis of an acyl complex as an elementary step.

Recently, Hazel and coworkers have observed that only in the presence of platinum(0) complex does $ReH_7(PR_3)_2$ react with ethylene to give $ReH_3(C_2H_4)_2(PR_3)_2$ (PR_3 = $PPhPr^i_2$ or P(cyclopentyl)$_3$).[23] It seems plausible that platinum-ethylene complex is first formed, and the coordinated ethylene is then transferred to the rhenium hydride *via* a platinum-rhenium mixed metal complex.

References

1 R.M. Laine, *J. Org. Chem.*, 45, 3370(1980).

2 A. Ceriotti, L. Garlaschelli, M.C. Malatesta, D. Strumolo, A. Fumagalli, and S. Martinengo, *J. Mol. Catal.*, 24, 309(1984); *idem*, *ibid.*, 24, 323(1984).

3 M. Hidai, M. Orisaku, M. Ue, Y. Uchida, K. Yasufuku, and H. Yamazaki, *Chem. Lett.*, 143(1981).

4 M. Hidai, M. Orisaku, M. Ue, Y. Koyasu, T. Kodama, and Y. Uchida, *Organometallics*, 2, 292(1983).

5 G. Doyle, *J. Mol. Catal.*, 18, 251(1983).

6 K. Kudo and N. Sugita, *Nippon Kagaku Kaishi*, 462(1982).

7 M. Hidai, Y. Koyasu, M. Yokota, M. Orisaku, and Y. Uchida, *Bull. Chem. Soc. Japan*, 55, 3951(1982).

8 H. Kheradmand, A. Kiennemann, and G. Jenner, *J. Organomet. Chem.*, 251, 339(1982).

9 J.F. Knifton, *J. Chem. Soc., Chem. Commun.*, 729(1983).

10 H. Alper and J.-F. Petrignani, *J. Chem. Soc., Chem. Commun.*, 1154(1983).

11 K.E. Hasam, J.-F. Petrignani, and H. Alper, *J. Mol. Catal.*, **26**, 285(1984).

12 C.R. Eady, P.F. Jackson, B.F.G. Johnson, J. Lewis, M.C. Malatesta, M. MacPartlin, and W.J.H. Nelson, *J. Chem. Soc., Dalton Trans.*, 383(1980).

13 A. Ahmad, S.D. Robinson, and M.F. Uttley, *J. Chem. Soc., Dalton Trans.*, 843(1972).

14 R. Whyman, *J. Organomet. Chem.*, **56**, 339(1973).

15 K. Issleib and H.P. Abicht, *J. Prakt. Chem.*, **312**, 456(1970).

16 Y. Koyasu, *Dissertation*, The University of Tokyo (1986).

17 I. Wender, S. Metlin, S. Ergun, H.W. Sternberg, and H. Greenfield, *J. Am. Chem. Soc.*, **78**, 5401(1956).

18 R.F. Heck and D.S. Breslow, *J. Am. Chem. Soc.*, **83**, 4023(1961).

19 D.S. Breslow and R.F. Heck, *Chem. Ind.(London)*, 467(1960).

20 N.H. Alemdaroglu, J.L.M. Penninger, and E. Oltay, *Monatsh. Chem.*, **107**, 1153(1976).

21 J.P. Collman, J.A. Belmont, and J.I. Brauman, *J. Am. Chem. Soc.*, **105**, 7288(1983).

22 R. Whyman, *J. Organomet. Chem.*, **81**, 97(1974).

23 N.J. Hazel, J.A.K. Howard, and J.L. Spencer, *J. Chem. Soc., Chem. Commun.*, 1663(1984).

2-2

HYDROGENOLYSIS OF ACYLCOBALT CARBONYL WITH METAL CARBONYL HYDRIDES

Summary

Investigation of dinuclear reductive reactions between hexanoylcobalt tetracarbonyl and various ruthenium and cobalt metal carbonyl hydrides showed that [PPN][$HRu(CO)_4$] reacts much faster to form hexanal than $HCo(CO)_4$. Other hydrides such as [Et_4N][$HRu_3(CO)_{11}$], [Ph_4P]$_2$[$H_2Ru_4(CO)_{12}$], $HRuCo_3(CO)_{12}$, and $HFeCo_3(CO)_{12}$ are less reactive than $HCo(CO)_4$ or [PPN][$HRu(CO)_4$].

Introduction

The hydrogenolysis step of a metal acyl intermediates forming an aldehyde is now the subject of controversy in the mechanism for the hydroformylation reaction of olefins (Figure 1)[1]. Recently several papers suggested the dinuclear reductive elimination of aldehydes from metal acyls and metal hydrides in the cobalt[2-4]- and rhodium[5]-catalyzed hydroformylation (see Scheme 1). In section 2-1, we found remarkable synergistic effect for cobalt and ruthenium in the hydroformylation of cyclohexene catalyzed by a mixture of $Co_2(CO)_8$ and $Ru_3(CO)_{12}$. This finding has led us to investigate the reaction of acylcobalt with ruthenium hydrides. Here we describe the kinetic results of the dinuclear reductive elimination of hexanal from an

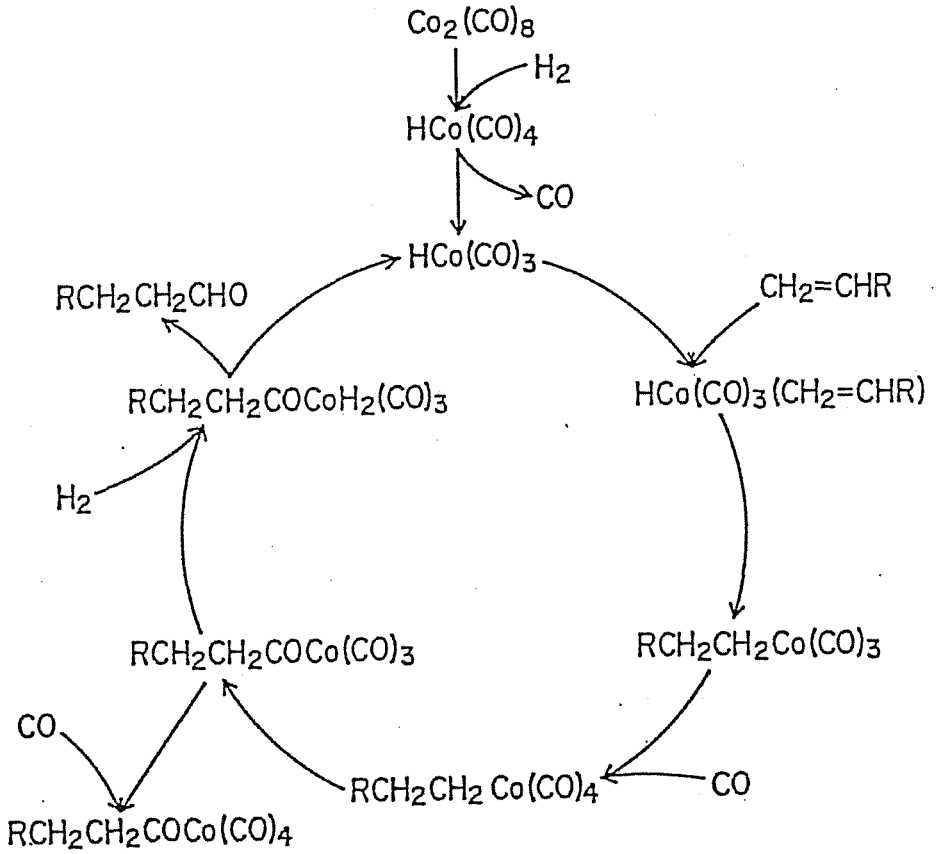

Figure 1. Proposed mechanism for hydroformylation of olefin by $Co_2(CO)_8$.[1]

$$RCOCo(CO)_3 + H_2 \rightarrow RCOCo(H)_2(CO)_3 \rightarrow RCHO + HCo(CO)_3$$
$$RCOCo(CO)_3 + HCo(CO)_4 \rightarrow RCHO + Co_2(CO)_7$$

Scheme 1. Hydrogenolysis of an acyl cobalt carbonyl with a hydrogen and a cobalt carbonyl hydride.

hexanoylcobalt tetracarbonyl and several kinds of metal carbonyl hydrides (eqs 1 and 2).

$$CH_3(CH_2)_4COCo(CO)_4 + HCo(CO)_4 \rightarrow CH_3(CH_2)_4CHO + Co_2(CO)_8 \quad (1)$$

$$CH_3(CH_2)_4COCo(CO)_4 + H_xRu_y(CO)_z \rightarrow CH_3(CH_2)_4CHO + \text{"Co"} + \text{"Ru"} \quad (2)$$

Experimental

$Co_2(CO)_8$ was obtained commercially and used without further purification. CD_2Cl_2 was distilled under CO atmosphere. Metal carbonyl hydrides such as $HCo(CO)_4$,[6] $HRuCo_3(CO)_{12}$,[7] $HFeCo_3(CO)_{12}$,[8] [PPN][$HRu(CO)_4$][9] (PPN = $(Ph_3P)_2N$)), [Et_4N][$HRu_3(CO)_{11}$],[10] [Ph_4P]$_2$[$H_2Ru_4(CO)_{12}$],[11] and $CH_3(CH_2)_4COCo(CO)_4$[12] were prepared according to the literature methods.

All reactions were performed in NMR tubes under CO using dry solvent. NMR spectra were obtained on a JEOL GX-400 spectrometer operating at 399.8 MHz for ^1H. Chemical shifts were recorded downfield from internal reference $Si(CH_3)_4$. The initial rates of the reactions were determined by measuring the intensity of a formyl proton (-C*H*O)of hexanal formed at various temperatures. In a typical experiment, a solution of a metal hydride in dry CD_2Cl_2 was syringed into an NMR tube containing a CD_2Cl_2 solution of the nearly equimolar acylcobalt with naphthalene as an internal standard under CO. The mixture was shaken vigorously for a short time at room temperature and measured the spectra periodically. In the reactions with $HCo(CO)_4$ or [PPN][$HRu(CO)_4$],

the mixtures were prepared at -78 °C and warmed up to 0 °C or 20 °C in the NMR probe just before the measurement.

Results and Discussion

Table 1 summarizes the initial rates of hexanal formation and the rate constants calculated by assuming that the reactions proceed with first-order in each reactant. Typical NMR spectrum is shown in Figure 2. It is noteworthy that the ruthenium hydride [PPN][$HRu(CO)_4$] which shows hydridic character reacts much faster with the acylcobalt to form hexanal than does $HCo(CO)_4$ which is a strong acid.[13] Other hydrides such as [Et_4N][$HRu_3(CO)_{11}$], [Ph_4P]$_2$[$H_2Ru_4(CO)_{12}$], $HRuCo_3(CO)_{12}$, and $HFeCo_3(CO)_{12}$ were less reactive compared with [PPN][$HRu(CO)_4$] and $HCo(CO)_4$. Though the pKa value[8] of $HFeCo_3(CO)_{12}$ is *ca.* 2.0 which is close to that of $HCo(CO)_4$ (*ca.* 1.0),[13] the reactivity of the hydride toward the acylcobalt is extremely lower than that of $HCo(CO)_4$. In the reaction with [PPN][$HRu(CO)_4$], the hydrides $[H_2Ru_4(CO)_{12}]^{2-}$ and $[HRu_3(CO)_{11}]^-$ were formed together with hexanal. The rates of the formation of those hydrides were similar to that of the aldehyde.

The hexanal formation from the reaction between [Et_4N][$HRu_3(CO)_{11}$] and the acylcobalt was accelerated under N_2, indicating that the slow step of the reaction may be the formation of coordinatively unsaturated acylcobalt species (Runs 3 and 4). The reaction gives both hexanal and two kinds of hydrides which exhibit the hydride resonance at δ = -13.9 and

Table 1. Initial Rates of Hexanal Formation and Rate Constants in the Reaction of $CH_3(CH_2)_4COCo(CO)_4$ with Various Metal Carbonyl Hydrides.[a]

Run	Metal carbonyl hydride (H-M)	[H-M] (x 10^2 M)	[$RCOCo(CO)_4$] (x 10^2 M)	Rate (x 10^{-7} Ms^{-1})	k[b] (x $10^{-4}M^{-1}s^{-1}$)
1[c]	$HCo(CO)_4$	3.79	1.85	150	210
2	[PPN][$HRu(CO)_4$]	2.07	1.87	300	780
3	[Et_4N][$HRu_3(CO)_{11}$]	2.81	3.03	1.4	1.6
4[d]	[Et_4N][$HRu_3(CO)_{11}$]	3.48	2.71	2.9	3.1
5	[Ph_4P]$_2$[$H_2Ru_4(CO)_{12}$]	2.56	2.68	2.9	4.2
6	$HRuCo_3(CO)_{12}$	1.49	1.60	0.18	0.74
7	$HFeCo_3(CO)_{12}$	1.72	2.20	0.29	0.78
8[e]	$HCo(CO)_4$	2.11	2.08	1.4	3.1
9[e]	[PPN][$HRu(CO)_4$]	2.55	2.49	58	92

[a] Reactions were carried out in dry CD_2Cl_2 under CO (1 atm). Reaction temperatures were between 19 and 21 °C.
[b] k = Rate/([$RCOCo(CO)_4$]x[H-M]).
[c] The NMR tube was sealed at -196 °C *in vacuo*.
[d] Under N_2, 1 atm.
[e] Reaction temp., 0 °C.

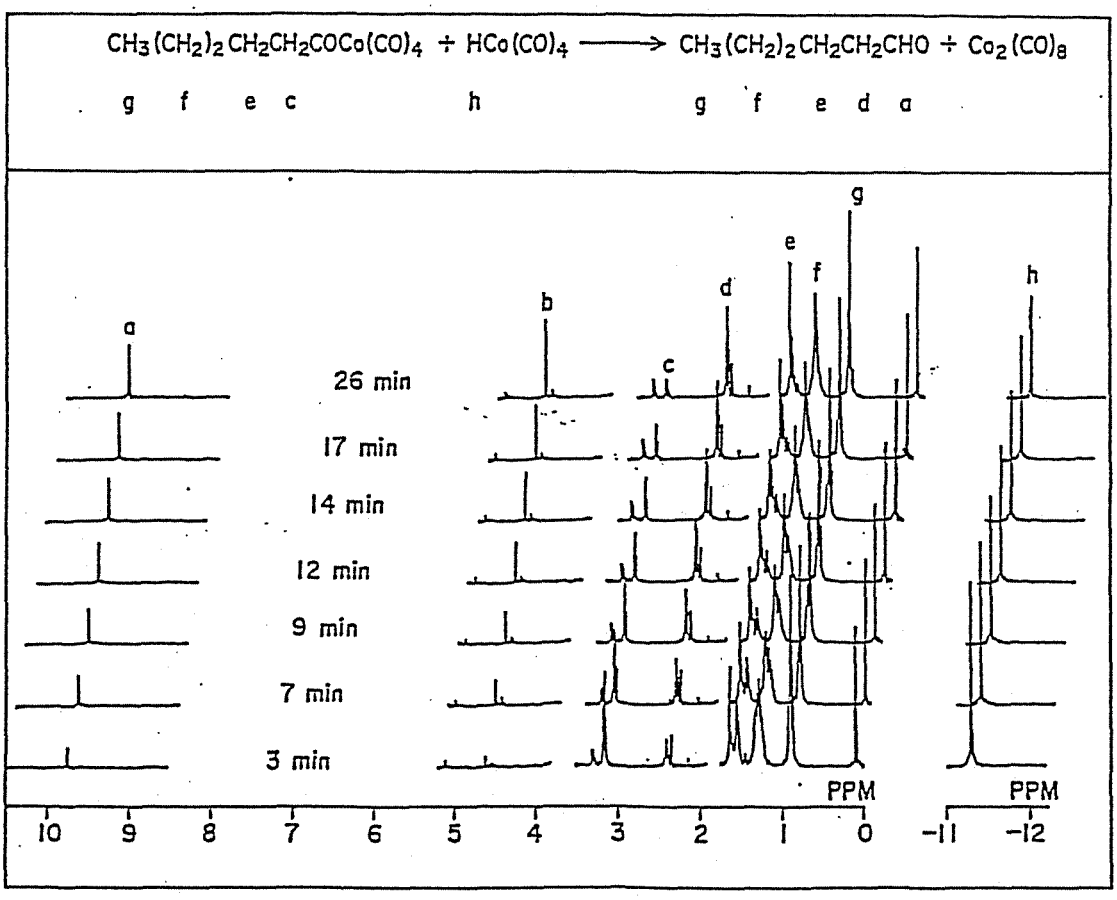

Figure 2. Stacked plot of ^1H NMR spectra during the reaction of hexanoylcobalt tetracarbonyl with $HCo(CO)_4$ at 20 °C (Table 1, Run 1). The peak b is uncharacterized.

-18.8, respectively, in the ^1H NMR spectra. When the reaction is carried out under CO, $Ru_3(CO)_{12}$ and a metal hydride which shows the hydride resonance at δ = -13.9 are formed together with hexanal. The reaction with $[Ph_4P]_2[H_2Ru_4(CO)_{12}]$ under CO gives $[HRu_3(CO)_{11}]^-$ and several metal carbonyl hydrides in addition to hexanal. However, in these reactions, the rates of the formation of the metal carbonyl hydrides were slower than those of the aldehyde.

The above results indicate that the remarkable rate increase in the hydroformylation with cobalt-ruthenium bimetallic systems is probably caused by dinuclear reductive elimination of aldehydes from acylcobalt carbonyls and ruthenium hydrides such as $[HRu(CO)_4]^-$.

IR spectral change was studied on the reaction solution after the hydroformylation of cyclohexene by $Co_2(CO)_8$ or $Co_2(CO)_8+Ru_3(CO)_{12}$ (1:1) catalysts.[14,15] The hydroformylation reaction was carried out for 9 min at 110 °C with a pressurized $CO+H_2$ gas (1:1, 80 atm at room temp.) in $C_{14}H_{30}$ solvent. After cooled rapidly, the reaction solution was subjected to IR analysis in an IR cell with NaCl windows at room temperature under 1 atm of CO, and the concentrations of metal carbonyls were estimated with the peak intensities. The conversions of $Co_2(CO)_8$ to $HCo(CO)_4$ were 19 % and 48 % in the $Co_2(CO)_8$ and the $Co_2(CO)_8+Ru_3(CO)_{12}$ catalysts, respectively. Notably, the formation of $HCo(CO)_4$ was promoted in the presence of $Ru_3(CO)_{12}$. Thus it is suggested that ruthenium not only reacts with an acylcobalt carbonyl to produce aldehyde by dinuclear reductive

elimination, but promotes the formation of an active precursor $HCo(CO)_4$.

References

1 R.F. Heck and D.S. Breslow, *J. Am. Chem. Soc.*, **83**, 4023(1961).

2 N.H. Alemdaroglu, J.L.M. Penninger, and E. Oltay, *Monatsh. Chem.*, **107**, 1153(1976).

3 F. Ungvary and L. Marko, *Organometallics*, **2**, 1608(1983).

4 J. Azran and M. Orchin, *Organometallics*, **3**, 197(1984).

5 J.P. Collman, J.A. Belmont, and J.I. Brauman, *J. Am. Chem. Soc.*, **105**, 7288(1983).

6 H.W. Sternberg, I. Wender, R.A. Friedel, and M. Orchin, *J. Am. Chem. Soc.*, **75**, 2717(1953).

7 M. Hidai, M. Orisaku, M. Ue, Y. Koyasu, T. Kodama, and Y. Uchida, *Organometallics*, **2**, 292(1983).

8 P. Chini, L. Colli, and M. Peraldo, *Gazz. Chim. Ital.*, **90**, 1005(1960).

9 H.W. Walker and P.C. Ford, *J. Organomet. Chem.*, **214**, C43(1981).

10 B.F.G. Johnson, J. Lewis, P.R. Raithby, and G. Suss, *J. Chem. Soc., Dalton Trans.*, 1356(1979).

11 K.E. Inkrott and S.G. Shore, *J. Am. Chem. Soc.*, **100**, 3954(1978).

12 J. Azran and M. Orchin, *Organometallics*, **3**, 197(1984).

13 W. Hieber and W. Hubel, *Z. Elektrochem.*, **57**, 235(1953).

14 Y. Koyasu, *Dissertation*, The University of Tokyo, 1986.

15 H. Matsuzaka, A. Fukuoka, Y. Koyasu, M. Ue, M. Orisaku, and M. Hidai, *Nippon Kagaku Kaishi*, 705(1988).

CHAPTER 3

SELECTIVE OLEFIN HYDROFORMYLATION ON CARBON-SUPPORTED RUTHENIUM AND RUTHENIUM-COBALT CARBONYL CLUSTER-DERIVED CATALYSTS

CHAPTER 3

SELECTIVE OLEFIN HYDROFORMYLATION ON CARBON-SUPPORTED RUTHENIUM AND RUTHENIUM-COBALT CARBONYL CLUSTER-DERIVED CATALYSTS

Summary

High activity and selectivity for direct alcohol production were achieved in hydroformylation of ethylene and propylene on carbon-supported RuCo bimetallic carbonyl cluster-derived catalysts at an atmospheric pressure. The selectivity toward normal-isomers of the C_4-alcohols and aldehydes was effectively improved on the $RuCo_3$ cluster/carbon catalyst in propylene hydroformylation.

Introduction

One promising method of obtaining well-defined metal catalysts is employing organometallic compounds as the precursors. Such an approach may provide a molecular-level elucidation of the elementary steps of heterogeneous catalysis in terms of surface organometallic chemistry.[1] Metal clusters have been paid much attention as the starting organometallic compounds because they can give highly-dispersed metal ensembles with uniform metal composition, and supported cluster-derived catalysts provide differences and advantages over the conventional ill-defined metal catalysts prepared by

co-impregnation or ion-exchange techniques of metal salts.[2] In fact, recent works[3,4] revealed that bimetallic cluster-derived catalysts exhibited a promotion of the catalytic activity and selectivity in some catalytic reactions, *e.g.*, syngas conversion to oxygenates and hydrocarbons, which are markedly different from those of the catalysts of constituent metals. Catalytic, electronic, and structural properties of the bimetallic catalysts are greatly associated with the compositions and geometric situation of bimetallic species generated on the surface of supports.

In homogeneous olefin hydroformylation reactions, ruthenium carbonyls exhibit a poor activity even under high pressure conditions compared with cobalt or rhodium carbonyls, but the competitive hydrogenation of olefin to paraffin preferentially occurs.[5] We discovered that $Co_2(CO)_8$+$Ru_3(CO)_{12}$ mixture showed the synergistic rate enhancement in homogeneous hydroformylation, as described in CHAPTER 2. We report here that carbon-supported Ru and RuCo bimetallic catalysts derived from the carbonyl clusters gave high catalytic activity to selectively produce normal alcohols in the vapor-phase hydroformylation of ethylene and propylene at an atmospheric pressure.

Experimental

The precursor complexes such as $[NEt_4][HRu_3(CO)_{11}]$,[7] $[NEt_4][Ru_3Co(CO)_{13}]$,[8] $H_3Ru_3Co(CO)_{12}$,[8] and $HRuCo_3(CO)_{12}$[9] were synthesized according to published procedures. $Co_4(CO)_{12}$ was

purchased from Strem Chem. Inc. and purified by recrystallization from pentane. An amorphous carbon (Wako Pure Chem. Ind. Ltd., surface area = 800 m^2/g, 12-20 mesh) was treated at 300 °C under vacuum for 2 h. Each carbonyl cluster was impregnated from the organic solutions under N_2 onto the amorphous carbon (1 wt% total metal loading). The organic solvent was carefully removed by vacuum distillation, followed with H_2-reduction at 200 °C (see Figure 1).

The hydroformylation reactions were carried out using an open flow-mode reactor. A mixture gas of C_2H_4 (or C_3H_6), CO and H_2 (1:1:1 molar ratio at a total pressure of 1 atm) was passed through the catalyst bed (3-4 g of catalyst) at a flow rate of 60 ml/min. The oxygenated products such as aldehydes and alcohols were collected in a water condenser (50 ml of H_2O) by bubbling the effluent gas. The analysis of C_2H_4 and C_2H_6 was performed by a Shimadzu GC-8AIT gas chromatograph with a thermal conductivity detector using a 4 mmϕ x 4 m Porapak Q (60-80 mesh) column at 70 °C. C_3H_6 and C_3H_8 were separated on a 4 mmϕ x 4 m *N,N*-dimethylformamide/Al_2O_3 (DMF 38 %, 60-80 mesh) column at room temperature. The concentration of gaseous products in the off-gas was calibrated with external standards by using a 5 ml of gas sampler. The analysis of the aldehydes and alcohols dissolved in the water trap was conducted by a Shimadzu GC-8APF gas chromatograph with a flame ionization detector. Propanal and 1-propanol, which were the products of hydroformylation of ethylene, were separated on a 4 mmϕ x 4 m Chromosorb 101 (60-80 mesh) column at 150 °C. The products of hydroformylation of

(a)

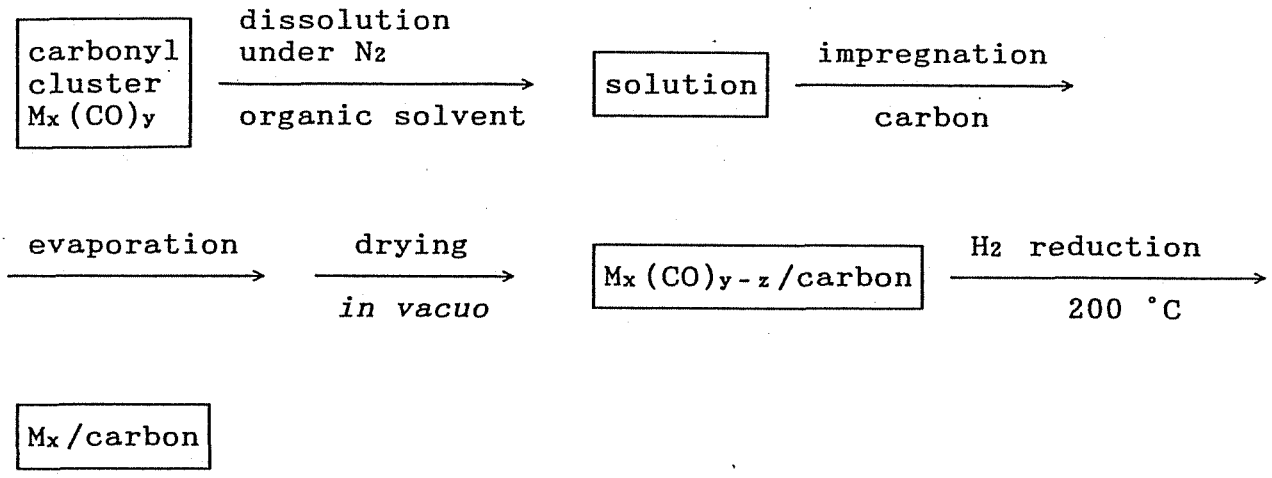

(b)

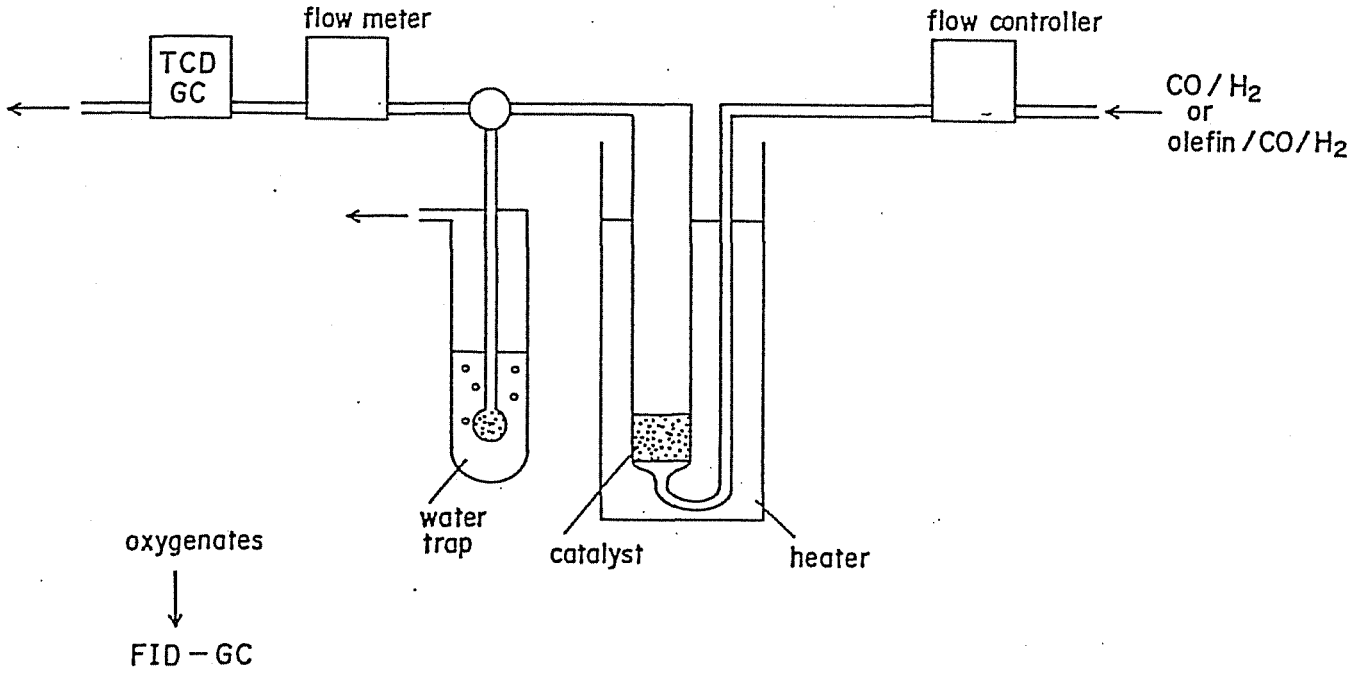

Figure 1.
(a) Procedures for catalyst preparation;
(b) A flow-mode reactor and a GLC system.

propylene such as butanal, 2-methylpropanal, 1-butanol, and 2-methylpropanol were separated on the same column at 155 °C. Ethanol was added as an internal standard to calibrate the concentration of the aldehydes and alcohols. In each gas chromatography, the amounts of the products were calculated with an integrator (Shimadzu Chromatopac CR-3A).

Results and Discussion

The results of hydroformylation of ethylene and propylene at atmospheric pressure in vapor-phase were presented in Table 1 and Table 2. It is of great interest that carbon-supported $[NEt_4][HRu_3(CO)_{11}]$-derived catalyst gave higher activity than did $Co_4(CO)_{12}$-derived one. Further hydrogenation of the aldehyde to the alcohol did not proceed on the Ru_3 cluster-derived one. The selectivities toward oxygenates (aldehydes + alcohols) by Ru or RuCo carbonyl cluster-derived catalysts were *ca.* 10 % in ethylene hydroformylation and *ca.* 5 % in propylene one. On the catalyst derived from $Co_4(CO)_{12}$, the rate of a simple hydrogenation as well as a hydroformylation reaction comparatively much lower than that by Ru carbonyl cluster-derived catalyst. These results suggest that ruthenium carbonyl hydrides as active species for olefin hydroformylation are formed on the carbon support under the reaction conditions.

The rates of hydroformylation (aldehyde + alcohol) per Ru atom are markedly enhanced with increasing the Co atoms in the precursor RuCo bimetallic clusters, relative to the rates by the

Table 1. Hydroformylation of Ethylene on Carbon-supported Ru, RuCo, and Co Carbonyl Cluster-derived Catalysts.[a]

precursor/carbon	at ratio Co/Ru	specific rate of formation,[b] min^{-1}		selectivity, mol %	
		C_2H_6	EtCHO + n-PrOH	oxygenates[c]	alcohol[d]
$[Et_4N][HRu_3(CO)_{11}]$	0	0.06(1)	0.007(1)	11	1
$[Et_4N][Ru_3Co(CO)_{13}]$	0.33	0.24(3.9)	0.033(4.5)	12	19
$H_3Ru_3Co(CO)_{12}$	0.33	0.27(4.4)	0.037(5.0)	12	10
$HRuCo_3(CO)_{12}$	3.0	1.1(18)	0.13(17)	10	47
$Co_4(CO)_{12}$	-	0.009	0.0008	8	0

[a] Reaction conditions: total metal loading 1 wt%, reaction temperature 172 ± 1 °C, flow rate $C_2H_4+CO+H_2$ = 20+20+20 ml/min, total pressure 1 atm. Values in parentheses are rates relative to $[Et_4N][HRu_3(CO)_{11}]$.
[b] $mmol/mmol_{Ru}/min$.
[c] (EtCHO + n-PrOH)/(C_2H_6 + EtCHO + n-PrOH) x 100.
[d] n-PrOH/(EtCHO + n-PrOH) x 100.

Table 2. Hydroformylation of Propylene on Carbon-supported Ru, RuCo, and Co Carbonyl Cluster-derived Catalysts.[a]

precursor/carbon	at ratio Co/Ru	specific rate of formation,[b] min^{-1}		selectivity, mol %		
		C_3H_8	n,i-PrCHO + n,i-BuOH	oxygenates[c]	alcohol[d]	n-isomer[e]
$[Et_4N][HRu_3(CO)_{11}]$	0	0.040(1)	0.0017(1)	4	1	80
$[Et_4N][Ru_3Co(CO)_{13}]$	0.33	0.15 (3.8)	0.0029(1.7)	2	0	74
$H_3Ru_3Co(CO)_{12}$	0.33	0.17 (4.3)	0.0029(1.7)	6	1	81
$HRuCo_3(CO)_{12}$	3.0	0.55(14)	0.027(16)	5	76	96
$Co_4(CO)_{12}$	-	0.006	0.0004	1	2	81

[a] Reaction conditions: total metal loading 1 wt%, reaction temperature 194 ± 1 °C, flow rate $C_3H_6+CO+H_2$ = 20+20+20 ml/min, total pressure 1 atm. Values in parentheses are rates relative to $[Et_4N][HRu_3(CO)_{11}]$.

[b] $mmol/mmol_{Ru}/min$.

[c] (n,i-PrCHO + n,i-BuOH)/(C_3H_8 + n,i-PrCHO + n,i-BuOH) x 100.

[d] (n-PrCHO + n-BuOH)/(n,i-PrCHO + n,i-BuOH) x 100.

catalyst prepared from $[NEt_4][HRu_3(CO)_{11}]$ or $Co_4(CO)_{12}$ alone. The catalyst prepared from $HRuCo_3(CO)_{12}$ provided the rate sixteen times higher than that by $[NEt_4][HRu_3(CO)_{11}]$ in propylene hydroformylation. The selectivity toward alcohols on the RuCo carbonyl cluster-derived catalysts was much higher than that on $[NEt_4][HRu_3(CO)_{11}]$ or $Co_4(CO)_{12}$-derived catalyst. Additionally, the selectivities toward normal alcohol were substantially improved by increasing Co contents in the precursor RuCo bimetallic clusters. In propylene hydroformylation, the highest selectivity toward normal alcohol (1-butanol) was achieved by $HRuCo_3(CO)_{12}$-derived catalyst, *i.e.*, the selectivity toward C_4-alcohol formation was 76% and the selectivity toward normal-isomers (butanal + 1-butanol) was 96%, although the $[NEt_4][HRu_3(CO)_{11}]$-derived catalyst gave 80% of normal-isomer selectivity. The results suggest that Co atoms are associated with the promotion for normal alcohol formation in the hydroformylation reaction catalyzed by Ru carbonyls.

Such higher rates and higher selectivity to normal alcohol production on the Co-rich RuCo bimetallic cluster-derived catalysts cannot be explained simply by the additional formation of aldehyde and alcohol from the individual Ru and Co carbonyl clusters without their cooperativity on carbon. It was previously reported that Co atoms in ZnO-supported RhCo carbonyl clusters such as $Rh_2Co_2(CO)_{12}$ and $RhCo_3(CO)_{12}$ markedly enhanced normal-isomer selectivity in propylene hydroformylation.[3] Co atoms in the RhCo carbonyl clusters are proposed to play a role as a ligand to stabilize n-alkyl intermediates and to accelerate

a migratory CO insertion into the alkyl-metal bond. Furthermore, they act effectively as a inert breaker to divide the Rh ensemble into an isolated Rh atom. Accordingly, in the olefin hydroformylation on RuCo bimetallic cluster-derived catalysts, the CO insertion may be accelerated by the two-site interaction on RuCo sites, *i.e.*, an oxygen atom of coordinated CO on Ru bound with the positively charged Co atom which has lower ionization potential than Ru, as shown in the following proposed model of an active site (Figure 2). In fact, Shriver *et al.* reported that Lewis acids such as $AlBr_3$ and BF_3 could greatly enhance the rate of the migratory CO insertion on metal carbonyls due to the adduct formation between the metal carbonyls and the Lewis acids.[10]

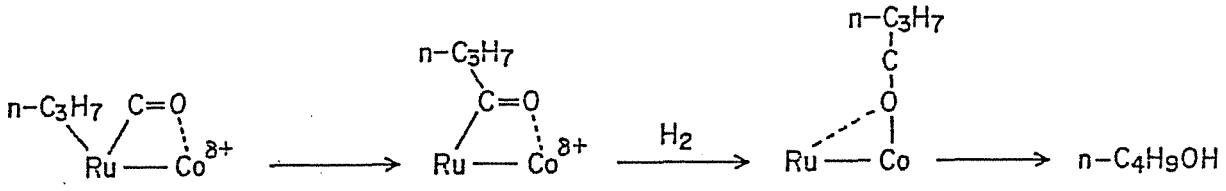

Figure 2.

References

1 Y.I. Yermakov and V. Likholobov eds., *"Homogeneous and Heterogeneous Catalysis"*, VNU Science Press, Utrecht, 1986.

2 M. Ichikawa, in *"Tailored Metal Catalysts"*, Y.Iwasawa ed., D. Reidel Pub., Dordrecht, 1986, p. 183 and references cited therein; T. Okuhara, K. Kobayashi, T. Kimura, M. Misono, and Y. Yoneda, *J. Chem. Soc., Chem. Commun.*, 1115(11981); Y. Iwasawa, Y. Yamada, S. Ogasawara, Y. Sato, and H. Kuroda, *Chem. Lett.*, 621(1983); T. Tatsumi, H. Odashima, and H. Tominaga, *J. Chem. Soc., Chem. Commun.*, 207(1985).

3 M. Ichikawa, *J. Catal.*, **56**, 127; **59**, 67(1979); *CHEMTECH*, 674(1982).

4 V.K. Kuznetsov, A.F. Danilyuk, I.E. Kolosova, and Y.I. Yermakov, *React. Kinet. Catal. Lett.*, **21**, 249(1982); A. Choplin, M. Leconte, and J.-M. Basset, *J. Mol. Catal.*, **21**, 389(1983); J.R. Budge, J.P. Scott, and B.C. Gates, *J. Chem. Commun., Chem. Commun.*, 342(1983); M. Kaminsky, K.J. Yoon, G.L. Geoffroy, and M.A. Vannice, *J. Catal.*, **91**, 338(1985); Y. Iwasawa and M. Yamada, *J. Chem. Soc., Chem. Commun.*, 675(1985).

5 P. Pino, F. Piacenti, and M. Bianchi, *"Organic Syntheses via Metal Carbonyls"*, Vol. 2, I. Wender and P. Pino eds., Wiley, New York, 1977, Vol. 2, p. 43; R.L. Pruett, *Adv. Organomet. Chem.*, **17**, 1(1979).

6 M. Hidai, A. Fukuoka, Y. Koyasu, and Y. Uchida, *J. Chem. Soc., Chem. Commun.*, 516(1984); *J. Mol. Catal.*, **35**, 29(1986).

7 B.F.G. Johnson, J. Lewis, P.R. Raithby, and G. Süss, *J. Chem. Soc., Dalton Trans.*, 1356(1979).

8 P.C. Steinhardt, W.L. Gladfelter, A.D. Harley, J.R. Fox, and G.L. Geoffroy, *Inorg. Chem.*, **19**, 332(1980); W.L. Gladfelter, G.L. Geoffroy, and J.C. Calabrese, *ibid.*, **19**, 2569(1980).

9 M. Hidai, M. Orisaku, M. Ue, Y. Koyasu, T. Kodama, and Y. Uchida, *Organometallics*, **2**, 292(1983).

10 S.B. Butts, S.H. Strauss, E.M. Holt, R.E. Stimson, N.W. Alcock, and D.F. Shriver, *J. Am. Chem. Soc.*, **102**, 5093(1980); C.P. Horwitz and D.F. Shriver, *Adv. Organomet. Chem.*, **23**, 219(1984); F. Correa, R. Nakamura, R.E. Stimson, R.L. Burwell, Jr., and D.F. Shriver, *J. Am. Chem. Soc.*, **102**, 5114 (1980).

CHAPTER 4

TWO-SITE ACTIVATION OF CO ON BIMETALLIC SITES IN HETEROGENEOUS CATALYSIS

CHAPTER 4

4-1

BIMETALLIC PROMOTION OF ALCOHOL PRODUCTION IN CO HYDROGENATION AND OLEFIN HYDROFORMYLATION ON RHODIUM-IRON, PLATINUM-IRON, PALLADIUM-IRON, AND IRIDIUM-IRON BIMETALLIC CLUSTER-DERIVED CATALYSTS.

Summary

Iron containing Fe_2Rh_4 cluster-derived catalysts showed high activities and selectivities for the formation of ethanol and methanol in CO hydrogenation. Fe_3Pt_3, Fe_6Pd_6, and $FeIr_4$ cluster catalysts gave methanol in high selectivity, while Fe-rich Fe_4Pt and Fe_4Pd were poor-selective catalysts. The RhFe cluster catalysts showed improved activity in hydroformylation of olefins; C_4-alcohols were substantially obtained in hydroformylation of propylene. Mössbauer and EXAFS studies on the Fe_2Rh_4/SiO_2 catalyst suggest that highly dispersed RhFe bimetallic particles are located on the SiO_2 surface, where Fe atoms exist preferentially in the state of Fe^{3+} even after H_2 reduction. FTIR spectrum of CO chemisorption on Fe_2Rh_4/SiO_2 exhibited a low-frequency band possibly due to the C- and O-bonded CO on Rh-Fe^{3+} sites. Bimetallic promotion of alcohol production in CO hydrogenation and olefin hydroformylation is proposed to originate from the two-site interaction of Rh-Fe^{3+} (or Pt-Fe^{3+}, Pd-Fe^{3+}, Ir-Fe^{3+}) sites with CO to enhance migratory CO insertion.

Introduction

The use of metal clusters as catalyst precursors is an important aspect of homogeneous and heterogeneous catalysis.[1-8] The chemical modification of solid surfaces by using clusters has been recently investigated for the sophisticated control of metal particle sizes as small as 10 Å and well-defined metal compositions. The bimetallic clusters offer prospects of synergistic effect for the two metal components in many useful catalytic reactions. Since Sinfelt *et al.* revealed by using EXAFS that alloys were formed in the reforming catalysts such as Pt-Ir and Ru-Cu on SiO_2 or Al_2O_3,[9] bimetallic clusters grafted on solid surfaces have attracted much attention, because they may provide the advantage of obtaining highly dispersed bimetallic particles which we can manage at the molecular-level.[10,11] It has been reported that the bimetallic cluster-derived catalysts are active in the reactions such as skeletal rearrangement of hydrocarbons,[12-15] hydrogenation of carbon-carbon multiple bonds,[15,16] CO hydrogenation[2,13,14,17-22], hydroformylation olefins,[23-25] and reductive carbonylation of nitro compounds.[26]

In CO hydrogenation on salt-derived Rh/SiO_2 catalysts, some additive metal ions such as Mn, Ti, Zr, and Fe promote the production of oxygenates including methanol, ethanol, and acetic acid.[27] In particular, Fe promotion in the salt-derived $Rh\text{-}Fe/SiO_2$,[28,29] $Pd\text{-}Fe/SiO_2$,[30] and $Ir\text{-}Fe/SiO_2$[31,32] catalysts is remarkable for enhancing alcohol production. EXAFS,[33] Mössbauer,[34,35] XPS,[36] and FTIR[37] studies on the $Rh\text{-}Fe/SiO_2$

catalysts suggested that this promotion was associated with Rh-Fe bimetallic sites formed on SiO_2 support.

Accordingly, as tailored models for the promoted Rh, Pt, Pd, and Ir, we have prepared RhFe, PtFe, PdFe, and IrFe bimetallic catalysts from bimetallic carbonyl clusters deposited on SiO_2. A CO hydrogenation reaction was conducted on the RhFe, PtFe, PdFe, and IrFe bimetallic catalysts. Hydroformylation reactions of ethylene and propylene have been carried out as a diagnostic reaction for migratory CO insertion which is an elementary step in CO hydrogenation. The structural properties of the bimetallic cluster-derived catalysts have been studied by means of Mössbauer, EXAFS, and FTIR spectroscopies. Here it is demonstrated that the bimetallic sites derived from carbonyl clusters are highly active for migratory CO insertion, and that they provide high activity and selectivity toward alcohols.

The origin of Fe promotion is discussed in terms of the two-site interaction of the bimetallic sites with CO.

Experimental

Catalysts

Carbonyl clusters $Rh_4(CO)_{12}$,[38] $[N(CH_3)_3(CH_2C_6H_5)]_2[Fe_3(CO)_{11}]$,[39] $[N(CH_3)_3(CH_2C_6H_5)][FeRh_5(CO)_{16}]$,[40] $[N(CH_3)_4]_2[FeRh_4(CO)_{15}]$,[40] $[N(CH_3)_3(CH_2C_6H_5)]_2[Fe_2Rh_4(CO)_{16}]$,[40] $Fe_3Rh_2(CO)_{14}C$,[41] $[N(C_2H_5)_4]_2[Pt_{12}(CO)_{24}]$,[42] $[N(CH_3)_3(CH_2C_6H_5)]_2[Fe_3Pt_3(CO)_{15}]$,[43] $[N(CH_3)_3(CH_2C_6H_5)]_2[Fe_4Pt(CO)_{16}]$,[44] $[N(CH_3)_3(CH_2C_6H_5)]_3[Fe_6Pd_6(CO)_{24}H]$,[44] $[N(CH_3)_3(CH_2C_6H_5)]_2$

$[Fe_4Pd(CO)_{16}]$,[44] $[N(CH_3)_3(CH_2C_6H_5)][HIr_4(CO)_{11}]$,[45] and $[N(CH_3)_3(CH_2C_6H_5)]_2[FeIr_4(CO)_{15}]$[46] were synthesized according to literature methods (see Figure 1). SiO_2 (Davison no. 57, 10-20 mesh, surface area = 280 m^2/g) was treated under vacuum (10^{-4} Torr) at 320 °C for 2 h, and was impregnated with each carbonyl cluster from a suitable organic solution under N_2 or CO atmosphere (Figure 2). After removal of the solvent *in vacuo* at room temperature, the impregnated catalysts were oxidized either by air at room temperature overnight or by O_2 at 150 °C for 2 h, followed with the reduction in flowing H_2 (1 atm, 50 ml/min) at the programmed temperature from 20 to 400 °C (Figure 2d). The total metal loadings of the catalysts were 2 wt% or 0.5 wt%. We shall use the notation $M_xM'_y/SiO_2$; the abbreviation refers only to the metal composition of the precursor cluster $M_xM'_y(CO)_z$ impregnated on SiO_2. Salt-derived Rh/SiO_2, $Rh-Fe/SiO_2$, Pt/SiO_2, Pd/SiO_2, $Pd-Fe/SiO_2$, and $Ir-Fe/SiO_2$ catalysts were prepared by the impregnation of SiO_2 with the ethanol solution of $RhCl_3 \cdot 3H_2O$, $RhCl_3 \cdot 3H_2O + FeCl_3$, $H_2PtCl_6 \cdot 6H_2O$, $PdCl_2$, $PdCl_2 + FeCl_3$, and $IrCl_4 \cdot H_2O + FeCl_3$. After removal of ethanol, they were reduced in flowing H_2 at 400 °C for 2 h and used as catalysts.

CO Hydrogenation Reactions

A CO hydrogenation reaction was conducted at 250 °C with an open flow-mode stainless-steel reactor (inner diameter = 14 mm, 240 mm long tubing) where 2.0 g of the catalyst (total metal loading 2 wt%) was charged. A gas mixture of CO and H_2 ($CO:H_2$ = 1:2 molar ratio, 5 kg/cm^2) was introduced into the reactor at a

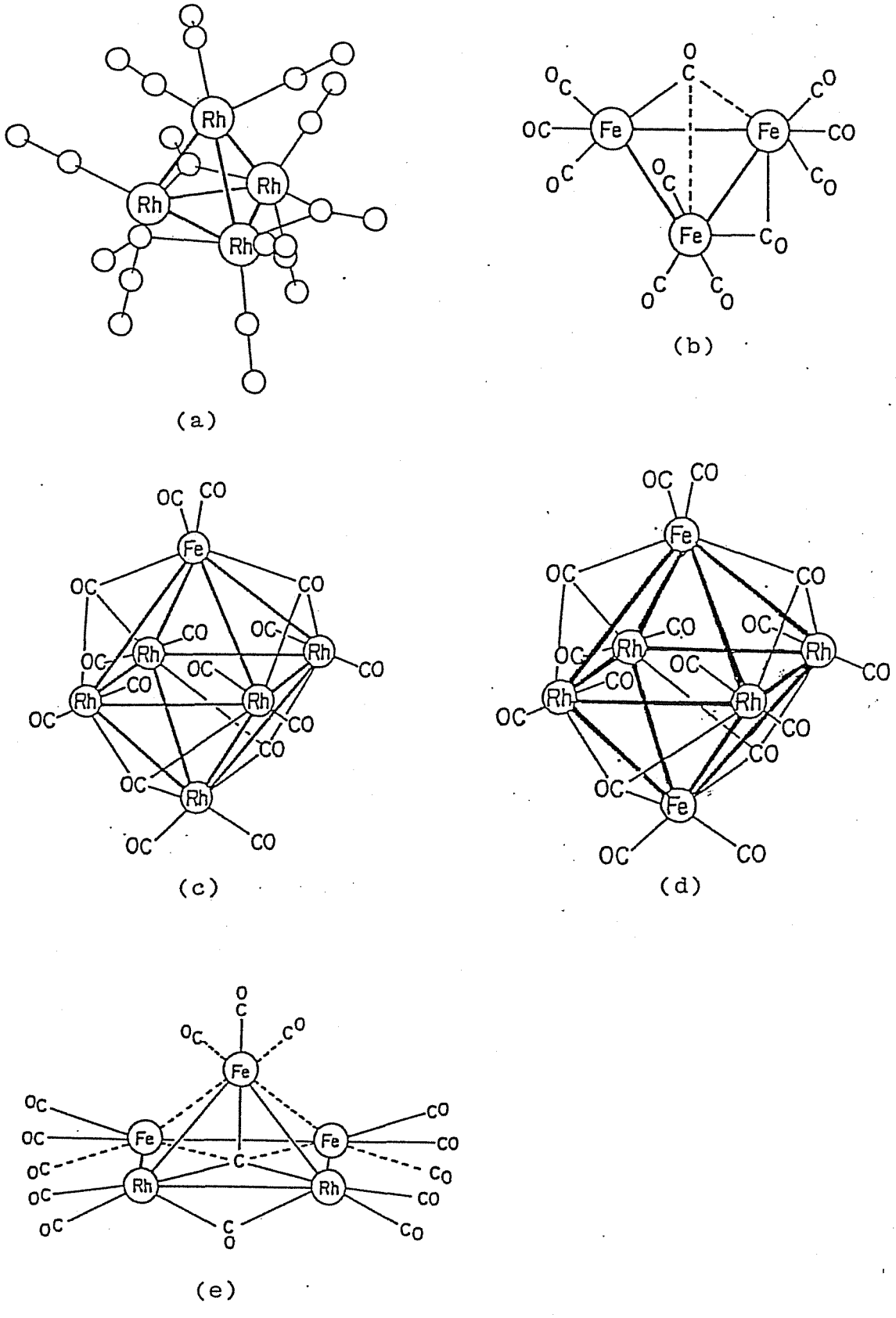

Figure 1. Rh, Fe, and RhFe carbonyl clusters: (a) $Rh_4(CO)_{12}$, (b) $[Fe_3(CO)_{11}]^{2-}$, (c) $[FeRh_5(CO)_{16}]^-$, (d) $[Fe_2Rh_4(CO)_{16}]^{2-}$, and (e) $Fe_3Rh_2C(CO)_{14}$.

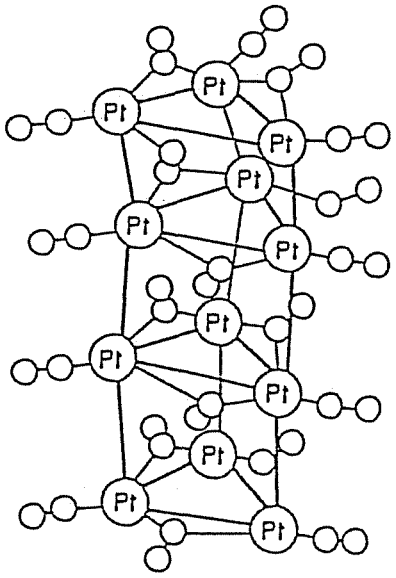

(f)

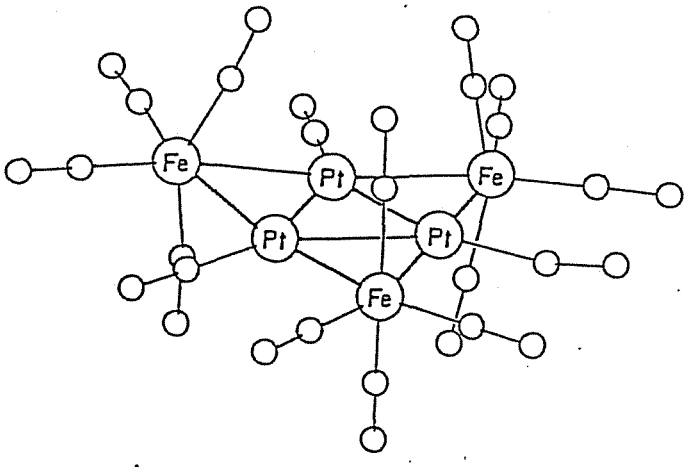

(g)

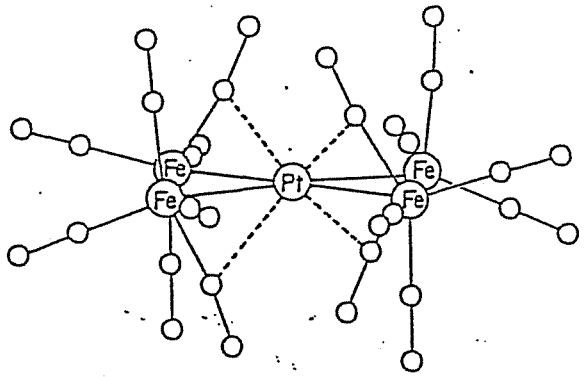

(h)

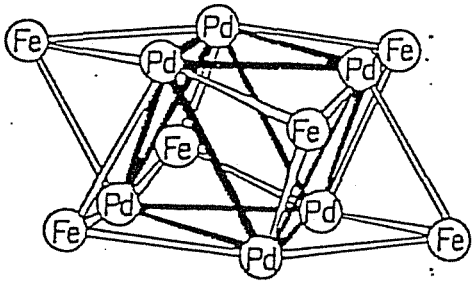

(i)

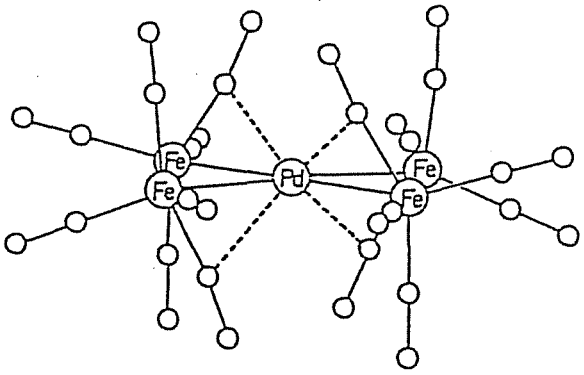

(j)

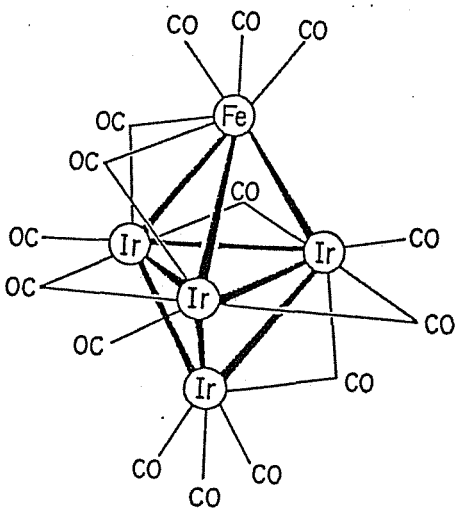

(k)

Figure 1 (continued). Pt, PtFe, PdFe, and IrFe carbonyl clusters: (f) $[Pt_{12}(CO)_{24}]^{2-}$, (g) $[Fe_3Pt_3(CO)_{15}]^{2-}$, (h) $[Fe_4Pt(CO)_{16}]^{2-}$, (i) $[Fe_6Pd_6(CO)_{24}H]^{3-}$, (j) $[Fe_4Pd(CO)_{16}]^{2-}$, and (k) $[FeIr_4(CO)_{15}]^{2-}$.

(a)

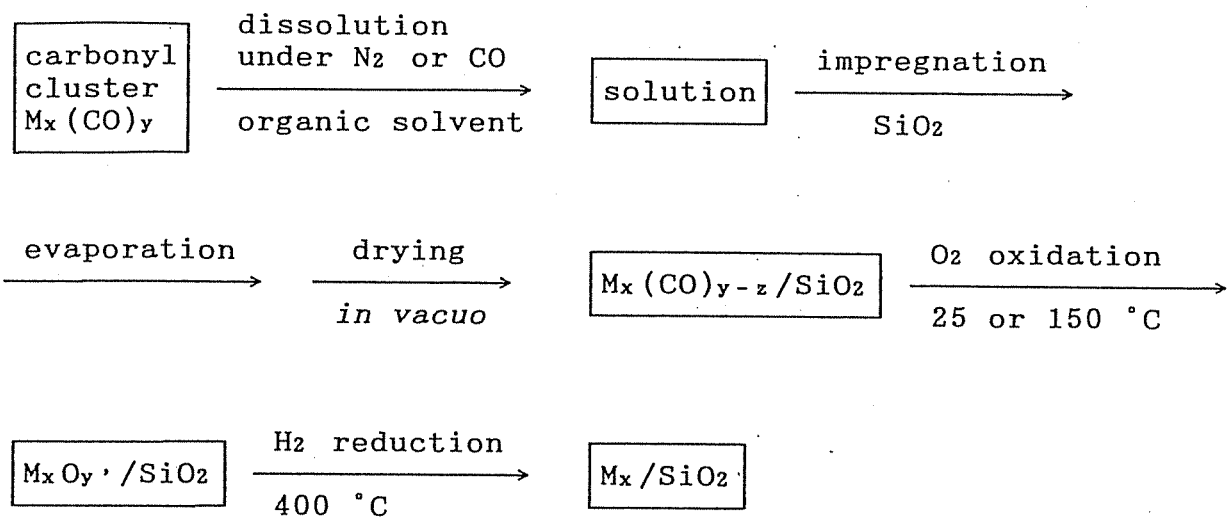

(b)

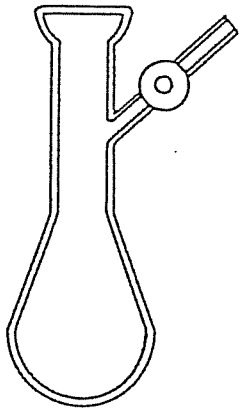

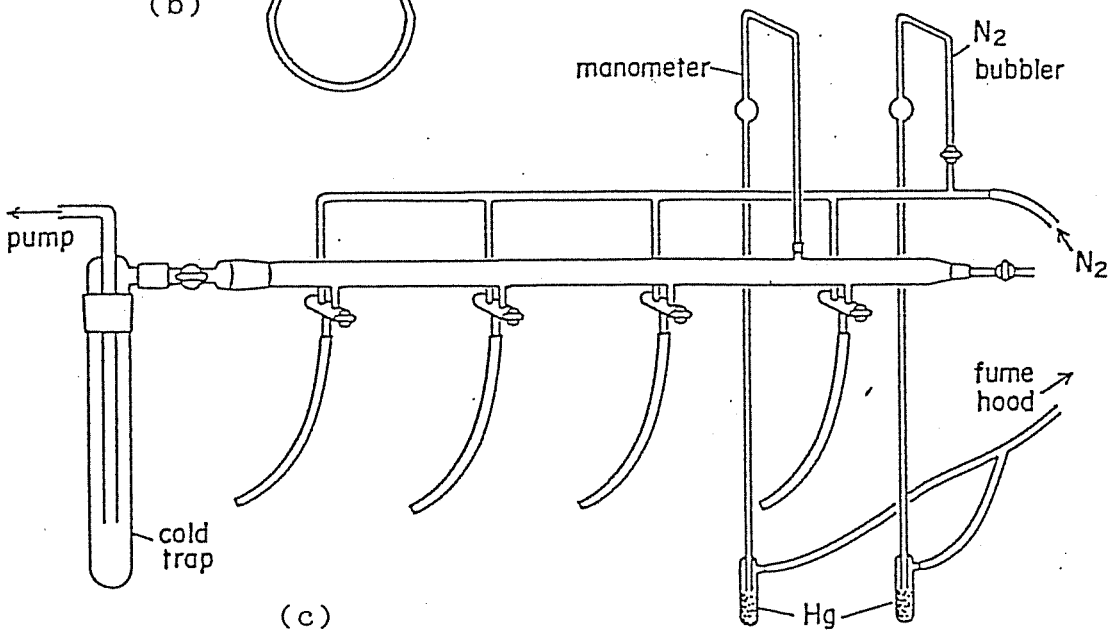

(c)

Figure 2.
(a) Procedures for catalyst preparation;
(b) A modern Schlenk tube with grease-free joint and valve, used in the catalyst preparation.
(c) A vacuum and N_2 line for Schlenk techniques;

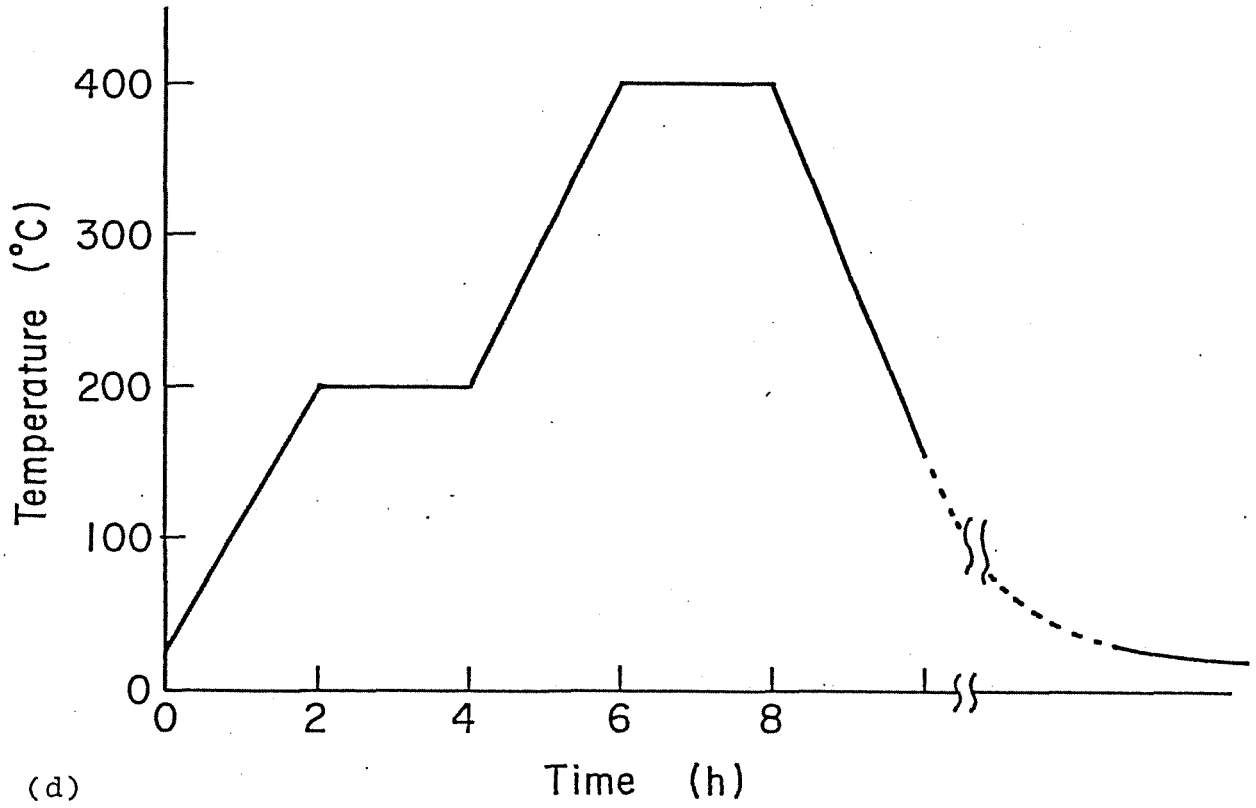

(d)

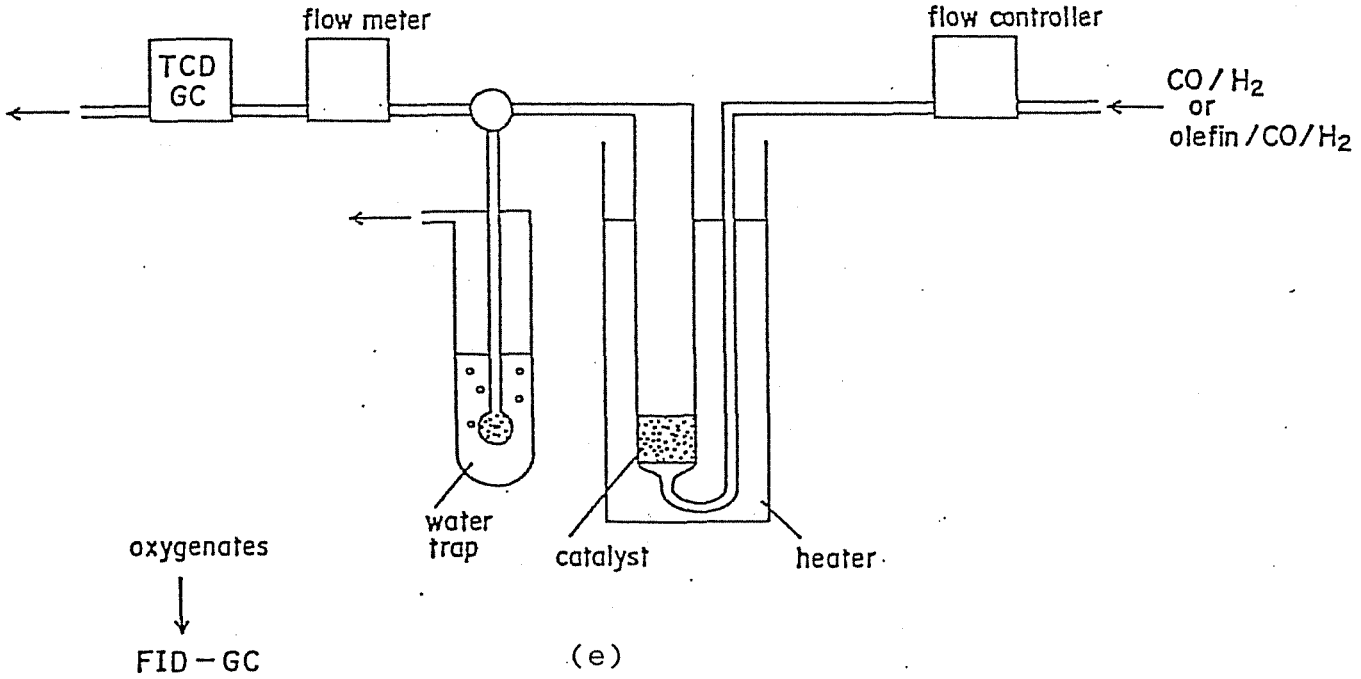

(e)

Figure 2 (continued).
(d) Temperature program for H_2 reduction;
(e) A flow-mode reactor with gas chromatographs.

flow rate of 90 ml/min and a space velocity of 1000 h^{-1} (Figure 2e). Oxygenated products such as CH_3OH, CH_3CHO, and C_2H_5OH were collected in a water trap (H_2O 50 ml) by bubbling the effluent gas. Products were analyzed by gas chromatography. CO, CO_2, and C_1-C_4 hydrocarbons were separated by using a Shimadzu GC-8AIT gas chromatograph with a thermal conductivity detector. A 4 mmϕ x 1 m of active carbon (60-80 mesh) column was used for the analysis of CH_4, CO, and CO_2 at room temperature. C_2-C_4 hydrocarbons such as ethylene and propylene were separated on a 4 mmϕ x 4 m *N,N*-dimethylformamide/Al_2O_3 (DMF 38 %, 60-80 mesh) column at room temperature. The concentration of the gaseous products in the off-gas was calibrated with external standards by using a 5 ml of gas sampler. The analyses of the oxygenates dissolved in the water trap were performed on a Shimadzu GC-8APF gas chromatograph with a flame ionization detector using a 4 mmϕ x 4 m Chromosorb 101 (60-80 mesh) column at 135 °C, and acetone was added as an internal standard to calibrate the concentration of the oxygenates. In each gas chromatography, the amounts of the products were calculated with an integrator (Shimadzu Chromatopac CR-3A).

Hydroformylations of Ethylene and Propylene

Hydroformylation reactions of ethylene and propylene were carried out in vapor phase at atmospheric pressure with a flow-mode Pylex glass reactor (i.d. = 14 mm, 240 mm long tubing) where 2.0 g of the catalyst (0.5 wt% or 2 wt% metal loading) was charged. Gas mixtures of C_2H_4 (or C_3H_6), CO, and H_2 (1:1:1 molar

ratio, total pressure 1 atm) were introduced into the reactor at a flow rate of 60 ml/min and a space velocity of 670 h^{-1}. The oxygenated products such as aldehydes and alcohols were collected by bubbling the effluent gas through a water trap (50 ml). Products were analyzed by gas chromatography. C_2H_4 and C_2H_6 were separated by a Shimadzu GC-8AIT gas chromatograph with a thermal conductivity detector using a 4 mmϕ x 4 m Porapak Q (60-80 mesh) column at 70 °C. C_3H_6 and C_3H_8 were separated on a 4 mmϕ x 4 m *N,N*-dimethylformamide/Al_2O_3 (DMF 38 %, 60-80 mesh) column at room temperature. The concentration of the gaseous products in the off-gas was calibrated with external standards by using a 5 ml of gas sampler. The analysis of the oxygenated products dissolved in the water trap was conducted by a Shimadzu GC-8APF gas chromatograph with a flame ionization detector. The products of hydroformylation of ethylene such as propanal and 1-propanol were separated on a 4 mmϕ x 4 m Chromosorb 101 (60-80 mesh) column at 150 °C. The products of hydroformylation of propylene such as butanal, 2-methylpropanal, 1-butanol, and 2-methylpropanol were separated on the same column at 155 °C. Ethanol was added as an internal standard to calibrate the amounts of the oxygenates. In each gas chromatography, the amounts of the products were calculated using an integrator (Shimadzu Chromatopac CR-3A).

Catalyst Characterization by Mössbauer, EXAFS, and FTIR Spectroscopies

Aerosil 300 (surface area = 300$\pm$30 m^2/g, average particle size = 7 mμ) was treated *in vacuo* at 320 °C for 2 h, and was

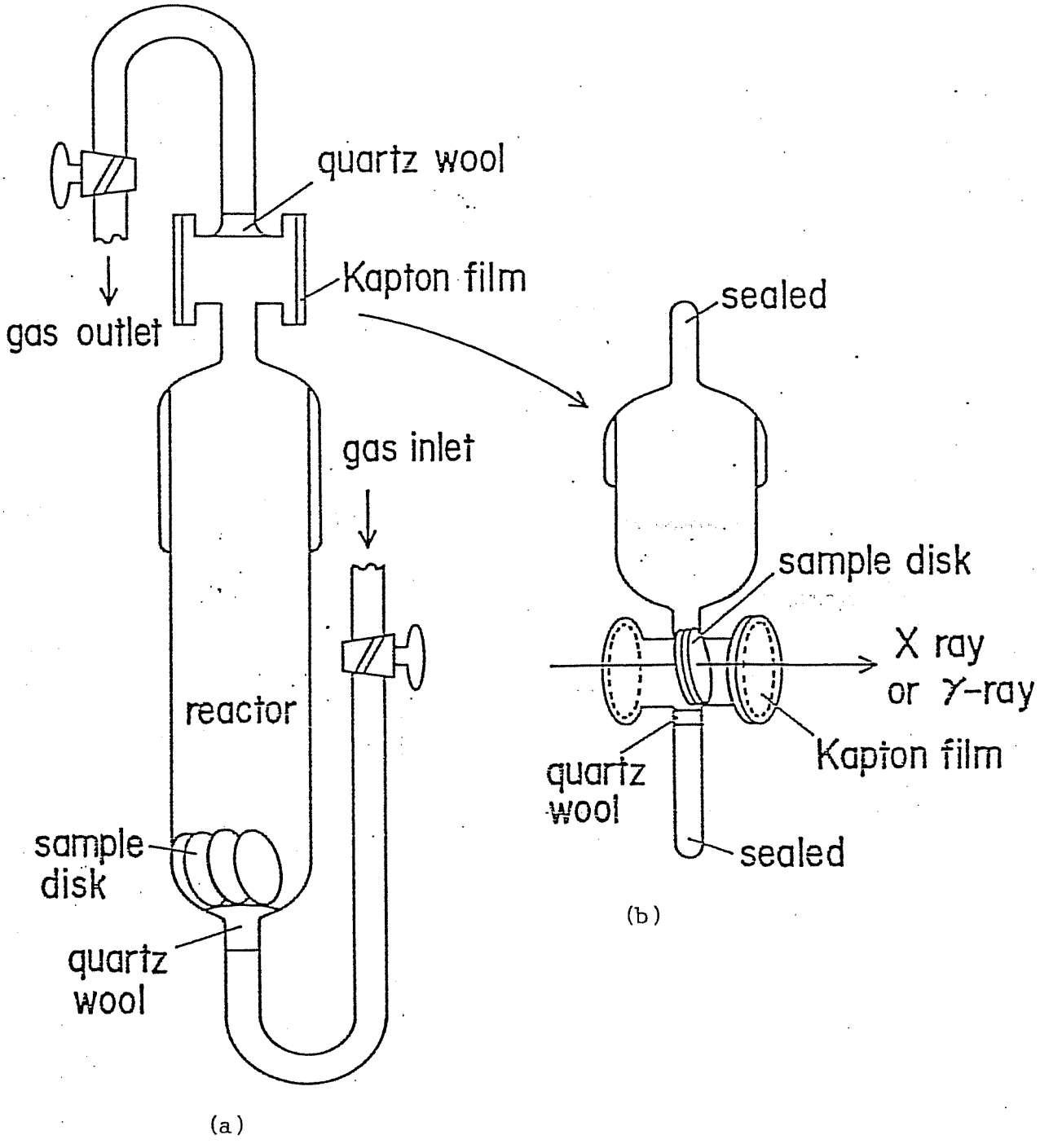

Figure 3.
(a) An apparatus for H_2 reduction of sample disks;
(b) A sealed-off cell for *in situ* EXAFS and ^{57}Fe Mössbauer spectroscopies;

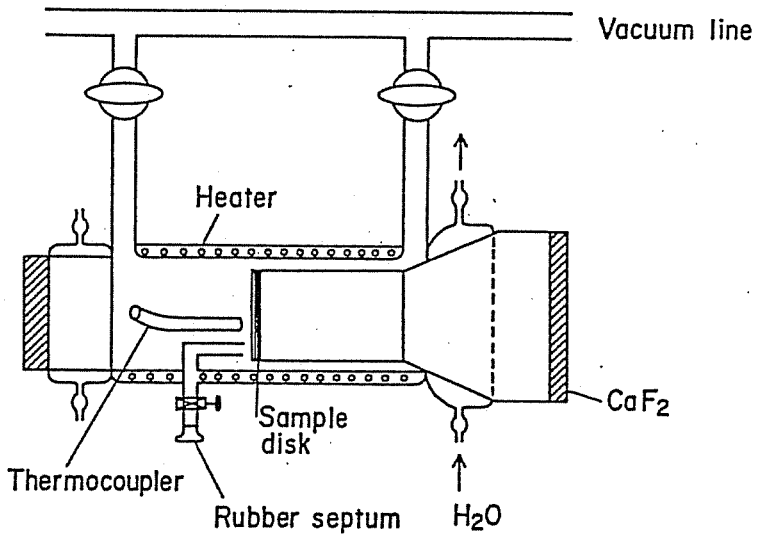

Figure 3 (continued).
(c) An *in situ* IR cell.

used as SiO_2 support to prepare the sample for spectroscopic studies. Carbonyl clusters were deposited onto the SiO_2 under N_2, and the sample was dried and oxidized by the same method described as above. The sample were pressed into disks (20-40 mg, 20 mmϕ). In Mössbauer and EXAFS study, the disks were reduced in an apparatus (Figure 3a) by flowing H_2 (50-100 ml/min) at the programmed temperature from 20 to 400 °C (Figure 2). After H_2 reduction, the H_2 atmosphere in the cells was substituted for dry N_2. The sample disks were transferred to an *in situ* cell of the upper part, the lower part was attached to a glass-joint under N_2, and the cell was sealed (Figure 3b). In FTIR study the sample disk was mounted into an *in situ* IR cell (Figure 3c), and was reduced in flowing H_2 by using the same temperature program as above. After H_2 reduction, the H_2 atmosphere in the cell was evacuated. The total metal loading of the sample in each spectroscopy was 4 wt%.

Mössbauer spectra were obtained from the disks in the cell with Kapton film window on a Shimadzu MEG-2 or an Austin Science S-600 spectrometer at 20 °C. In order to determine Mössbauer parameters and relative absorption areas, the spectra were fitted by computer as linear combination of Lorentzians with the least-squares method. Isomer shifts are given relative to α-Fe.

Extended X-ray absorption fine structure (EXAFS) spectra were obtained at 25 °C from the disks in the same cell as above on the synchrotron radiation source of Beam Line-10B in the Photon Factory of the National Laboratory for High Energy Physics (KEK-PF). Analysis of the EXAFS data was performed with Program

EXAFS-1 and EXAFS-2 of The University of Tokyo; *i.e.*, the EXAFS oscillations were extracted from the observed spectra, the Fourier transform of k^3-weighted EXAFS oscillation $k^3\chi(k)$ was calculated, and the curve-fitting analysis was carried out on the inverse Fourier transform of the selected region of k by using the theoretical amplitude and phase-shift functions given by Teo and Lee.[47] Coordination numbers and interatomic distances were determined with the EXAFS data of standard materials: foils of Fe, Rh, Pd, and Pt.

Infrared spectra were obtained from the disk in the IR cell with CaF_2 windows on a double-beam Fourier transform infrared spectrometer (Shimadzu FTIR-4100) at a resolution of 2 cm^{-1}. Generally, 25-50 interferograms were coadded to improve signal-to-noise ratios.

Results and Discussion

CO Hydrogenation on RhFe, PtFe, PdFe, and IrFe Carbonyl Cluster-derived Catalysts

The results of CO hydrogenation at 5 kg/cm^2 are summarized in Table 1, where the specific rates of product formation and selectivities are evaluated on mmol/min/mmol of Rh (or Pt, Pd, Ir) in CO base.

Rh_4/SiO_2 prepared from $Rh_4(CO)_{12}$ converted the 0.5 % of CO under the reaction conditions, and it produced methane in 97 % selectivity. The selectivity toward oxygenates among products was 3 %; acetaldehyde was mainly obtained and methanol was

Table 1. CO Hydrogenation on SiO_2-supported RhFe, PtFe, PdFe, and IrFe Carbonyl Cluster-derived Catalysts.[a]

precursor/SiO_2	at ratio Fe/M	CO conv. (%)	specific rate of formation[b] x 10^{-3} min^{-1}						selectivity,[c] %					
			CH_3OH	CH_3CHO	C_2H_5OH[d]	CH_4	CO_2	C_{2+}	CH_3OH	CH_3CHO	C_2H_5OH[d]	CH_4	CO_2	C_{2+}
$RhCl_3 \cdot 3H_2O$	0	0.1	0.03	0.18	0	36	0	0	1	9	0	90	0	0
$Rh_4(CO)_{12}$	0	0.5	0.05	0.18	0	12	0	0	<1	3	0	97	0	0
$[NMe_4]_2[FeRh_4(CO)_{15}]$	0.25	1.5	3.7	1.4	1.7	39	0	0	8	6	7	79	0	0
[TMBA][e]$_2[Fe_2Rh_4(CO)_{16}]$	0.50	2.4	7.0	1.3	13	45	0	0	9	3	33	56	0	0
$[TMBA]_2[Fe_3(CO)_{11}]$	-	0	-	-	-	-	-	-	-	-	-	-	-	-
$H_2PtCl_6 \cdot 6H_2O$	0	0.03	1.5	0	0	0	0	0	100	0	0	0	0	0
$[NEt_4]_2[Pt_{12}(CO)_{24}]$	0	0.1	4.2	0	0	0	0	0	100	0	0	0	0	0
$[TMBA]_2[Fe_3Pt_3(CO)_{15}]$	1.0	0.2	13	0	0	0	0	0	100	0	0	0	0	0
$[TMBA]_2[Fe_4Pt(CO)_{16}]$	4.0	1.7	12	0	0	31	88	23	7	0	0	18	50	26
$PdCl_2$	0	0.03	1.5	0	0	0	0	0	100	0	0	0	0	0
$[TMBA]_3[Fe_6Pd_6(CO)_{24}H]$	1.0	0.5	20	0	0	5	0	0	79	0	0	21	0	0
$PdCl_2$ + $FeCl_3$	1.0	0.5	5.4	0	0.2	11	9.2	4.8	17	0	1	34	28	20
$[TMBA]_2[Fe_4Pd(CO)_{16}]$	4.0	1.1	12	0	0	36	21	16	12	0	0	35	21	32
$[TMBA][HIr_4(CO)_{11}]$	0	0.01	0.2	0	0	0.3	0	<0.1	40	0	0	48	0	12
$[TMBA]_2[FeIr_4(CO)_{15}]$	0.25	0.66	45	0	0	4.3	0	0.4	90	0	0	9	0	1
$IrCl_4 \cdot H_2O$ + $FeCl_3$	0.25	0.17	7.8	0	0.4	3.4	0	0.6	61	0	6	27	0	6
$[TMBA][HIr_4(CO)_{11}]$ + $[TMBA]_2[Fe_3(CO)_{11}]$	0.25	0.05	3.0	0	<0.1	0.8	0	0.1	79	0	0	20	0	2

[a] Reaction conditions: total metal loading 2 wt%, reaction temerature 250 $\pm$ 2 °C, CO/H_2 = 0.5 molar ratio, total pressure 5 kg/cm^2, space velocity 1000 l/l/h.

[b] $mmol/mmom_{Rh,Pt,Pd,Ir}/min$.

[c] Selectivities were calculated from the carbon efficiency: 100 x $iC/CO_{converted}$, i = carbon number of the product molecule, C = molar concentration of the product molecule.

[d] Including $CH_3COOC_2H_5$.

[e] TMBA = $N(CH_3)_3(CH_2C_6H_5)$, trimethylbenzylammonium.

slightly produced. Ethanol was not produced on Rh_4/SiO_2. Fe_3/SiO_2 prepared from an anion cluster $[TMBA]_2[Fe_3(CO)_{11}]$ had no catalytic activity under the reaction conditions of 250 °C and 5 kg/cm^2. On the RhFe bimetallic catalysts prepared from $[TMBA]_2[Fe_2Rh_4(CO)_{16}]$ and $[NMe_4]_2[FeRh_4(CO)_{15}]$, the CO conversion and the rates for oxygenates were substantially increased. Notably, the rate for ethanol was strikingly enhanced on the Fe_2Rh_4/SiO_2 catalyst and the selectivity toward ethanol reached to 33 %. The RhFe bimetallic cluster-derived catalysts improved the rates for methane as well, but relative rate enhancement for oxygenates was much higher than that for methane. Accordingly, the selectivities toward methane were decreased to 79 % and 56 % on $FeRh_4/SiO_2$ and Fe_2Rh_4/SiO_2 catalysts, respectively, which was in contrast with the substantial increase of the selectivities toward oxygenates such as methanol and ethanol. The conventional Rh-Fe/SiO_2 catalyst was prepared from co-impregnation of $RhCl_3 \cdot 3H_2O$ and $FeCl_3$. The Rh-Fe/SiO_2 catalyst showed higher rates and selectivity toward oxygenates than did Fe-free Rh_4/SiO_2, but the selectivity toward ethanol was lower than that on Fe_2Rh_4/SiO_2 at the same Fe/Rh ratio of 0.5.

Remarkable Fe promotion for methanol production was observed on PtFe, PdFe, and IrFe cluster-derived catalysts. Pt_{12}/SiO_2 prepared from $[NEt_4][Pt_{12}(CO)_{24}]$ produced only methanol, and the rate for methanol was larger than that on the $H_2PtCl_6 \cdot 6H_2O$-derived catalyst. Fe_3Pt_3/SiO_2 (Fe/Pt = 1 atomic ratio) prepared from $[TMBA]_2[Fe_3Pt_3(CO)_{15}]$ gave higher activity for methanol with the selectivity of 100 %. Interestingly, hydrocarbons and

CO_2 along with methanol were produced on the catalyst derived from Fe-rich $[TMBA]_2[Fe_4Pt(CO)_{16}]$ (Fe/Pt = 4). This poor selectivity may be due to the segregation of the bimetallic cluster to make a Fe metal active for hydrocarbons and CO_2; their product distribution is like typical Fischer-Tropsch synthesis. Higher activity for methanol to produce methanol was achieved on the catalyst derived from $[TMBA]_3[Fe_6Pd_6(CO)_{24}H]$ (Fe/Pd = 1), and the methanol selectivity was 79 %. The Pd-Fe/SiO_2 catalyst prepared from $PdCl_2$ + $FeCl_3$ (Fe/Ir = 1) gave lower selectivity toward methanol. The Fe-rich Fe_4Pd/SiO_2 catalyst from $[TMBA]_2[Fe_4Pd(CO)_{16}]$ provided the activity and poor selectivity similar to those on the Fe_4Pt/SiO_2 catalyst.

Iron is an effective promoter for methanol production in the IrFe bimetallic cluster-derived catalyst. The rate of methanol production on $FeIr_4/SiO_2$ prepared from $[TMBA]_2[FeIr_4(CO)_{15}]$ was dramatically enhanced by a factor of over 200 times compared with the Fe-free Ir_4/SiO_2 catalyst. In addition, the selectivity toward methanol was as high as 90 % but the selectivity toward methane was suppressed to 9 % on $FeIr_4/SiO_2$. To determine the effect of proximity of Ir and Fe in the precursor compounds, two Ir-Fe catalysts were prepared from $IrCl_4 \cdot H_2O$ + $FeCl_3$ and a mixture of monometallic clusters $[TMBA][HIr_4(CO)_{11}]$ and $[TMBA]_2[Fe_3(CO)_{11}]$ at the same Fe/Ir atomic ratio of 0.25 as that of $[TMBA]_2[FeIr_4(CO)_{15}]$. Both catalysts gave larger rates for methanol than did Ir_4/SiO_2, but the rate enhancement was much lower than that with the $FeIr_4$ cluster catalyst. On the salt- and the mixed cluster-derived catalysts, methanol selectivities

were 60-80 % and methane was substantially produced in above 20 % of selectivity.

The activity of cluster-derived Fe_2Rh_4 and $FeIr_4/SiO_2$ catalysts was retained for *ca.* 60 h.

Hydroformylation of Ethylene and Propylene on RhFe, PtFe, PdFe, and IrFe Bimetallic Cluster-derived Catalysts

Since CO hydrogenation reaction over the supported metal catalysts is composed of many elementary steps, it is difficult to discriminate between the influence of Fe on the individual elementary steps for alcohol production. Sachtler and Ichikawa[27] have insisted that alcohols are produced through surface acyls formed by the CO insertion into metal-alkyl bonds (Figure 4), and that hydroformylation of olefin enabled them to observe the specific influence of the promoter on the migratory CO insertion and the H addition to surface alkyl group on the Rh/SiO_2 catalysts. Accordingly, to ravel the promotion effect for production of methanol and ethanol from syngas on Fe-containing Rh, Pt, Pd, and Ir cluster catalysts, hydroformylations of ethylene and propylene were chosen as diagnostic reactions to evaluate the CO insertion in elementary steps for syngas conversion.

Table 2 summarizes the results of hydroformylation of ethylene on the SiO_2-supported RhFe bimetallic cluster-derived catalysts. Under the reaction conditions of 135 °C and 1 atm, simple hydrogenation of ethylene to ethane is predominant over hydroformylation on the Rh_4/SiO_2 catalyst; the selectivity toward

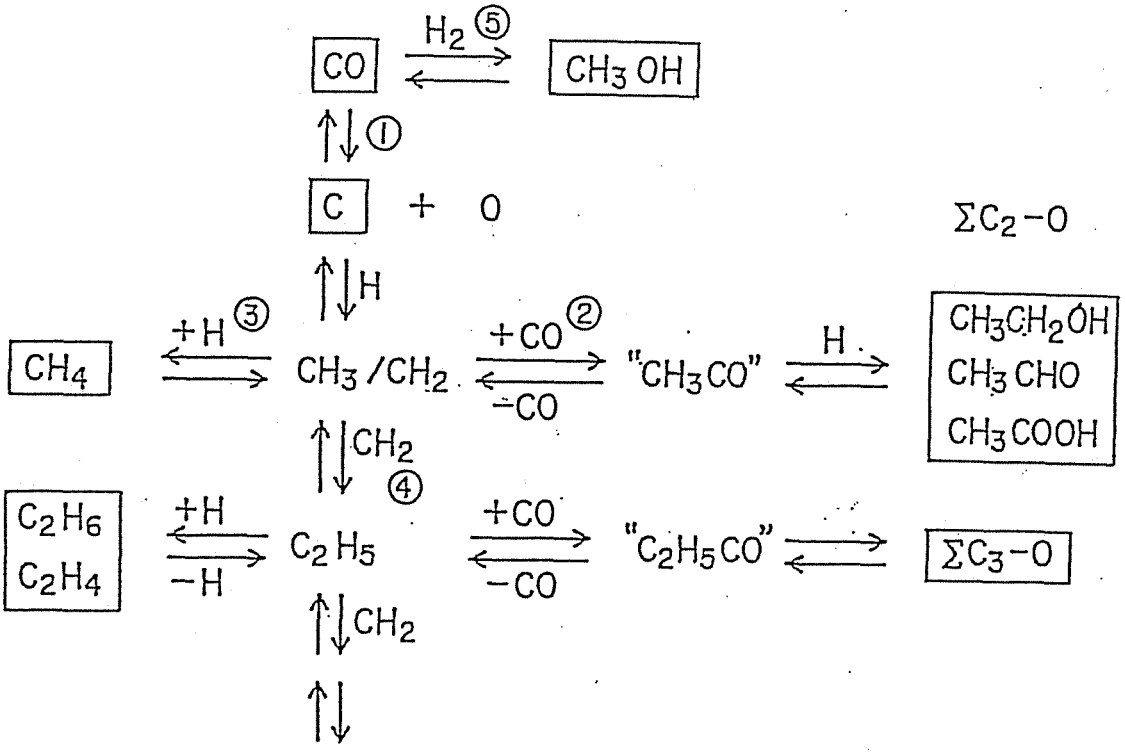

Figure 4. Proposed elementary steps in syngas conversion.[27]

oxygenates, expressed by the percentage of (propanal + 1-propanol) to (ethane + propanal + 1-propanol), is only 28 %. On the Fe_3/SiO_2 catalyst derived from $[TMBA]_2[Fe_3(CO)_{11}]$, neither hydroformylation nor simple hydrogenation occurred under the reaction conditions.

The activity for hydroformylation was greatly increased for the catalysts derived from RhFe bimetallic clusters having the metal composition of $FeRh_5$, $FeRh_4$, Fe_2Rh_4, and Fe_3Rh_2; the rates for C_2H_5CHO + 1-C_3H_7OH were improved by factors of 62-110 compared with Fe-free Rh_4/SiO_2. The RhFe catalysts improved the activity for the simple hydrogenation, but the relative rate enhancement for the hydrogenation was lower than that for the hydroformylation. The selectivity toward oxygenates was thus substantially increased on the RhFe catalysts: 28 % on Rh_4/SiO_2, 37-50 % on $RhFe/SiO_2$. A small amount of 1-propanol was obtained on the RhFe cluster-derived catalysts, although Rh_4/SiO_2 gave only propanal as oxygenate. To clarify the effect of the proximity of Rh and Fe in the catalysts, a mixed Rh-Fe catalyst was prepared by the impregnation of SiO_2 with a tetrahydrofuran solution of $Rh_4(CO)_{12}$ and $[TMBA]_2[Fe_3(CO)_{11}]$ at the Fe/Rh atomic ratio of 0.26. The Rh_4+Fe_3/SiO_2 catalyst gave much lower activity for the hydroformylation of ethylene than that from $[NMe_4]_2[FeRh_4(CO)_{15}]$ (Fe/Rh = 0.25). In addition, the two catalysts Rh_4/SiO_2 and Fe_3/SiO_2 were mixed at the Fe/Rh atomic ratio of 0.24 and charged into the reactor. The resulting Rh_4/SiO_2 + Fe_3/SiO_2 catalyst showed the activity for hydroformylation and hydrogenation as low as that by Rh_4/SiO_2.

Table 2. Hydroformylation of Ethylene on SiO_2-supported Rh, RhFe, and Fe Carbonyl Cluster-derived Catalysts.[a]

precursor/SiO_2	at ratio Fe/Rh	C_2H_4 conv.(%)	specific rate of formation,[b] min^{-1}		selectivity, mol %	
			C_2H_6	EtCHO + 1-PrOH	oxygenates[c]	alcohol[d]
$Rh_4(CO)_{12}$	0	<0.1	0.006 (1)	0.002 (1)	28	0
[TMBA][$FeRh_5(CO)_{16}$][e]	0.20	3	0.16 (30)	0.13 (62)	45	4
[NMe_4]$_2$[$FeRh_4(CO)_{15}$]	0.25	5	0.28 (53)	0.20 (96)	42	2
[TMBA]$_2$[$Fe_2Rh_4(CO)_{16}$]	0.5	5	0.30 (57)	0.18 (86)	37	3
$Fe_3Rh_2(CO)_{14}C$	1.5	3	0.22 (41)	0.22(110)	50	6
[TMBA]$_2$[$Fe_3(CO)_{11}$]	-	0	0	0	-	-
$Rh_4(CO)_{12}$ + [TMBA]$_2$[$Fe_3(CO)_{11}$]	0.26	0.7	0.039 (7)	0.036(17)	48	0
$Rh_4(CO)_{12}/SiO_2$ + [TMBA]$_2$[$Fe_3(CO)_{11}$]/SiO_2	0.24	<0.1	0.003 (0.6)	0.001 (0.6)	27	0
[TMBA]$_2$[$Fe_2Rh_4(CO)_{16}$][f]	0.5	7	0.046	0.14	75	28

[a]Reaction conditions: total metal loading 0.5 wt%, reaction temperature 135±2 °C, flow rate C_2H_4+CO+H_2 = 20+20+20 ml/min, total pressure 1 atm, space velocity 670 h^{-1}. Values in parentheses are rates relative to $Rh_4(CO)_{12}$.

[b]$mmol/mmol_{Rh}/min$.

[c](EtCHO + 1-PrOH)/(C_2H_6 + EtCHO + 1-PrOH) x 100.

[d]1-PrOH/(EtCHO + 1-PrOH) x 100.

[e]TMBA = $N(CH_3)_3(CH_2C_6H_5)$, trimethylbenzylammonium

[f]Total pressure 5 kg/cm^2, flow rate C_2H_4+CO+H_2 = 20+20+20 ml/min.

Hydroformylation of ethylene at 5 kg/cm^2 on the Fe_2Rh_4/SiO_2 derived from $[NMe_4]_2[Fe_2Rh_4(CO)_{16}]$ was conducted in a stainless steel reactor. Compared with the catalytic performance at 1 atm, the simple hydrogenation of C_2H_4 to C_2H_6 was effectively suppressed and thus the selectivity toward oxygenates reached up to 75 % with the considerable formation of 1-propanol (28 % selectivity among oxygenates).

Likewise, Fe promotion for the formation of oxygenates, in particular alcohols, were observed in hydroformylation of propylene, as shown in Table 3. Under the conditions of 162 °C and 1 atm, the rates of hydroformylation were dramatically increased on the catalysts derived from $FeRh_5$, $FeRh_4$, Fe_2Rh_4, and Fe_3Rh_2 carbonyl clusters, *i.e.*, 130, 260, 300, and 290 times larger, respectively, relative to the $Rh_4(CO)_{12}$-derived catalyst. The selectivity toward hydroformylation was substantially increased on the RhFe catalysts; 13 % on Rh_4/SiO_2, 32-45 % on $RhFe/SiO_2$. Additionally, alcohols such as 1-butanol and 2-methylpropanol were also obtained on the RhFe catalysts, while the $Rh_4(CO)_{12}$-derived catalyst gave only aldehydes as oxygenates. Interestingly, the selectivity toward normal isomers of aldehydes and alcohols, *i.e.*, (butanal + 1-butanol)/(butanal + 2-methyl-propanal + 1-butanol + 2-methyl-1-propanol) x 100, was not affected by the Fe content in precursor clusters. For example, the selectivity was 75% on the catalyst from $Rh_4(CO)_{12}$, and the RhFe cluster-derived catalysts gave the normal selectivities of 70-74 %. This implies that the CO insertion of metal-C_3H_8 to form metal-COC_3H_8, which determines the selectivity toward normal

Table 3. Hydroformylation of Propylene on SiO_2-supported Rh, RhFe, and Fe Carbonyl Cluster-derived Catalysts.[a]

precursor/SiO_2	at ratio Fe/Rh	C_3H_6 conv.(%)	specific rate of formation,[b] min^{-1}		selectivity, mol %		
			C_3H_8	n,i-PrCHO[c] + n,i-BuOH[d]	oxygenates[e]	alcohol[f]	n-isomer[g]
$Rh_4(CO)_{12}$	0	<0.1	0.001	0.0003 (1)			
$Rh_4(CO)_{12}$[h]	0	0.7	0.027	0.0038	13	0	75
[TMBA][$FeRh_5(CO)_{16}$][i]	0.20	1	0.078	0.037 (130)	32	46	72
[NMe_4]$_2$[$FeRh_4(CO)_{15}$]	0.25	2	0.12	0.075 (260)	38	42	74
[TMBA]$_2$[$Fe_2Rh_4(CO)_{16}$]	0.50	2	0.13	0.088 (300)	41	44	73
$Fe_3Rh_2(CO)_{14}C$	1.5	1	0.10	0.084 (290)	45	63	70
[TMBA]$_2$[$Fe_3(CO)_{11}$]	-	0	0	0			
$Rh_4(CO)_{12}$ + [TMBA]$_2$[$Fe_3(CO)_{11}$]	0.26	0.2	0.015	0.010 (34)	41	33	78

[a]Reaction conditions: total metal loading 0.5 wt%, reaction temperature 162±2 °C, flow rate C_3H_6+CO+H_2 = 20+20+20 ml/min, total pressure 1 atm, space velocity 670 h^{-1}. Values in parentheses are rates relative to $Rh_4(CO)_{12}$.

[b]$mmol/mmol_{Rh}/min$.

[c]n-PrCHO = butanal, i-PrCHO = 2-methylpropanal.

[d]n-BuOH = 1-butanol, i-BuOH = 2-methylpropanol.

[e](n,i-PrCHO + n,i-BuOH)/(C_3H_8 + n,i-PrCHO + n,i-BuOH) x 100.

[f](n,i-BuOH)/(n,i-PrCHO + n,i-BuOH) x 100

[g](n-PrCHO + n-BuOH)/(n,i-PrCHO + n,i-BuOH) x 100.

[h]Total metal loading 4 wt%.

[i]TMBA = $N(CH_3)_3(CH_2C_6H_5)$, trimethylbenzylammonium

isomers, occurs on Rh atoms. Fe does not impose such a steric hindrance around Rh as is caused by PPh_3 in homogeneous hydroformylation with $HRh(CO)(PPh_3)_3$.

From these results of hydroformylations of ethylene and propylene on the RhFe catalysts, it is suggested that RhFe bimetallic carbonyl clusters provide Rh-Fe sites where Rh and Fe atoms are in close proximity, and that they are highly active for hydroformylation, *i.e.*, CO insertion and successive hydrogenation to give alcohols.

Tables 4 and 5 present the results of hydroformylation of ethylene and propylene on PtFe, PdFe, and IrFe cluster-derived catalysts. In ethylene hydroformylation (Table 4), PtFe, PdFe, and IrFe cluster-derived catalysts exhibited substantial promotion for the rates of hydroformylation compared with Fe-free Pt, Pd, and Ir catalysts, although the rates were much smaller than those on $RhFe/SiO_2$ (Table 2). Fe_6Pd_6/SiO_2 gave a modest rate for hydroformylation, but the hydrogenation of C_2H_4 to C_2H_6 was greatly predominant under the reaction conditions of 135 °C and 1 atm. Likewise in RhFe-catalyzed hydroformylation, selectivity toward the alcohol was increased on PtFe, PdFe, and $IrFe/SiO_2$ catalysts. Also, the improved selectivity toward alcohol was obtained in the hydroformylation of propylene on PtFe and PdFe cluster-derived catalysts. The selectivities toward n-isomer was 74 % on Fe_3Pt_3/SiO_2 and 41 % on Fe_6Pd_6/SiO_2, while the rates for hydroformylation were very small.

Table 4. Hydroformylation of Ethylene on SiO_2-supported PtFe, PdFe, and IrFe Carbonyl Cluster-derived Catalysts.[a]

precursor/SiO_2	at ratio Fe/M	C_2H_4 conv.(%)	specific rate of formation,[b] min^{-1}		selectivity, mol %	
			C_2H_6	EtCHO + 1-PrOH	oxygenates[c]	alcohol[d]
$[NEt_4][Pt_{12}(CO)_{24}]$	0	0.7	0.021	0.0056 (1)	2	8
$[TMBA]_2[Fe_3Pt_3(CO)_{15}]$[e]	1.0	0.8	0.021	0.019 (3.5)	48	37
$[TMBA]_2[Fe_4Pt(CO)_{16}]$	4.0	<0.1	0.003	0.0043 (0.8)	61	50
$PdCl_2$	0	9	0.20	0.0009 (1)	<1	≃0
$[TMBA]_3[Fe_6Pd_6(CO)_{24}H]$	1.0	55	1.80	0.035 (39)	2	79
$[TMBA]_2[Fe_4Pd(CO)_{16}]$	4.0	8	0.54	0.0041 (4.6)	1	91
$[TMBA][HIr_4(CO)_{11}]$[f]	0	0.3	0.0094	0.0003 (1)	3	70
$[TMBA]_2[FeIr_4(CO)_{15}]$[f]	0.25	0.4	0.012	0.0039(13)	3	94

[a]Reaction conditions: total metal loading 2 wt%, reaction temperature 135±2 °C, flow rate C_2H_4+CO+H_2 = 20+20+20 ml/min, total pressure 1 atm, space velocity 670 h^{-1}. Values in parentheses are rates relative to Fe-free catalysts.

[b]mmol/$mmol_{Pt,Pd,Ir}$/min.

[c](EtCHO + 1-PrOH)/(C_2H_6 + EtCHO + 1-PrOH) x 100.

[d]1-PrOH/(EtCHO + 1-PrOH) x 100.

[e]TMBA = $N(CH_3)_3(CH_2C_6H_5)$, trimethylbenzylammonium

[f]Reaction temperature 170 °C.

Table 5. Hydroformylation of Propylene on SiO_2-supported PtFe and PdFe Carbonyl Cluster-derived Catalysts.[a]

precursor/SiO_2	at ratio Fe/M	C_3H_6 conv.(%)	specific rate of formation,[b] min^{-1}		selectivity, mol %		
			C_3H_8	n,i-PrCHO[c] + n,i-BuOH[d]	oxygenates[e]	alcohol[f]	n-isomer[g]
$[NEt_4]_2[Pt_{12}(CO)_{24}]$	0	0.1	0.0035	0.001 (1)	21	41	74
$[TMBA]_2[Fe_3Pt_3(CO)_{15}]$[h]	1.0	0.4	0.011	0.0074 (7.7)	40	97	60
$[TMBA]_2[Fe_4Pt(CO)_{16}]$	4.0	0.4	0.0014	0.0014 (1.5)	51	88	50
$[TMBA]_3[Fe_6Pd_6(CO)_{24}H]$	1.0	24	0.81	0.005	<1	98	41
$[TMBA]_2[Fe_4Pd(CO)_{16}]$	4.0	2	0.16	0.0007	<1	≃100	42

[a]Reaction conditions: total metal loading 0.5 wt%, reaction temperature 162 ± 2 °C, flow rate $C_3H_6+CO+H_2$ = 20+20+20 ml/min, total pressure 1 atm, space velocity 670 h^{-1}. Values in parentheses are rates relative to $[NEt_4]_2[Pt_{12}(CO)_{24}]$.

[b]$mmol/mmol_{Pt,Pd}/min$.

[c]n-PrCHO = butanal, i-PrCHO = 2-methylpropanal.

[d]n-BuOH = 1-butanol, i-BuOH = 2-methylpropanol.

[e](n,i-PrCHO + n,i-BuOH)/(C_3H_8 + n,i-PrCHO + n,i-BuOH) x 100.

[f](n,i-BuOH)/(n,i-PrCHO + n,i-BuOH) x 100

[g](n-PrCHO + n-BuOH)/(n,i-PrCHO + n,i-BuOH) x 100.

[h]TMBA = $N(CH_3)_3(CH_2C_6H_5)$, trimethylbenzylammonium

Characterization of Cluster-derived RhFe, PtFe, PdFe, and IrFe Bimetallic Catalysts

^{57}Fe Mössbauer spectroscopy

The valence states of Fe in RhFe, PtFe, and PdFe bimetallic cluster-derived catalysts were studied by ^{57}Fe Mössbauer spectroscopy. The spectra of $FeRh_5/SiO_2$ and Fe_2Rh_4/SiO_2 at 20 °C are shown in Figure 5 and the Mössbauer parameters are summarized in Table 6. The isomer shifts and quadrupole splittings for $FeRh_5/SiO_2$ and Fe_2Rh_4/SiO_2 are very similar to those for the salt-derived Rh-Fe/SiO_2 catalysts previously reported.[35] In the spectra of $FeRh_5/SiO_2$ and Fe_2Rh_4/SiO_2, two absorption bands were observed and resolved into a singlet and a pair of quadrupole doublets by the computer fitting. The singlets at δ = *ca.* 0.15 mm/s were assigned to Fe^0 alloyed with Rh but metallic iron was absent because the isomer shift was higher than that of α-Fe (0 mm/s). The isomer shifts and quadrupole splittings indicate that the doublets were attributed to Fe^{3+}. Niemantsverdriet *et al.* assigned the similar doublet in the salt-derived Rh-Fe/SiO_2 catalysts to high spin Fe^{3+} of iron(III) oxides with high dispersion.[34] Bands of Fe^{+} and Fe^{2+} were negligible for $FeRh_5/SiO_2$ and Fe_2Rh_4/SiO_2.

It is notable that Fe atoms of the RhFe bimetallic catalysts mostly exist in the state of Fe^{3+} even after H_2 reduction at 400 °C. The ratios of peak area of Fe^{3+} to Fe^0 were 88/12 for $FeRh_5/SiO_2$ (Fe/Rh = 0.2) and 73/27 for Fe_2Rh_4/SiO_2 (Fe/Rh = 0.5). The Fe^{3+}/Fe^0 ratio decreased with increasing the Fe/Rh atomic

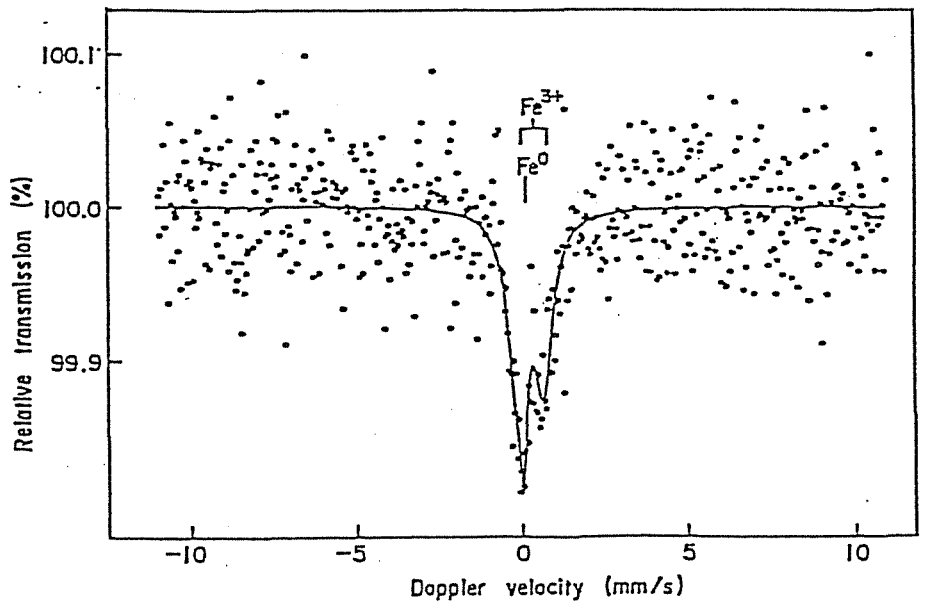

(a)

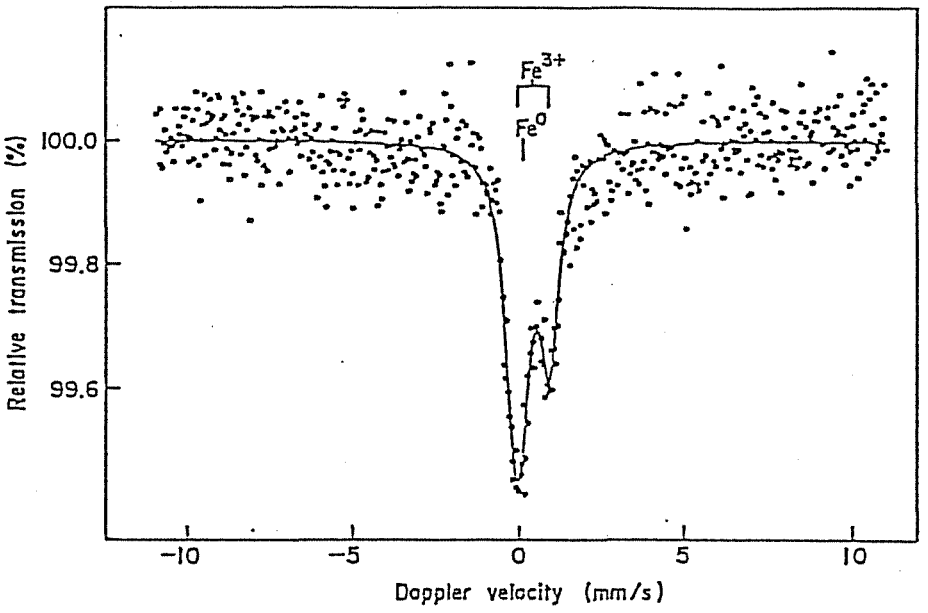

(b)

Figure 5. ^{57}Fe Mössbauer spectra of H_2-reduced RhFe cluster-derived catalysts at 20 °C: H_2 reduction at 400 °C for 2 h, isomer shifts are relative to α-Fe.
(a) $FeRh_5/SiO_2$ derived from [TMBA][$FeRh_5(CO)_{16}$];
(b) Fe_2Rh_4/SiO_2 derived from [TMBA]$_2$[$Fe_2Rh_4(CO)_{16}$].

Table 6. Mössbauer Parameters of H_2-reduced RhFe, PtFe, and PdFe Bimetallic Cluster-derived Catalysts at 20 °C.[a]

precursor/SiO_2	at ratio Fe/M	iron state	δ[b] mm/s	Δ[c] mm/s	peak area %
[TMBA][$FeRh_5(CO)_{16}$][d]	0.2	Fe^0	0.15	-	12
		Fe^{3+}	0.37	0.82	88
[TMBA]$_2$[$Fe_2Rh_4(CO)_{16}$]	0.5	Fe^0	0.17	-	27
		Fe^{3+}	0.46	1.00	73
[TMBA]$_2$[$Fe_3Pt_3(CO)_{15}$]	1.0	Fe^0	-0.06	-	35
		Fe^{3+}	0.72	0.76	65
[TMBA]$_3$[$Fe_6Pd_6(CO)_{24}H$]	1.0	Fe^{2+}	1.24	2.50	36
		Fe^{3+}	0.35	0.43	64
[TMBA]$_2$[$Fe_4Pd(CO)_{16}$]	4.0	Fe^0	0.59	-	14
		Fe^{2+}	1.16	2.15	86

[a] Total metal loading 4 wt%, H_2 reduction at 400 °C for 2 h.
[b] Isomer shift relative to α-Fe.
[c] Quadrupole splitting.
[d] TMBA = $N(CH_3)_3(CH_2C_6H_5)$, trimethylbenzylammonium

ratio of precursor clusters, implying that the reduction of Fe^{3+} to Fe^0 was easier on the Rh-rich bimetallic catalysts.

Similar contribution of Fe^{3+} and Fe^0 were obtained for the Fe_3Pt_3/SiO_2 which was a selective catalyst for methanol production in CO hydrogenation. The spectrum for Fe_6Pd_6/SiO_2 shows the presence of Fe^{3+} and Fe^{2+}, but the band associated with Fe^0 was not observed. On the other hand, Fe^{2+} had a large contribution in Fe_4Pd/SiO_2; the relative peak areas of Fe^{2+} and Fe^0 were 86 % and 14 %, respectively. Fe^{3+} species, which was found in the selective alcohol catalysts such as Fe_2Rh_4/SiO_2 and Fe_6Pd_6/SiO_2, was not observed in the ill-selective catalyst Fe_4Pd/SiO_2.

EXAFS spectroscopy

EXAFS analysis was performed on the ethanol selective Fe_2Rh_4/SiO_2 catalyst after H_2 reduction at 400 °C. Figure 6 shows the k^3 weighted EXAFS oscillation $k^3\chi(k)$ at Rh K-edge and Fe K-edge, and their Fourier transforms. The results of the curve fitting analysis are summarized with the previous results for salt-derived Rh-Fe/SiO_2 catalysts in Table 7. Since the EXAFS data of the cluster-derived catalysts were quite similar to those of the salt-derived catalysts, we could estimate the contribution around Rh or Fe in Fe_2Rh_4/SiO_2 according to the procedures of analysis for the salt-derived Rh-Fe catalysts.[33]

As outlined in Figure 6, the Fourier transform of $k^3\chi(k)$ for the Rh K-edge EXAFS shows a strong peak at about 2.3 Å which is attributable to Rh-Rh. From the curve-fitting analysis of

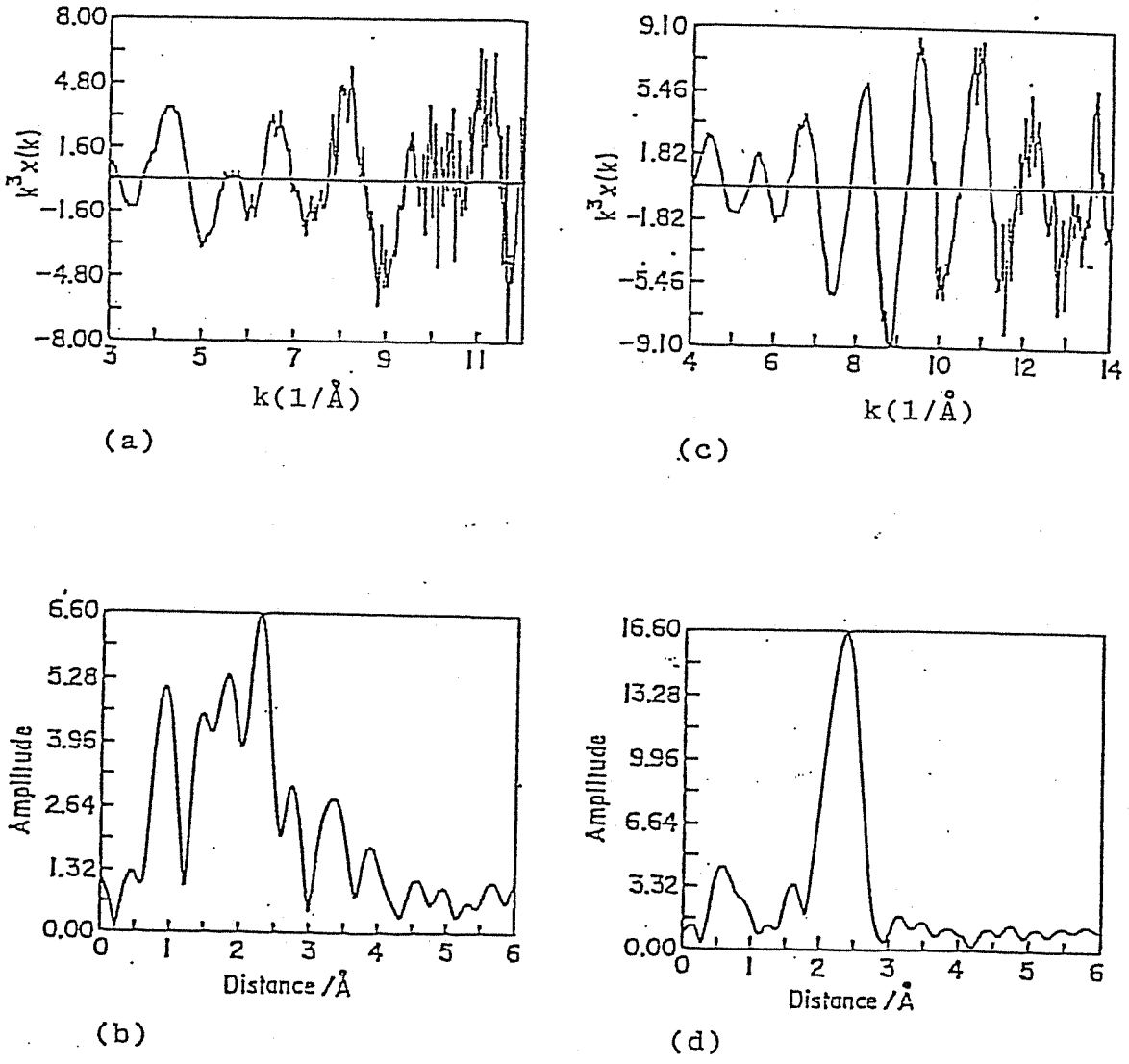

Figure 6. EXAFS study on Fe_2Rh_4/SiO_2 at 25 °C: H_2 reduction at 400 °C for 2 h.
(a) Fe *K*-edge EXAFS oscillation $k^3\chi(k)$;
(b) Fourier transform of (a);
(c) Rh *K*-edge EXAFS oscillation $k^3\chi(k)$;
(d) Fourier transform of (c);

Table 7. Results of the Curve-fitting Analysis of $k^3\chi(k)$ of H_2-reduced RhFe Bimetallic Cluster-derived Catalyst.[a]

		Fe *K*-edge EXAFS				Rh *K*-edge EXAFS		
		Fe-O		Fe-Rh		Rh-Rh		
precursor/SiO_2	at ratio Fe/Rh	C.N.[c]	R(Å)[d]	C.N.	R(Å)	C.N.	R(Å)	Fe^{3+},[b] (%)
$[TMBA]_2[Fe_2Rh_4(CO)_{16}]$	0.5	3.0	1.99	1.8	2.54	7.2	2.65	73
$RhCl_3 \cdot 3H_2O$ + $FeCl_3$[e]	0.5	0.9	1.99	4.0	2.62	9.5	2.66	86

[a] Total metal loading 4 wt%, H_2 reduction at 400 °C for 2 h. The EXAFS spectra were obtanined at 25 °C.
[b] From Mössbauer results (Table 6, ref. 35).
[c] C.N. = coordination number.
[d] R = interatomic distance.
[e] From ref. 33.

inverse Fourier transform of the peak, it is assigned to Rh-Rh: the interatomic distance (R) = 2.65 Å, the coordination number (C.N.) = 7.2. The contribution of Rh-Fe interaction was not found in the curve-fitting. In the Fourier transform of $k^3\chi(k)$ for the Fe *K*-edge EXAFS of Fe_2Rh_4/SiO_2, a peak at *ca.* 2.2 Å is assigned to Fe-Rh from the curve-fitting analysis: R = 2.54 Å and C.N. = 1.8. A shoulder peak at *ca.* 1.8 Å is Fe-O (R = 1.99 Å, C.N. = 3.0) where O may be the surface oxygen of SiO_2. There is negligible contribution of Fe-Fe in the curve-fitting analysis. In comparison to Rh-Fe/SiO_2 (Fe/Rh = 0.5) prepared from $RhCl_3 \cdot 3H_2O$ + $FeCl_3$, the contribution of Rh-Rh is decreased but that of Fe-O is increased for Fe_2Rh_4/SiO_2, *i.e.*, Rh-Rh: C.N. = 7.2 for Fe_2Rh_4/SiO_2, 9.5 for Rh-Fe/SiO_2 (Fe/Rh = 0.5); Fe-O: C.N. = 3.0 for Fe_2Rh_4/SiO_2, 0.9 for Rh-Fe/SiO_2 (Fe/Rh = 0.5). In addition, the total coordination number around Rh and Fe in Fe_2Rh_4/SiO_2 are about 7 and 5, respectively, which indicates that the average particle size is as small as 10 Å.

The image of $[TMBA]_2[Fe_2Rh_4(CO)_{16}]$ deposited on the silica surface of small particles of silicon were obtained by using high resolution transmission electron microscopy.[48] The shape of one molecule of cluster was hemispherical and its diameter was less than 10 Å at the metal loading of 2-4 wt%. Continued irradiation of electrons imposed the aggregation of two or three molecules during the observation. The particle size of the Rh-Fe/SiO_2 (Fe/Rh = 0.3) by transmission electron microscopy is reported to be 25 Å.[33]

From above EXAFS and Mössbauer studies for Fe_2Rh_4/SiO_2

catalyst, we propose the following structural model (Figure 7). Fe atoms mostly in the state of Fe^{3+} are located between Rh and O to form chemical bonds with the oxygen atoms of SiO_2 support. Since the contribution of Fe-Fe is negligible and the total coordination number around Fe is as low as 5, Fe atoms/ions are highly dispersed. Thus Fe^{3+} ions anchor Rh atoms onto the SiO_2 support to generate Rh-Fe^{3+}-O bimetallic sites, and these Fe^{3+} ions are stable and not reduced by H_2 at 400 °C. Minor amounts of Fe are in the state of Fe^0 which may be located on the Rh surface to be subject to H_2 reduction in the presence of the noble metal Rh.

EXAFS analysis was performed on H_2-reduced Fe_6Pd_6/SiO_2 and Fe_4Pd/SiO_2 catalysts derived from bimetallic clusters. The Fourier transforms of $k^3\chi(k)$ for Fe_6Pd_6/SiO_2 at Fe *K*- and Pd *K* edges are shown in Fig. 8, and the results of the curve-fitting analysis are summarized in Table 8. Two-strong peaks were observed at 2.1-2.8 Å and 1.0-2.1 Å in the Fourier transform of EXAFS at the Fe *K*-edge. From the curve-fitting analysis, the former peak is assigned to the overlap of Fe-Fe (R = 2.50 Å, C.N. = 0.4) and Fe-Pd (R = 2.62 Å, C.N. = 0.9), and the latter to Fe-O (R = 1.93 Å, C.N. = 3.8). The large contribution of Fe-O is consistent with the preferential existence of Fe^{3+} and Fe^{2+} in the Mössbauer results of Fe_6Pd_6/SiO_2. In the Fourier transform of EXAFS at the Pd *K*-edge, a strong peak was obtained at 1.9-2.8 Å, which was assigned to Pd-Pd (R = 2.75 Å, C.N. = 6.5) in the curve-fitting analysis. The contribution of Pd-Fe and Pd-O was negligible. Although Fe-Pd was found in the Fe *K*-

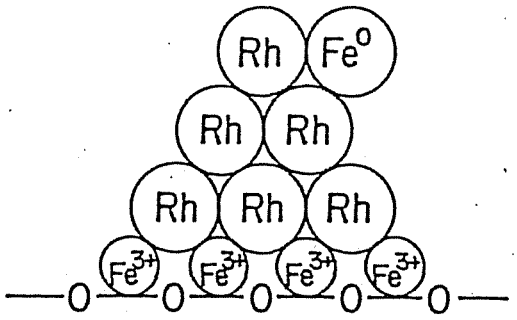

Figure 7. A structural model of Rh-Fe bimetallic sites of Fe_2Rh_4/SiO_2.

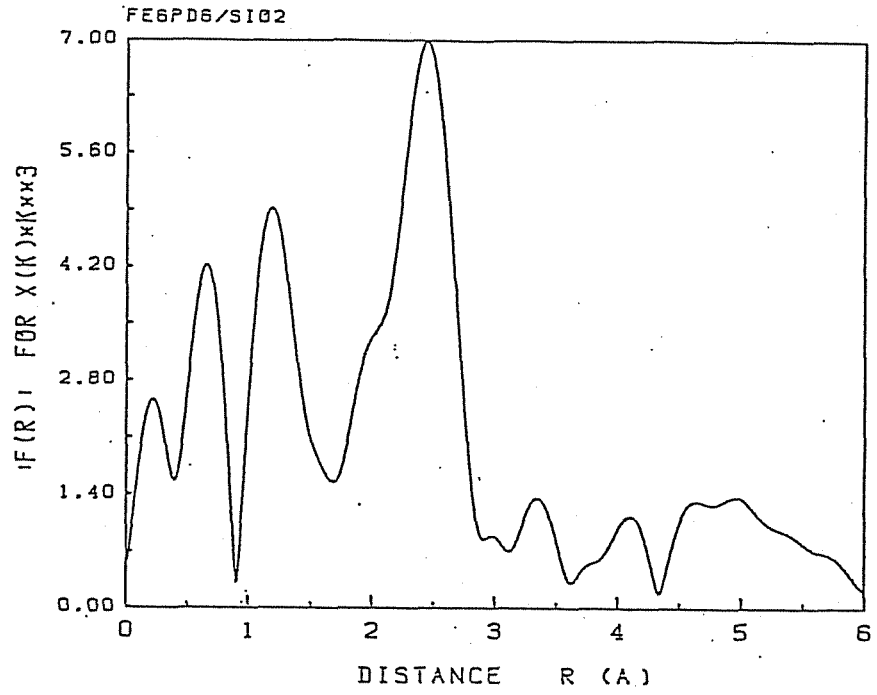

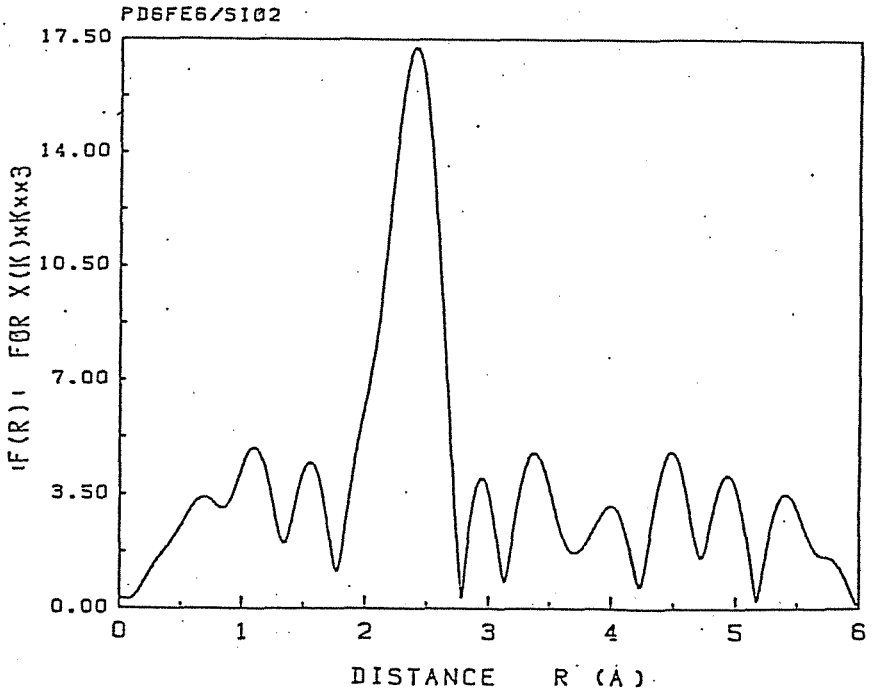

Figure 8. Fourier transforms of $k^3\chi(k)$ for Fe_6Pd_6/SiO_2 at Fe *K*-edge (a) and at Pd *K*-edge (b). Under N_2 at 25 °C after H_2 reduction at 400 °C for 2 h.

Table 8. Results of the Curve-fitting Analysis of $k^3\chi(k)$ of H_2-reduced PdFe Bimetallic Cluster-derived Catalyst.[a]

		Fe *K*-edge EXAFS						Pd *K*-edge EXAFS			
		Fe-O		Fe-Fe		Fe-Pd		Pd-Fe		Pd-Pd	
precursor/SiO_2	at ratio Fe/Pd	C.N.[b]	R(Å)[c]	C.N.	R(Å)	C.N.	R(Å)	C.N.	R(Å)	C.N.	R(Å)
$[TMBA]_3[Fe_6Pd_6(CO)_{24}H]$	1.0	3.8	1.93	0.4	2.50	0.9	2.62	-	-	6.5	2.75
$RhCl_3 \cdot 3H_2O + FeCl_3$[d]	0.45	-	-	0.9	2.46	9.0	2.62	4.6	2.63	7.7	2.76

[a]Total metal loading 4 wt%, H_2 reduction at 400 °C for 2 h. The EXAFS spectra were obtained at 25 °C.
[b]C.N. = coordination number.
[c]R = interatomic distance.
[d]From ref. 49.

edge EXAFS, the contribution of Pd-Fe was not detectable in the Pd *K*-edge EXAFS.

By contrast, large contribution of Fe-Fe and Fe-O was observed in the EXAFS results of Fe_4Pd/SiO_2, but Fe-Pd was negligible. The absence of Fe-Pd is reasonably reflected in the catalytic performance of Fe_4Pd catalyst with a poor selectivity for oxygenates in CO hydrogenation. In H_2-reduced $Pd-Fe/SiO_2$ catalysts prepared from $PdCl_2$ + $FeCl_3$, Fe-O bonding was not found and Fe atoms were proposed to be uniformly distributed in the metal particles forming $Pd-Fe^0$ alloy.[49] In contrast to this salt-derived catalyst, the results of Mössbauer and EXAFS on Fe_6Pd_6/SiO_2 imply that Fe^{3+} ions are located at the $Pd-SiO_2$ interface to anchor Pd atoms, where $Pd-Fe^{3+}$ sites are generated on SiO_2 similarly as in the case of Fe_2Rh_4/SiO_2.

FTIR spectroscopy

FTIR studies were performed on the CO chemisorption on cluster-derived Rh_4/SiO_2, $FeRh_5/SiO_2$, and Fe_2Rh_4/SiO_2 catalyst after H_2 reduction at 400 °C. The spectrum for Fe_2Rh_4/SiO_2 is shown in Figure 9. Two absorption bands at 2058 and 1806 cm^{-1} are assigned to terminal and bridging CO on Rh atoms, respectively. The relative intensities of the bridging CO to terminal CO for $FeRh_5/SiO_2$ and Fe_2Rh_4/SiO_2 were appreciably suppressed compared to Fe-free Rh_4/SiO_2. This is possibly due to the isolation of Rh sites with Fe^0 and/or Fe^{3+}. Moreover, it is notable that a low-frequency band appeared at *ca.* 1630 cm^{-1} in the spectra of $FeRh_5/SiO_2$ and Fe_2Rh_4/SiO_2 (1628 cm^{-1} in Figure

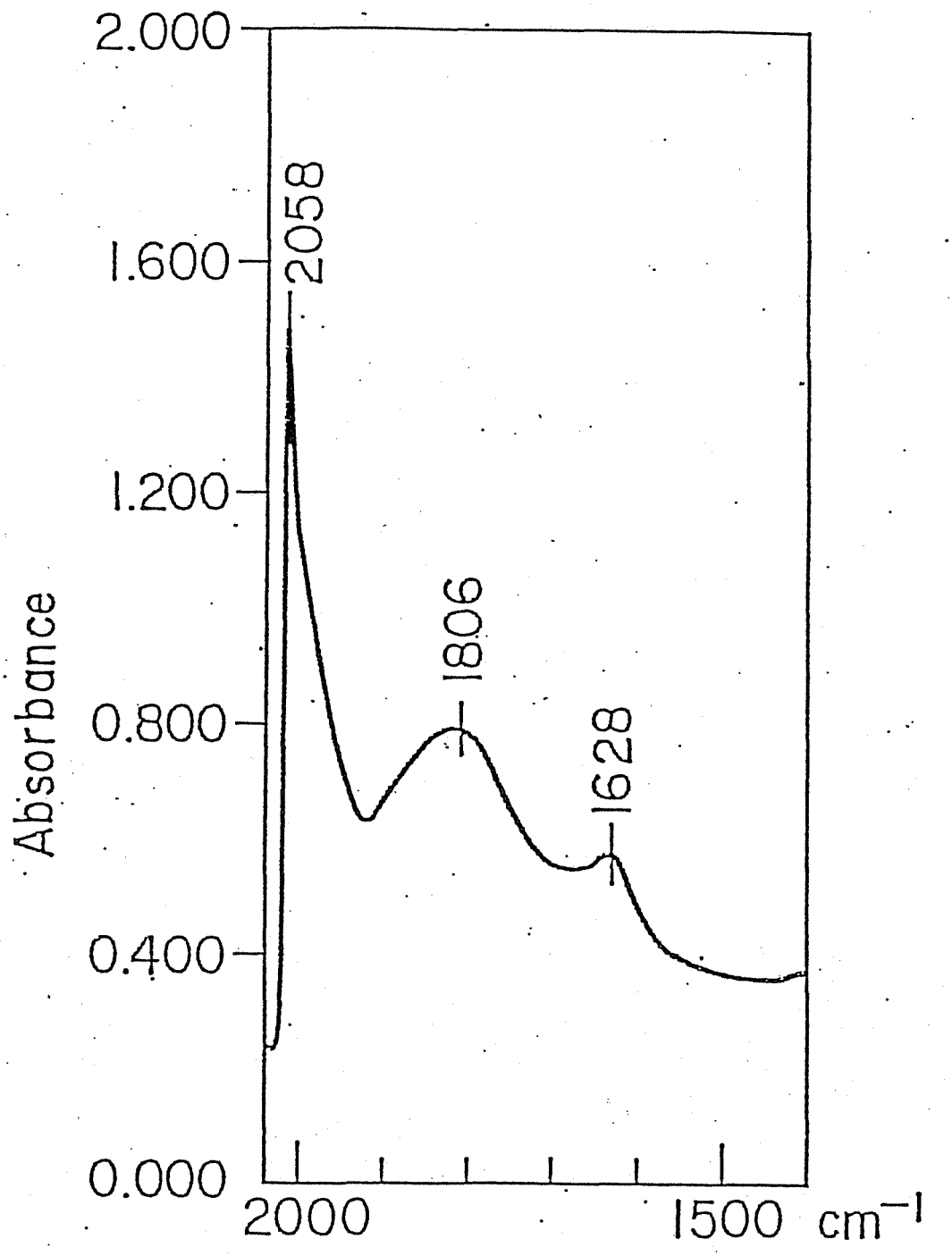

Figure 9. FTIR spectrum of CO chemisorption on H_2-reduced Fe_2Rh_4/SiO_2: H_2 reduction at 400 °C for 2 h, CO chemisorption at 25 °C and 22 Torr for 30 min. The background spectrum was obtained on the sample disk which had been reduced with H_2 but not exposed to CO.

9). This may arise from η^2-CO with the bonding of C-Rh and O-Fe^{3+} on the Rh-Fe^{3+} bimetallic sites. Such a low frequency band was not observed for Rh_4/SiO_2. It was previously suggested that similar bifunctional chemisorption of CO occurred on salt-derived Rh-Mn, Rh-Ti, and Rh-Zr/SiO_2 catalysts, where a large reduction of the CO frequency was induced.[37] Shriver *et al.*[50,51] demonstrate that the stoichiometric formation of adducts between carbonyl complexes and Lewis acids arises from C- and O-bonded CO, and that the rate of the methyl migration, *i.e.*, CO insertion, to form the acetyl complex in $Mn(CH_3)(CO)_5$ is greatly increased by the adduct formation with Lewis acids such as $AlBr_3$, BF_3, and γ-Al_2O_3 (Figure 10a-c).

By combining the FTIR data with the structural model (Figure 7) suggested by Mössbauer and EXAFS studies, it is conceivable that Fe promotion for alcohol production could be explained in terms of the two-site activation of CO with Rh-Fe^{3+} to enhance the migratory CO insertion into Rh-H and Rh-R (R = alkyl), and to enhance the successive hydrogenation to alcohols (Figure 11). Electropositive Fe^{3+} contiguous Rh atoms are located at the interface of Rh and SiO_2 may play a role not only to anchor Rh atoms to prevent their aggregation but also to affect catalytic performances to promote the oxygenate formation in CO hydrogenation and olefin hydroformylation. Similar two-site activation is suggested for the methanol production on Fe_3Pd_3, Fe_6Pd_6, and $FeIr_4$ cluster-derived catalysts.

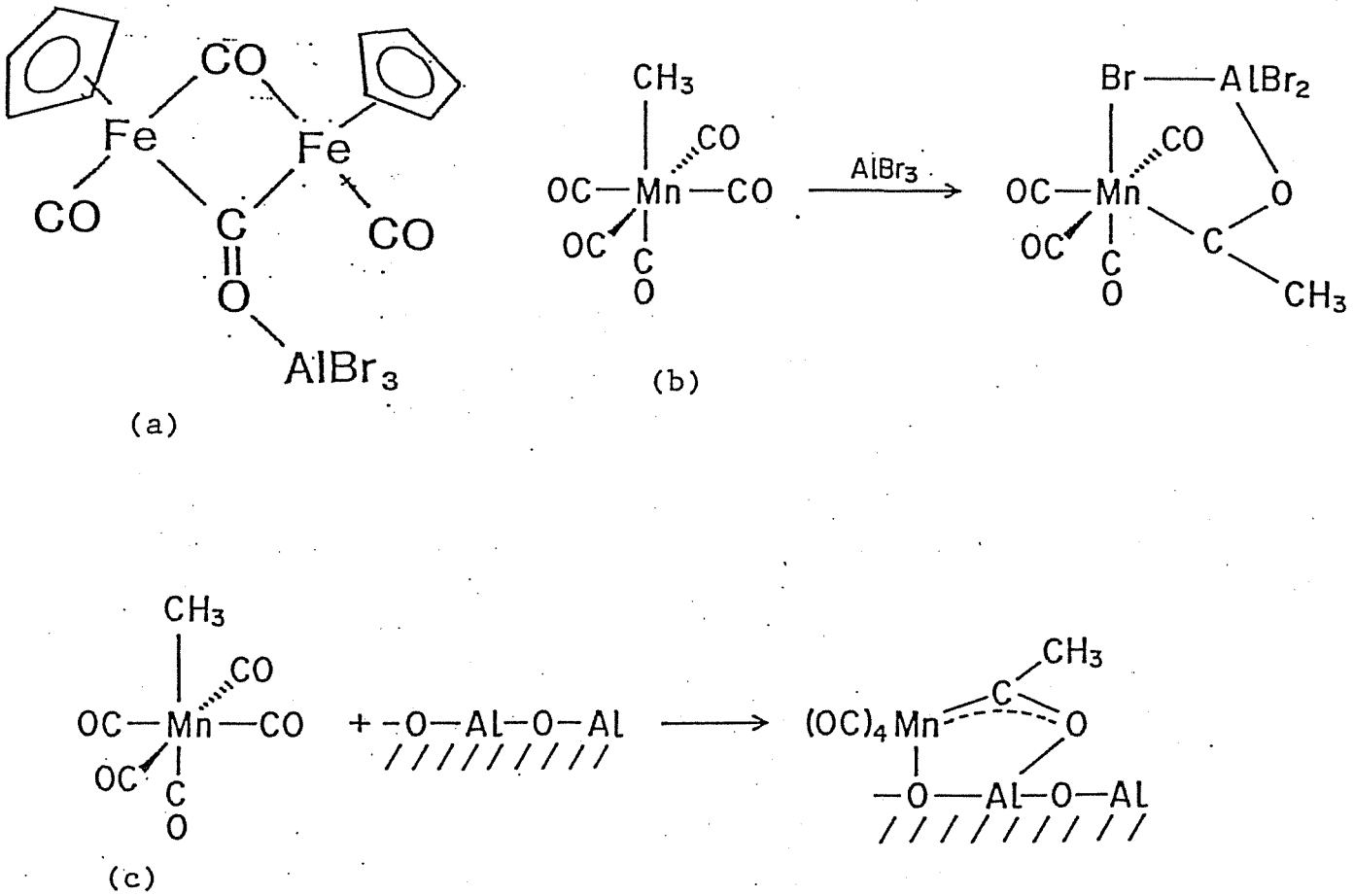

Figure 10. Adduct formation between metal carbonyls and Lewis acids: (a) $Cp_2Fe_2(CO)_4$ with $AlBr_3$, (b) $Mn(CH_3)(CO)_5$ with $AlBr_3$, and (c) $Mn(CH_3)(CO)_5$ with Al_2O_3. In (b) and (c), Lewis acids greatly enhance the methyl migration (CO insertion).

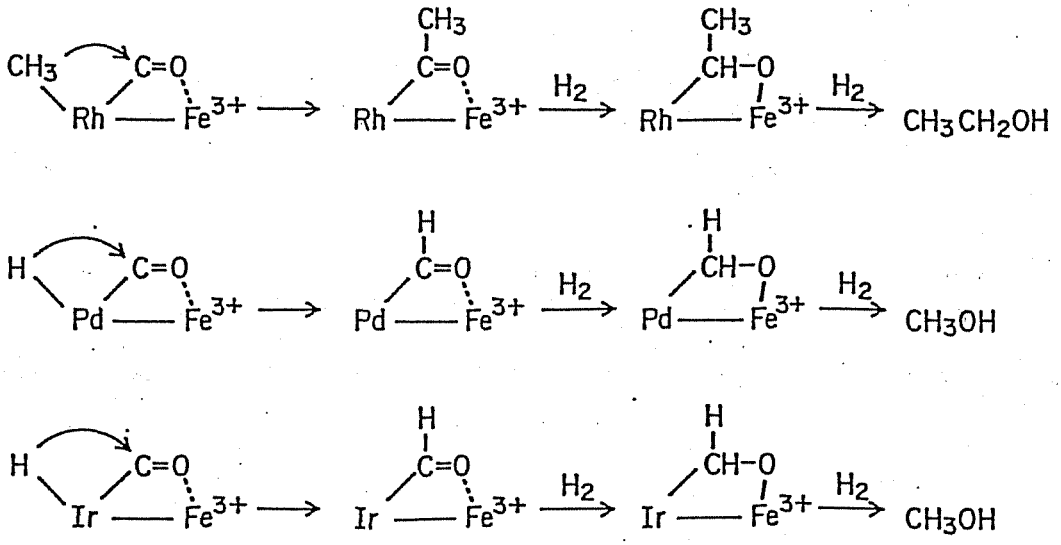

Figure 11. Two-site activation of CO on M-Fe^{3+}/SiO_2 (M = Rh, Pd, and Ir).

Conclusion

We have revealed the benefits of bimetallic carbonyl clusters as precursors for the preparation of tailored RhFe, PtFe, PdFe, and IrFe bimetallic catalysts. $RhFe/SiO_2$ catalysts derived from bimetallic clusters gave high activity and selectivity toward oxygenates, particularly toward ethanol in CO hydrogenation. PtFe, PdFe, and IrFe clusters with the atomic ratios of Fe/Pt = Fe/Pd = 1 and Fe/Ir = 0.25 provided the highly active catalysts for methanol production from syngas. The Fe-containing bimetallic catalysts effectively promote migratory CO insertion as judged by activity for olefin hydroformylation. This activity and selectivity may be due to the two-site interaction of C- and O-bonded CO on $M-Fe^{3+}$ sites (M = Rh, Pt, Pd, and Ir), which appear to be generated from bimetallic clusters supported on SiO_2.

References

1 E.L. Muetterties, T.N. Rhoudui, E. Band, C.F. Brucker, and W.R. Pretzer, *Chem. Rev.*, 79, 9 (1979).

2 M. Ichikawa, *CHEMTECH*, 674(1982).

3 M. Ichikawa, in *"Tailored Metal Catalysts"*, Y. Iwasawa ed., p. 183, D. Reidel Pub., Dordrecht 1986.

4 J.M. Basset and R. Ugo, in *"Aspects of Homogeneous Catalysis"*, R. Ugo ed., Vol. 3, p. 127, D. Reidel Pub., Dordrecht 1977.

5 Y.I. Yermakov, B.N. Kuznetsov, and V.A. Zakharov, *"Catalysis by Supported Complexes"*, Elsevier, Amsterdam 1981.

6 B.C. Gates, L. Guczi, and H. Knözinger eds., *"Metal Clusters in Catalysis"*, Elsevier, Amsterdam 1986.

7 J.M. Basset, B.C. Gates, J.P. Candy, A. Choplin, M. Leconte, F. Quignard, and C. Santini eds., *"Surface Organometallic Chemistry: Molecular Approaches to Surface Catalysis"*, Kluwer Academic Pub., Dordrecht 1988.

8 P. Braunstein and J. Rose, in *"Stereochemistry of Organometallic and Inorganic Compounds"*, I. Bernal Ed., Vol. 3, Elsevier, Amsterdam 1988.

9 J.H. Sinfelt, *Acc. Chem. Res.*, **10**, 15(1977); **20**, 134(1987).

10 T. Yokoyama, K. Yamazaki, N. Kosugi, H. Kuroda, M. Ichikawa, and T. Fukushima, *J. Chem. Soc., Chem. Commun.*, 962(1984).

11 A. Choplin, L. Huang, A. Theolier, P. Gallezot, J.M. Basset, U. Siriwardane, S.G. Shore, and R. Mathieu, *J. Am. Chem. Soc.*, **108**, 4224(1986).

12 J.R. Anderson and D.E. Mainwaring, *J. Catal.*, **35**, 162(1974).

13 J.R. Shapley, S.J. Hardwick, D.S. Foose, G.D. Stucky, M.R. Churchill, C. Bueno, and J.P. Hutchinson, *J. Am. Chem. Soc.*, **103**, 7383(1981).

14 Y. Iwasawa and M. Yamada, *J. Chem. Soc., Chem. Commun.*, 675(1985).

15 M. Castiglioni, R. Giodano, and E. Sappa, *J. Mol. Catal.*, **40**, 65(1987).

16 J.P. Scott, J.R. Budge, A.L. Rheingold, and B.C. Gates, *J. Am. Chem. Soc.*, **109**, 7736(1987).

17 L. Guczi, Z. Schay, K. Lazar, A. Vizi, and L. Marko, *Surf. Sci.*, 106, 516(1981).

18 V.L. Kuznetsov, A.F. Danilynk, I.E. Kolosova, and Y.I. Yermakov, *React. Kinet. Catal. Lett.*, 21, 249(1982).

19 H.E. Ferkul, D.J. Stanton, J.D. McCowen, and M.C. Baird, *J. Chem. Soc., Chem. Commun.*, 955(1982).

20 A. Choplin, M. Leconte, J.M. Basset, S.G. Shore, and W.-L. Hsu, *J. Mol. Catal.*, 21, 389(1983).

21 J.R. Budge, B.F. Lucke, B.C. Gates, and J. Toran, *J. Catal.*, 91, 272(1985).

22 M. Kaminsky, K.J. Yoon, G.L. Geoffroy, and M.A. Vannice, *J. Catal.*, 91, 338(1985).

23 M. Ichikawa, *J. Catal.*, 56, 127(1979); 59, 67(1979).

24 A. Fukuoka, H. Matsuzaka, M. Hidai, and M. Ichikawa, *Chem. Lett.*, 941(1987).

25 A. Fukuoka, M. Ichikawa, J.A. Hriljac, and D.F. Shriver, *Inorg. Chem.*, 26, 3643(1987).

26 P. Braunstein, R. Bender, and J. Kervennal, *Organometallics*, 1, 1236(1982).

27 W.M.H. Sachtler and M. Ichikawa, *J. Phys. Chem.*, 90, 4752(1986).

28 M.M. Bhasin, W.J. Bartley, P.C. Ellgen, and T.P. Wilson, *J. Catal.*, 54, 120(1978).

29 T. Fukushima, H. Arakawa, and M. Ichikawa, *J. Phys. Chem.*, 89, 4440(1985).

30 T. Fukushima, K. Araki, and M. Ichikawa, *J. Chem. Soc., Chem. Commun.*, 148(1986).

31 T. Fukushima, Y. Ishii, Y. Onda, and M. Ichikawa, *J. Chem. Soc., Chem. Commun.*, 1752(1985).

32 D.C. Koningsberger, C.P.J.H. Borgmans, A.M.J. van Elderen, B.J. Kip, and J.W. Niemantsverdriet, *J. Chem. Soc., Chem. Commun.*, 892(1987).

33 M. Ichikawa, T. Fukushima, T. Yokoyama, N. Kosugi, and H. Kuroda, *J. Phys. Chem.*, **90**, 1222(1986).

34 J.W. Niemantsverdriet, A.M. van der Kraan, and W.N. Delgass, *J. Catal.*, **89**, 138(1984).

35 Y. Minai, T. Fukushima, M. Ichikawa, and T. Tominaga, *J. Radioanal. Nucl. Chem.*, **87**, 189(1984).

36 J.W. Niemantsverdriet, J.A.C. van Kaam, C.F.J. Flipse, and A.M. van der Kraan, *J. Catal.*, **96**, 58(1985).

37 M. Ichikawa and T. Fukushima, *J. Phys. Chem.*, **89** 1564(1985).

38 P. Chini and S. Martinengo, *Inorg. Chim. Acta*, **3**, 315(1969).

39 H.A. Hodali and D.F. Shriver, *Inorg. Synth.*, **20**, 222(1980).

40 A. Ceriotti, G. Longoni, R.D. Pergola, B.T. Heaton, and D.O. Smith, *J. Chem. Soc., Dalton Trans.*, 1433(1983).

41 J.A. Hriljac, E.M. Holt, and D.F. Shriver, *Inorg. Chem.*, **26**, 2943(1987).

42 G. Longoni and P. Chini, *J. Am. Chem. Soc.*, **98**, 7225(1976).

43 G. Longoni, M. Manassero, and M. Sansoni, *J. Am. Chem. Soc.*, **102**, 7973(1980).

44 G. Longoni, M. Manassero, and M. Sansoni, *J. Am. Chem. Soc.*, **102**, 3242(1980).

45 L. Malatesta and G. Caglio, *J. Chem. Soc., Chem. Commun.*, 420 (1967).

46 A. Fumagalli, *private communication*.

47 B.-K. Teo and P.A. Lee, *J. Am. Chem. Soc.*, **101**, 2815(1979).

48 S. Iijima, K. Moriyama, A. Fukuoka, and M. Ichikawa, *unpublished results*.

49 H. Kuroda, T. Yokoyama, N. Kosugi, M. Ichikawa, and T. Fukushima, *J. de Phys.*, **47**, C8-301(1986).

50 S.B. Butts, E.M. Holt, S.H. Strauss, N.W. Alcock, R.E. Stimson, and D.F. Shriver, *J. Am. Chem. Soc.*, **101**, 5864(1979).

51 F. Correa, R. Nakamura, R.E. Stimson, R.L. Burwell, Jr., and D.F. Shriver, *J. Am. Chem. Soc.*, **102**, 5112(1980).

4-2

^{13}C AND ^{18}O LABELLING FTIR STUDIES ON C- AND O-ENDED CO CHEMISORPTION ON MANGANESE-PROMOTED RHODIUM/SILICA CATALYSTS

Summary

IR spectroscopic evidence demonstrates the low frequency band of C- and O-ended CO which interacts with Rh and promoter Mn ion on Rh-Mn/SiO_2 catalyst in the chemisorption and exchange of CO using ^{13}CO and $C^{18}O$.

Introduction

It has been reported previously that additive metal ions such as Mn, Ti, and Zr provide a great enhancement of the CO conversion rates on Rh/SiO_2 catalysts in a CO hydrogenation reaction to give high yields of C_2-oxygenates such as ethanol and acetic acid.[1] In fact, the bifunctional promotion of the additive metals is a subject of recent interest and debate.[2] Ichikawa *et al.* found low frequency IR bands in the CO chemisorption on Rh-Mn and Rh-Ti/SiO_2 catalysts,[3] and characterized it as activated CO on the promoted Rh. It has been proposed that the low frequency band arises from the CO chemisorbed in a tilted manner, *i.e.*, the carbon is bonded to two Rh atoms with the oxygen interacting with the promoter cations.[4] Such a low frequency band was observed in the CO chemisorption on cluster-derived RhFe/SiO_2 catalyst, as described in Section 4-1.

In this section, the further FTIR spectroscopic evidence are presented for the C- and O-ended CO on Rh-Mn/SiO_2 by using ^{13}CO and $C^{18}O$.

Experimental

Rh-Mn/SiO_2 (Rh:Mn = 1:2 atomic ratio, 4 wt% Rh loading) was prepared by co-impregnation of SiO_2 (Aerosil 300) with a methanol solution of $RhCl_3 \cdot 3H_2O$ and $MnCl_2 \cdot 4H_2O$. After removal of the solvent under vacuum, followed by reduction in flowing H_2 (1 atm, 100 ml/min) with programmed heating from 25 to 400 °C for 6 h, the resultant Rh-Mn/SiO_2 was pressed into a thin disk (20 mm ϕ, 25 mg) for mounting in the *in situ* IR cell. IR spectra were recorded on a Fourier transform double-beam infrared spectrometer (Shimadzu FTIR-4100) with a resolution of 2 cm^{-1}. ^{13}CO (98 % enriched) and $C^{18}O$ (90 % enriched) were purchased from MSD Isotope Co. and dried with Molecular Sieve 5A.

Results and Discussion

Upon admission of CO (150 Torr) at 25 °C on the freshly reduced Rh-Mn/SiO_2, a characteristic low frequency CO band (LF CO) appeared at 1713 cm^{-1} as well as the bands of the linear (at 2055 cm^{-1}) and bridging CO (at 1815 cm^{-1}), as shown in Figure 1. The relative rates of growth for each band on CO chemisorption at 25 °C on Rh-Mn/SiO_2 were in the following order: LF CO >> bridging CO > linear CO. This suggests that the CO species

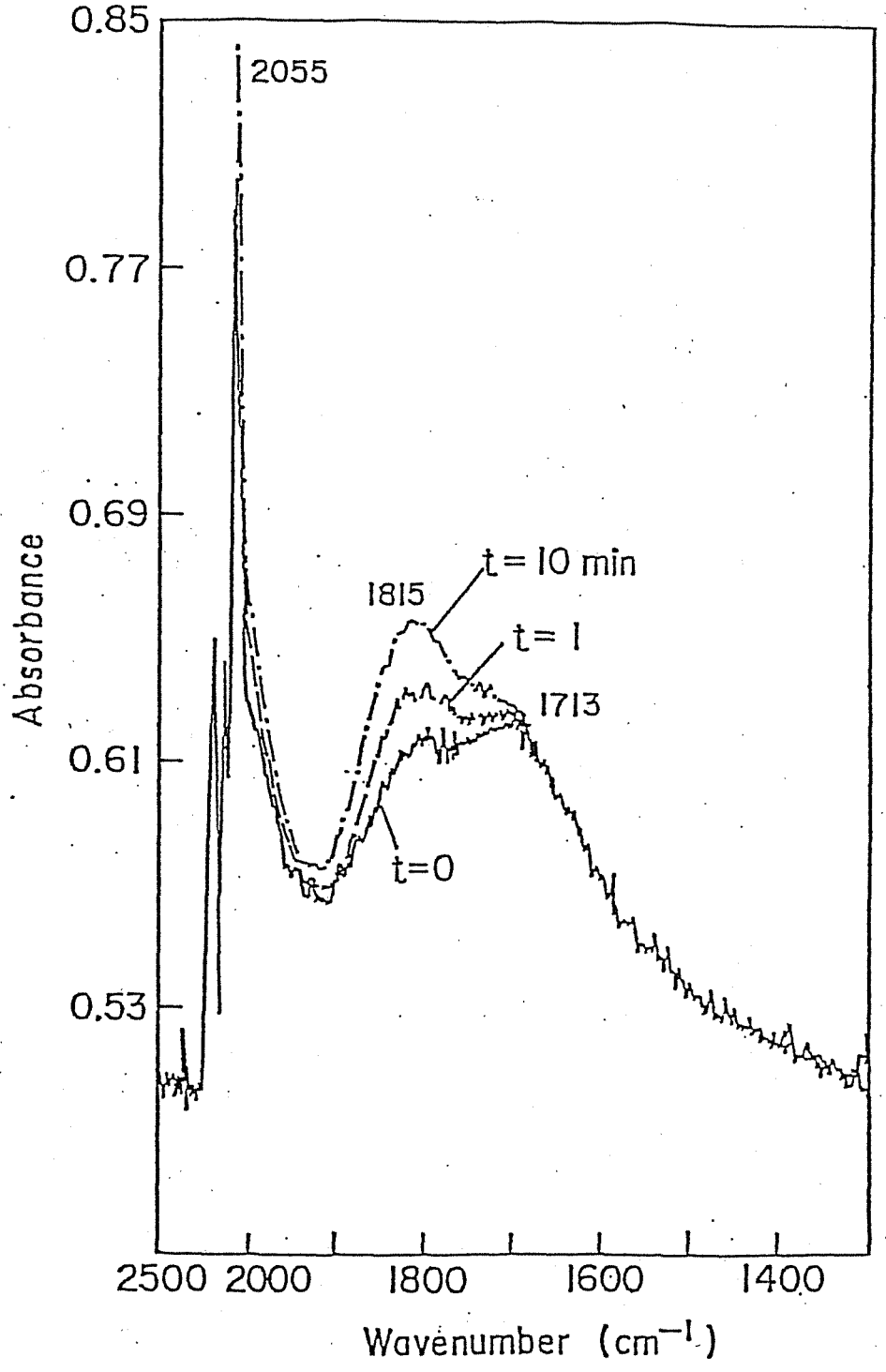

Figure 1. FTIR spectra of CO chemisorption on Rh-Mn/SiO_2 (Rh:Mn = 1:2) at 25 °C: CO 150 Torr. t = 0, 1, and 10 min are the time of CO admission on the H_2-reduced catalyst.

giving LF CO band is more activated with the Rh-Mn sites compared with the bridging and linear CO species.

In the FTIR spectrum of the chemisorption of ^{13}CO (50 Torr) at 25 °C on the H_2-reduced Rh-Mn/SiO_2 catalyst (Figure 2A), the bands at 2012 and 1770 cm^{-1} are assigned to linear and bridging ^{13}CO, respectively, with a shift of *ca.* 40 cm^{-1} from the bands on CO chemisorption due to the isotope effect. The LF ^{13}CO band was observed at 1670 cm^{-1} overlapping with the broad band of bridging ^{13}CO. It is notable that among the chemisorbed ^{13}CO, the linear and bridging ^{13}CO exchanged rapidly with gaseous ^{12}CO at 25 °C, while the LF ^{13}CO gave a very low rate of the exchange even at 50 °C. This indicates that the LF CO species has a stronger bonding with the Rh-Mn sites than do the linear and the bridging CO species. On chemisorption of $C^{18}O$ (25 Torr) at 25 °C (Figure 2B), we observed the bands at 2010 and 1797 cm^{-1} attributable to linear and bridging $C^{18}O$, respectively. Additionally, the broad band in the region of 1850-1650 cm^{-1} consists of two collapsed bands; a shoulder band is observed at *ca.* 1700 cm^{-1} which is similar position to that of LF $C^{16}O$. When $C^{16}O$ (150 Torr) was admitted onto the $C^{18}O$ chemisorbed Rh-Mn/SiO_2 at 25 °C (Figure 2C), the broad band was resolved into two bands; one for the bridging $C^{16}O$ at 1815 cm^{-1} and the other for the LF $C^{16}O$ at 1713cm^{-1} which is in good agreement with the bridging $C^{16}O$ and the LF $C^{16}O$ band observed in the $C^{16}O$ chemisorption on Rh-Mn/SiO_2 in Figure 1. Accordingly, it is proposed that the LF CO species is active for the facile exchange of oxygen possibly with promoter MnO on Rh-Mn/SiO_2 (see Figure 3). The formation of the

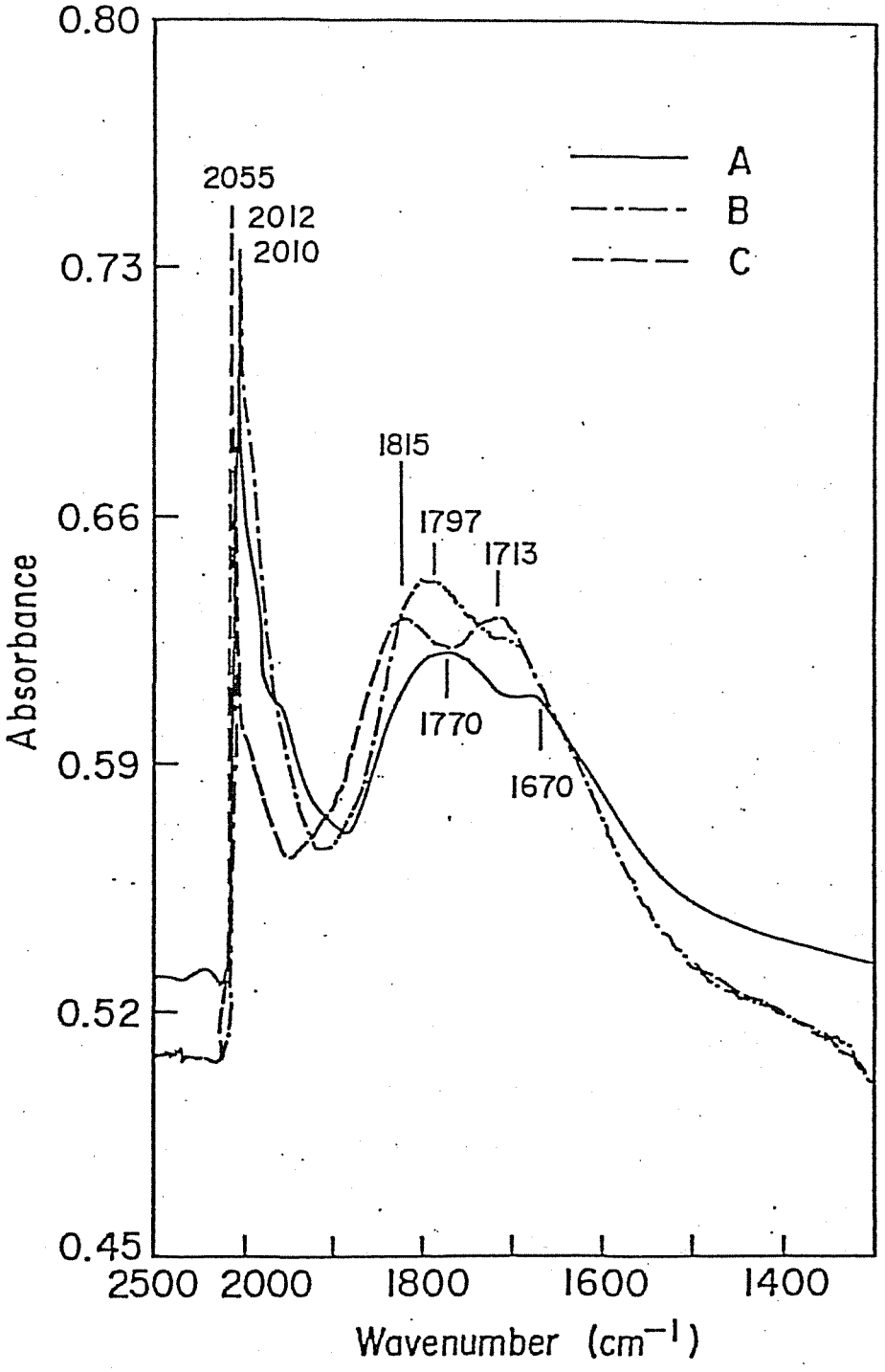

Figure 2. IR spectrum of ^{13}CO and $C^{18}O$ chemisorption on Rh-Mn/SiO_2 (Rh:Mn =1:2) at 25 °C.
A: ^{13}CO chemisorption, ^{13}CO = 50 Torr,
B: $C^{18}O$ chemisorption, $C^{18}O$ = 25 Torr,
C: admission of CO (150 Torr) on the $C^{18}O$ chemisorbed Rh-Mn/SiO_2 at 25 °C.

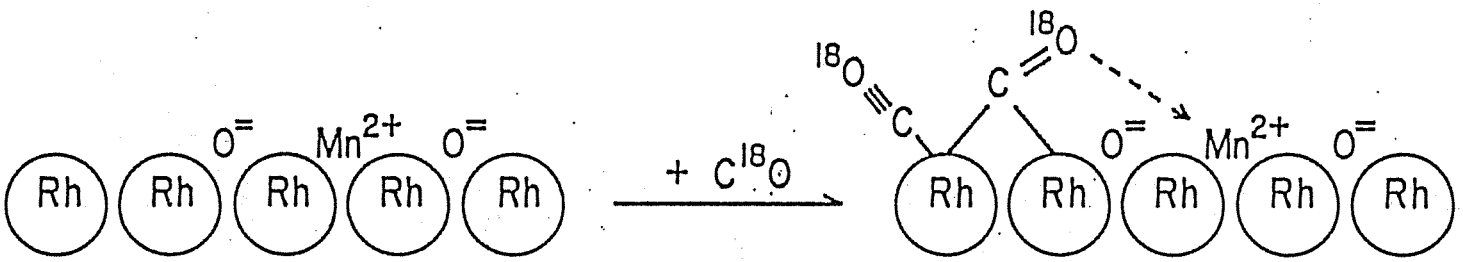

Figure 3. $C^{18}O$ chemisorption on $Rh\text{-}Mn/SiO_2$.

C- and O-ended CO on Rh-Mn/SiO_2 is suggested to promote the CO dissociation, resulting in the increase of CO conversion rates and high yields of C_2-oxygenates in the CO hydrogenation reaction.

References

1 T.P. Wilson, P.H. Kasai, and P.C. Ellgen, *J. Catal.*, **69**, 193 (1981); M. Ichikawa, K. Sekizawa, K. Shikakura, and M. Kawai, *J. Mol. Catal.*, 11, 167(1981).

2 J. Santos, J. Phillips, and J.A. Dumesic, *J. Catal.*, **81**, 147 (1983); C.S. Kellner and A.T. Bell, *ibid.*, 71, 296(1981); M.A. Vannice and C. Sudhakar, *J. Phys. Chem.*, 88, 2429(1984); M. Ichikawa, T. Fukushima, and K. Shikakura, *Proc. 8th Intnl. Congr. Catal.(Berlin)*, Vol II, 69(1984).

3 M. Ichikawa and T. Fukushima, *J. Phys. Chem.*, **89**, 1564(1985).

4 W.M.H. Sachtler, *Proc. 8th Intnl. Congr. Catal.(Berlin)*, Vol I, 151(1984); W.M.H. Sachtler and M. Ichikawa, *J. Phys. Chem.*, **90**, 4752(1986).

CHAPTER 5

SYNTHESIS, CHARACTERIZATION, AND CATALYSIS OF RHODIUM, IRON, RHODIUM-IRON, IRIDIUM, AND RHODIUM-IRIDIUM CARBONYL CLUSTERS ENTRAPPED IN SODIUM-Y ZEOLITE

CHAPTER 5

SYNTHESIS, CHARACTERIZATION, AND CATALYSIS OF RHODIUM, IRON, RHODIUM-IRON, IRIDIUM, AND RHODIUM-IRIDIUM CARBONYL CLUSTERS ENTRAPPED IN SODIUM-Y ZEOLITE

Summary

A series of monometallic and bimetallic carbonyl clusters comprising Rh, Fe, RhFe, Ir, and RhIr were prepared by the reductive carbonylation of small precursors introduced into NaY framework. EXAFS and FTIR results suggest that $Rh_6(CO)_{16}$, $[HFe_3(CO)_{11}]^-$, $Rh_xFe_y(CO)_z$, $Ir_6(CO)_{16}$, and $Rh_{6-x}Ir_x(CO)_{16}$ (x = 2 and 3) were formed uniformly in the framework. H_2 reduction of the carbonyl clusters resulted in the formation of small metal particles less than 10 Å in size with the similar metal compositions to those of the original carbonyl clusters; their structure and electronic states were studied by means of EXAFS and FTIR. H_2-reduced Rh_6/NaY catalyst gave C_2-C_4 olefins in CO hydrogenation at an atmospheric pressure, whereas Rh_xFe_y/NaY bimetallic catalyst showed a unique activity for the formation of ethanol and methanol. In hydroformylations of ethylene and propylene, Rh_6/NaY gave aldehydes as the main oxygenated products. By contrast, Rh_xFe_y/NaY exhibited higher rates for alcohols with an improved n/iso ratio. The promotion role of the bimetallic catalysts is discussed.

Introduction

Mono- and bimetallic carbonyl clusters have been used as precursors for the preparation of metal particles less than 10 Å in size with the metal composition of original clusters.[1-3] The structural characterization of the cluster-derived catalysts has been conducted by using extended X-ray absorption fine structure (EXAFS),[4,5] infrared (IR),[6-8] X-ray photoelectron spectroscopy (XPS),[9,10] and transmission electron microscopy (TEM)[11,12]. In some instances, the cluster-derived catalysts provide advantages of high activity and improved selectivity over conventional salt-derived metal catalysts.[13-20] In catalytic CO hydrogenation and olefin hydroformylation, remarkable Fe-promotion for alcohol production has been reported on SiO_2-supported RhFe, PdFe, and IrFe cluster-derived catalysts.[21-23] The Fe-promotion is proposed to be associated with bimetallic M-Fe^{3+} (M = Rh, Pd, Ir) sites to enhance migratory CO insertion.

In order to improve the selectivity of products on supported metal catalysts, zeolites have been used as supports to impose a shape selectivity on the catalysis[24] or to control the performance through metal particle size effects.[25]

In this section, we report the *"ship-in-a-bottle"* synthesis of Rh_6, Rh_xFe_y, Ir_6, and RhIr carbonyl clusters in the framework of NaY zeolite. The diameters of a supercage and a cage aperture are *ca.* 13 Å and 7 Å, respectively.[26] We introduced small subcarbonyls or metal ions into the framework, and reductive carbonylation of the precursors led to the formation and

encapsulation[27,28] of carbonyl clusters with diameters of *ca.* 10 Å in the zeolite framework. Structural characterization of those entrapped clusters and cluster-derived metal catalysts was investigated by means of EXAFS, and FTIR. CO hydrogenation and hydroformylations of ethylene and propylene were carried out to probe the catalysis of NaY entrapped Rh_6 and Rh_xFe_y cluster-derived metal particles.

Experimental

Catalysts

Rh^{3+} on NaY (Rh^{3+}-NaY) was prepared by the ion-exchange of NaY (Linde LZ-Y52, 1 g) with an aqueous solution of $RhCl_3 \cdot 3H_2O$ (0.2 mmol) at 90 °C for 12 h.[29-31] The loading of Rh was 2 wt%. After dried at 110 °C overnight, Rh^{3+}-NaY was exposed to the vapor of water (*ca.* 15 Torr) for several hours, and reductive carbonylation of the hydrated Rh^{3+}-NaY under CO (600 Torr) at 120 °C led to the pale gray sample. An FTIR spectrum of this sample gave a band at 1760 cm^{-1}, which was characteristic of $Rh_6(CO)_{16}$.[32] We shall use the notation $Rh_6(CO)_{16}$/NaY for this sample. $[HFe_3(CO)_{11}]^-$/NaY (3.5 wt% Fe) (pink-purple) were prepared by the reaction of $Fe_2(CO)_9$ with hydrated NaY at 70 °C.[33] Rh_xFe_y bimetallic carbonyl cluster ($Rh_xFe_y(CO)_z$/NaY, pale red-brown) was prepared by the reaction between $[HFe_3(CO)_{11}]^-$/NaY and $Rh_4(CO)_{12}$ *in vacuo* at 80-100 °C. On the other hand, the reaction of $Rh_6(CO)_{16}$/NaY with $Fe_2(CO)_9$ at 70 °C resulted in the formation of a mixture of $Rh_6(CO)_{16}$ and $[HFe_3(CO)_{11}]^-$ in the

zeolite: $Rh_6(CO)_{16}+[HFe_3(CO)_{11}]^-/NaY$, RhFe bimetallic clusters were not formed from $Rh_6(CO)_{16}/NaY$ and $Fe_2(CO)_9$.

The reaction of ion-exchanged Ir^{4+}-NaY, derived from $IrCl_4 \cdot H_2O$, with $CO+H_2$ (1:2 molar ratio, 1 atm) at 200 °C gave $Ir_6(CO)_{16}/NaY$.[32] $Rh_{6-x}Ir_x(CO)_{16}/NaY$ (x = 2,3) were prepared according to the preparation of $Rh_6(CO)_{16}/NaY$ and $Ir_6(CO)_{16}/NaY$; the ion-exchanged NaY was obtained from the aqueous solution of $RhCl_3 \cdot 3H_2O$ and $IrCl_4 \cdot H_2O$ mixture at the ratios of Rh:Ir = 4:2 and 3:3. The total metal atoms were 4 mmol per 1 g of zeolite. The reductive carbonylation of the resulting sample under $CO+H_2$ (1:2, 1 atm) at 200 °C for 24 h led to the formation of the corresponding bimetallic carbonyl clusters: $Rh_4Ir_2(CO)_{16}$ and $Rh_3Ir_3(CO)_{16}$.

H_2-reduced samples were obtained by the oxidation of carbonyl clusters in NaY with O_2 at 200 °C, followed with the reduction in flowing H_2 at 200 °C. The reduced samples are abbreviated to Rh_6/NaY, Fe_3/NaY, Rh_6+Fe_3/NaY, and Rh_xFe_y/NaY.

Characterization

Infrared spectra were obtained from the disk in *in situ* cells with KBr or CaF_2 windows. The spectra were acquired on a double-beam Fourier transform infrared spectrometer (Shimadzu FTIR-4100) at a resolution of 2 cm^{-1}. Generally, 25-50 interferograms were coadded to improve signal-to-noise ratios.

Extended X-ray absorption fine structure (EXAFS) spectra were obtained from the disk in *in situ* cells with Kapton film windows. The spectra were acquired at 25 °C on the synchrotron

radiation source of Beam Line-10B in the Photon Factory of the National Laboratory for High Energy Physics (KEK-PF). Analysis of the EXAFS data were performed with Program EXAFS-1 and EXAFS-2.[35] Coordination numbers and interatomic distances were determined by using the data of standard materials: foils of Rh and Fe, $Rh_6(CO)_{16}$, $Fe_3(CO)_{12}$, Ir powder, and $Ir_4(CO)_{12}$.

Catalytic Reactions

CO hydrogenation reactions were conducted at 196-250 °C with an open flow-mode glass reactor where 0.6 g of the catalyst (total metal loading 2 wt%) was charged. After the H_2 reduction at 200 °C for 2 h, a gas mixture of CO and H_2 ($CO:H_2$ = 1:1 molar ratio, 1 atm) was introduced into the reactor at a flow rate of 20 ml/min. Oxygenated products such as methanol, acetaldehyde, and ethanol were collected in a water trap (H_2O 25 ml) by bubbling the effluent gas. Products were analyzed by gas chromatography. CO, CO_2, and C_1-C_5 hydrocarbons were separated by a Shimadzu GC-8AIT gas chromatograph with a thermal conductivity detector; a 4 mmϕ x 1 m of active carbon (60-80 mesh) column at room temp. for the separation of CO, CO_2, and CH_4, a 4 mmϕ x 4 m of Porapak Q (60-80 mesh) column at 70 °C for C_2H_4 and C_2H_6, a 4 mmϕ x 4 m of *N,N*-dimethylformamide/Al_2O_3 (DMF 38 %, 60-80 mesh) column at room temp. for C_3-C_5 hydrocarbons. The concentrations of gaseous products in the off-gas were calibrated with external standards by using a 5 ml of gas sampler. The analysis of oxygenated products dissolved in the water trap was performed on a Shimadzu GC-8APF gas chromatograph

with a flame ionization detector using a 4 mmϕ x 4 m Chromosorb 101 (60-80 mesh) column at 135 °C, and acetone was added as an internal standard to calibrate the concentration of oxygenates. In each gas chromatography, the amounts of the products were calculated with an integrator (Shimadzu Chromatopac CR-3A).

Hydroformylation reactions of ethylene and propylene were carried out with the same procedures as those of the CO hydrogenation. A gas mixture of C_2H_4 (or C_3H_6), CO, and H_2 (1:1:1 molar ratio, total pressure 1 atm) was flowed into the reactor at a flow rate of 20 ml/min. The products were analyzed by gas chromatography; C_2H_4 and C_2H_6 were separated on the Porapak Q column (4 mmϕ x 4 m) in the TCD-GC at 70 °C, and C_3H_6 and C_3H_8 on the DMF/Al_2O_3 column (4 mmϕ x 4 m) at room temp.. The products of hydroformylation of ethylene such as propanal and 1-propanol were separated on the Chromosorb 101 (4 mmϕ x 4 m) at 150 °C. The products of hydroformylation of propylene such as butanal, 2-methylpropanal, 1-butanol, and 2-methylpropanol were separated on the same column at 155 °C. Ethanol was used as an internal standard.

Results and Discussion

Synthesis and Characterization of $Rh_6(CO)_{16}$/NaY, Rh_6/NaY, and $Rh_xFe_y(CO)_z$/NaY

As shown in Figure 1, $Rh_6(CO)_{16}$/NaY (1) showed IR peaks of terminal carbonyls at 2098(s) and 2060(w) cm^{-1} and a peak of face-bridging carbonyl at 1760(m) cm^{-1}. Since the peak positions

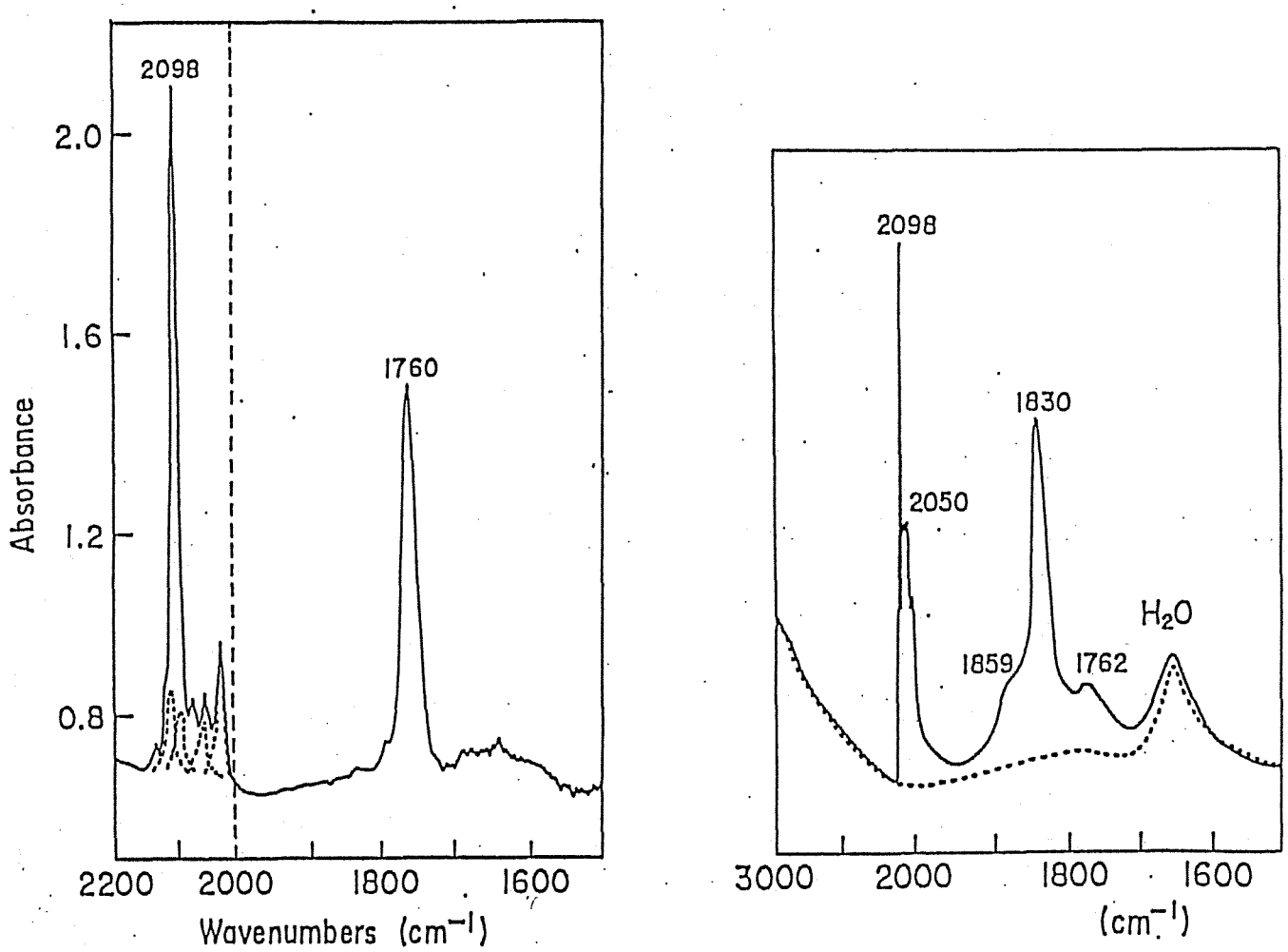

Figure 1. FTIR spectra of $Rh_6(CO)_{16}$ (a) and Rh_6/NaY(200)+CO (b).

of $Rh_6(CO)_{16}$ crystalline in nujol are 2070(s), 2022(mw), 2020(mw), and 1798(s) cm^{-1},[36] the bridging CO shifted to lower position by 38 cm^{-1} and the terminal COs to higher positions by 20-40 cm^{-1}. Presumably, the peak shifts are ascribed to the interaction of the carbonyls with Al^{3+} or H^+ located on the cage wall.[32] We attempted to prepare $Rh_6(CO)_{16}$ on the external surface of NaY by the deposition of $[Rh(CO)_2Cl]_2$ onto the surface and the successive carbonylation under CO at 100 °C. The resulting sample has the bridging CO at 1805 cm^{-1}, which is almost the same position as that of $Rh_6(CO)_{16}$ crystalline. Thus $Rh_6(CO)_{16}$ on the NaY surface seems to have negligible interaction with Al^{3+} or H^+ in contrast to (1) where $Rh_6(CO)_{16}$ is surrounded closely by the cage wall. Accordingly, the above FTIR results strongly suggest the formation of $Rh_6(CO)_{16}$ in the NaY framework. In addition, the spectrum of (1) in Figure 1 contains the peaks of two weak doublets shown as dotted lines;[37] the peaks at 2098 and 2022 cm^{-1} are the symmetric and asymmetric CO stretching of $Rh^I(CO)_2(O_z)_2$ and the peaks at 2114 and 2048 cm^{-1} are of $Rh^I(CO)_2(O_z)(H_2O)$, where O_z denotes zeolite framework oxygen.[29] In the region of terminal carbonyls in the IR spectrum, the total contribution of the two doublets is estimated at about 15-20 %. Therefore, 80-85 % of Rh ions were converted to $Rh_6(CO)_{16}$ in the framework of NaY zeolite.

The Fourier transforms of the k^3-weighted Rh *K*-edge EXAFS $k^3\chi(k)$ of (1) and reduced Rh_6/NaY are shown in Figure 2, and the results of curve-fitting analysis are summarized in Table 1. In the Fourier transform of (1), a major peak at *ca.* 2.5 Å is

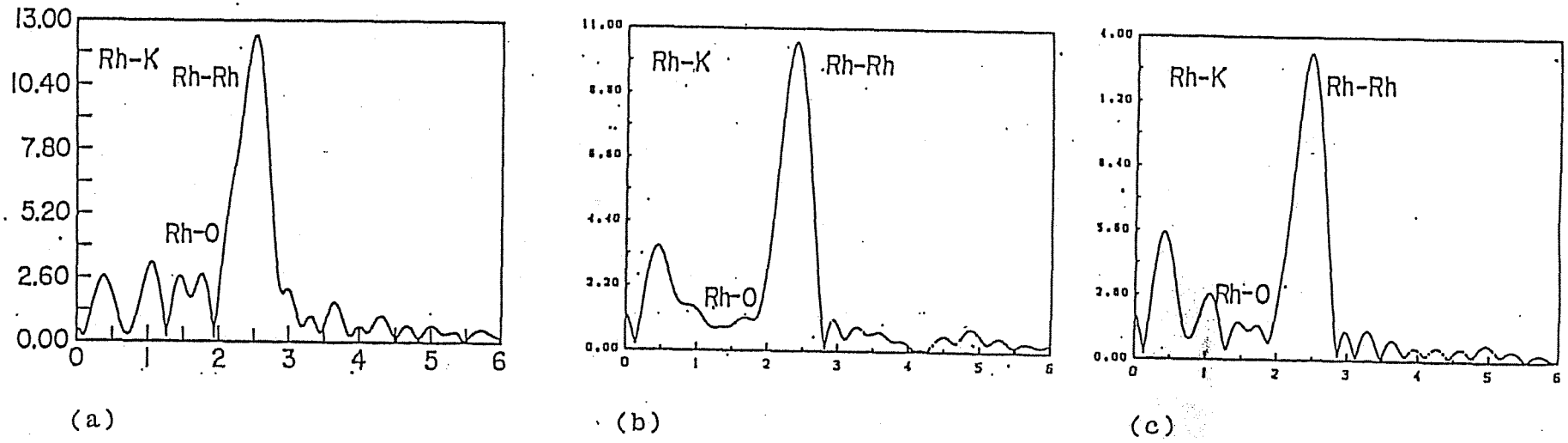

Figure 2. Fourier transforms of $k^3\chi(k)$ of $Rh_6(CO)_{16}$ (a), Rh_6/NaY(200) (b), and Rh_6/NaY(200)+CO (c).

Table 1. Results of the Curve-Fitting Analysis of $k^3\chi(k)$ of Rh_6 Clusters/NaY

Sample	*Rh*-*C*O(terminal) C.N.	R (Å)	*Rh*-*C*O(bridge) C.N.	R (Å)	Rh-O(support) C.N.	R (Å)	Rh-Rh C.N.	R (Å)
$Rh_6(CO)_{16}$/NaY (1)	1.5	1.88	1.6	2.15	1.9	2.06	3.1	2.74
Rh_6/NaY (200) (2)	-	-	-	-	0.7	2.10	4.6	2.70
Rh_6/NaY (400) (3)	-	-	-	-	0.7	2.09	4.6	2.70
Rh_6/NaY (200) + CO (4)	1.4	1.85	1.4	2.15	0.8	2.03	3.2	2.72
$Rh_6(CO)_{16}$ crystalline	2.1	1.97	2.0	2.17	-	-	4.0	2.76

attributed to Rh-Rh. From the curve-fitting analysis of the peak, the interatomic distance (R) is 2.74 Å and the coordination number (C.N.) is 3.1. The first and the second neighbor Rh-C interactions of Rh-CO are also observed and they correspond to Rh-CO(terminal) and Rh-CO(bridging), respectively, Rh-CO(terminal): R = 1.88 Å, C.N. = 1.5; Rh-CO(bridging): R = 2.15 Å, C.N. = 1.6. The results of curve-fitting analysis of (1) are fairly in good agreement with those of $Rh_6(CO)_{16}$ crystalline used as a standard (Rh-Rh: R = 2.76 Å, C.N. = 4.0; Rh-CO(terminal): R = 1.87 Å, C.N. = 2.1; Rh-CO(bridging): R = 2.17 Å, C.N. = 2.0). Therefore, the EXAFS data confirm the formation of $Rh_6(CO)_{16}$. In addition, the contribution of Rh-O was observed in (1) possibly due to $Rh^I(CO)_2(O_z)_2$ and $Rh^I(CO)_2(O_z)(H_2O)$; Rh-O: R = 2.06 Å, C.N. = 1.9. Gallezot *et al.* also suggested the formation of $Rh_6(CO)_{16}$ in the zeolite supercage by using radial electron distribution derived from X-ray scattering and IR.[38]

After O_2-oxidation of (1) at 200 °C to eliminate carbonyl ligands and the successive H_2-reduction at 200 °C or 400 °C, the reduced samples Rh_6/NaY (200) (2) and Rh_6/NaY (400) (3) were obtained. From EXAFS study on (2) and (3) (Table 1), the interatomic distance of Rh-Rh is 2.70 Å and the coordination number is 4.6, which substantiated the retention of a framework of Rh-Rh as small as a Rh_6 cluster without the aggregation of Rh atoms. (2) chemisorbed CO and H_2 at 25 °C with stoichiometries of CO/Rh = 2.0 and H/Rh = 0.6. The FTIR spectrum of CO chemisorbed (2) (Rh_6/NaY (200) + CO, (4)) has a bridging peak at

1830 cm^{-1} (Figure 1), which seems to be a edge-bridging carbonyl in $Rh_4(CO)_{12}$.[37] However, *in situ* FTIR study showed that (4) converted to (1) by the reaction with $CO+H_2$ (1:1, 1 atm) at 150 °C. The EXAFS data of (4) gave similar interatomic distance and coordination number to those of (1) (Table 1). We suggest that (4) is $Rh_6(CO)_{12}(\mu_2\text{-}CO)_4$ with edge-bridging carbonyls stabilized in the supercage, although the edge-bridging isomer of $Rh_6(CO)_{16}$ has not been isolated. Ir has the same d^9 configuration as Rh, and $Ir_6(CO)_{16}$ exists in two isomeric forms: $Ir_6(CO)_{12}(\mu_3\text{-}CO)_4$ and $Ir_6(CO)_{12}(\mu_2\text{-}CO)_4$.[42] Consequently, the Rh_6 clusters are stabilized in the zeolite framework through oxidation and reduction without the formation of large metal particles migrating onto the surface:

$$\underset{(1)}{Rh_6(CO)_{16}/NaY} \xrightarrow[-\,CO_2]{+\,O_2} [Rh_6]_{ox}/NaY \xrightarrow[-\,H_2O]{+\,H_2} \underset{(2),(3)}{Rh_6/NaY}$$

$$\xrightarrow{+\,CO} \underset{(4)}{Rh_6(CO)_{12}(\mu_2\text{-}CO)_4/NaY} \xrightarrow[150\,^\circ C]{+\,CO/H_2} \underset{(1)}{Rh_6(CO)_{12}(\mu_3\text{-}CO)_4/NaY}$$

$[HFe_3(CO)_{11}]^-$ was entrapped in the NaY zeolite by the reaction of $Fe_2(CO)_9$ and hydrated NaY. We attempted to extract $[HFe_3(CO)_{11}]^-$ formed on the external surface of NaY as ammonium salts by washing the sample with a tetraglyme solution of bulky ammonium halides such as $[N(n\text{-}C_6H_{13})_4]Br$ and $[NMe_3(CH_2Ph)]Cl$. However, the concentration of $[HFe_3(CO)_{11}]^-$ in the extracted solution was very low; the amounts of the anion cluster on the surface was estimated below 1 % based on Fe. The analysis of EXAFS at Fe *K*-edge of $[HFe_3(CO)_{11}]^-/NaY$ is shown in Table 2.

Table 2. Results of the Curve-Fitting Analysis of $k^3\chi(k)$ of $[HFe_3(CO)_{11}]^-/NaY$

Sample	*Fe-C*O C.N.	R (Å)	Fe-O C.N.	R (Å)	Fe-Fe C.N.	R (Å)
$[HFe_3(CO)_{11}]^-/NaY$	0.8	1.81	1.6	2.09	1.8	2.58
$[HFe_3(CO)_{11}]^-$	2.3	1.81	-	-	2.2	2.62

RhFe bimetallic carbonyl clusters were attempted to prepare in NaY framework. Longoni *et al.* reported the synthesis and characterization of a series of RhFe carbonyl clusters such as $[NMe_3(CH_2Ph)][FeRh_5(CO)_{16}]$ and $[NMe_3(CH_2Ph)]_2[Fe_2Rh_4(CO)_{16}]$, where the redox condensation of $[Fe_3(CO)_{11}]^{2-}$ with $Rh_4(CO)_{12}$ or $[Rh(CO)_2Cl]_2$ was used.[39] Ballivet-Tkatchenko *et al.* suggested that $[HFe_3(CO)_{11}]^-$/NaY was deprotonated and converted to $[Fe_3(CO)_{11}]^{2-}$ by heating at 70-120 °C.[40] Thus, in our study, the reaction between $[HFe_3(CO)_{11}]^-$/NaY and $Rh_4(CO)_{12}$ was chosen for the preparation of RhFe carbonyl clusters in NaY.

The IR spectrum of the resulting $Rh_xFe_y(CO)_z$/NaY (5) is shown in Figure 3, coupled with the spectra of $[NMe_3(CH_2Ph)]_2[Fe_2Rh_4(CO)_{16}]$ deposited onto the NaY surface and in acetonitrile. (5) has terminal carbonyls at 2078(s) and 2020(m) cm^{-1}, and bridging carbonyls at 1744(m) and 1711(m) cm^{-1}, which are very similar to the peak positions of $[Fe_2Rh_4(CO)_{16}]^{2-}$ deposited on NaY. As described in the preparation of $[HFe_3(CO)_{11}]^-$/NaY, $[HFe_3(CO)_{11}]^-$ does not migrate from the framework to the external surface at 70 °C *in vacuo*. Consequently, $[HFe_3(CO)_{11}]^-$ might react with small Rh carbonyls derived from $Rh_4(CO)_{12}$ to form the RhFe bimetallic carbonyl cluster in the NaY framework. *In situ* FTIR spectra of (5) showed that the O_2 oxidation at room temperature led to the elimination of carbonyls, and that after the H_2 reduction at 200 °C (5) was regenerated by the reaction with $CO+H_2O$ at 120 °C. Further investigation on the composition of $Rh_xFe_y(CO)_z$/NaY is now under way.

Synthesis and Characterization of $Ir_6(CO)_{16}$/NaY and $Rh_{6-x}Ir_x(CO)_{16}$/NaY (x = 2,3)

Since Ir has the same d electron configuration (d^9) as does Rh, and $Ir_6(CO)_{16}$ and $Rh_6(CO)_{16}$ are known to have the same octahedral framework structure, we attempted to prepare $Ir_6(CO)_{16}$ and RhIr bimetallic clusters in NaY zeolite. Up to date tetranuclear $Rh_2Ir_2(CO)_{12}$ and $Rh_3Ir(CO)_{12}$ are known as RhIr bimetallic carbonyl clusters,[41] but hexanuclear RhIr bimetallic clusters have not been reported.

NaY-zeolite entrapped Ir_6 and $Rh_{6-x}Ir_x$ carbonyl clusters were prepared from the ion-exchanged samples with Ir^{4+} and/or Rh^{3+}. Figure 4 shows IR spectra of the cluster/NaY and Table 3 summarizes their characteristic frequencies. The sample from Ir^{4+}-NaY gave carbonyl peaks at 2099(s), 2060(w), 2038(w), and 1733(m) cm^{-1}, which resemble the peaks of the red isomer of $Ir_6(CO)_{16}$ crystalline with four face-bridging carbonyls reported by Garlaschelli *et al.*.[42] As found in $Rh_6(CO)_{16}$/NaY, the face-bridging CO shifted to lower position by *ca.* 30 cm^{-1}, possibly due to the interaction with the cage wall. In preliminary Ir *L*-edge EXAFS study on this sample (Table 4), the interatomic distance and the coordination number of Ir-Ir are 2.71 Å and 3.8. The above FTIR and EXAFS data suggest the formation of $Ir_6(CO)_{16}$ in NaY.

Likewise, the reductive carbonylation of Rh^{3+}+Ir^{4+} on NaY with the Rh:Ir ratios of 4:2 and 3:3 was conducted. The IR spectra of the resulting samples are shown in Figure 4, and the carbonyl frequencies are summarized in Table 3. The peak in the

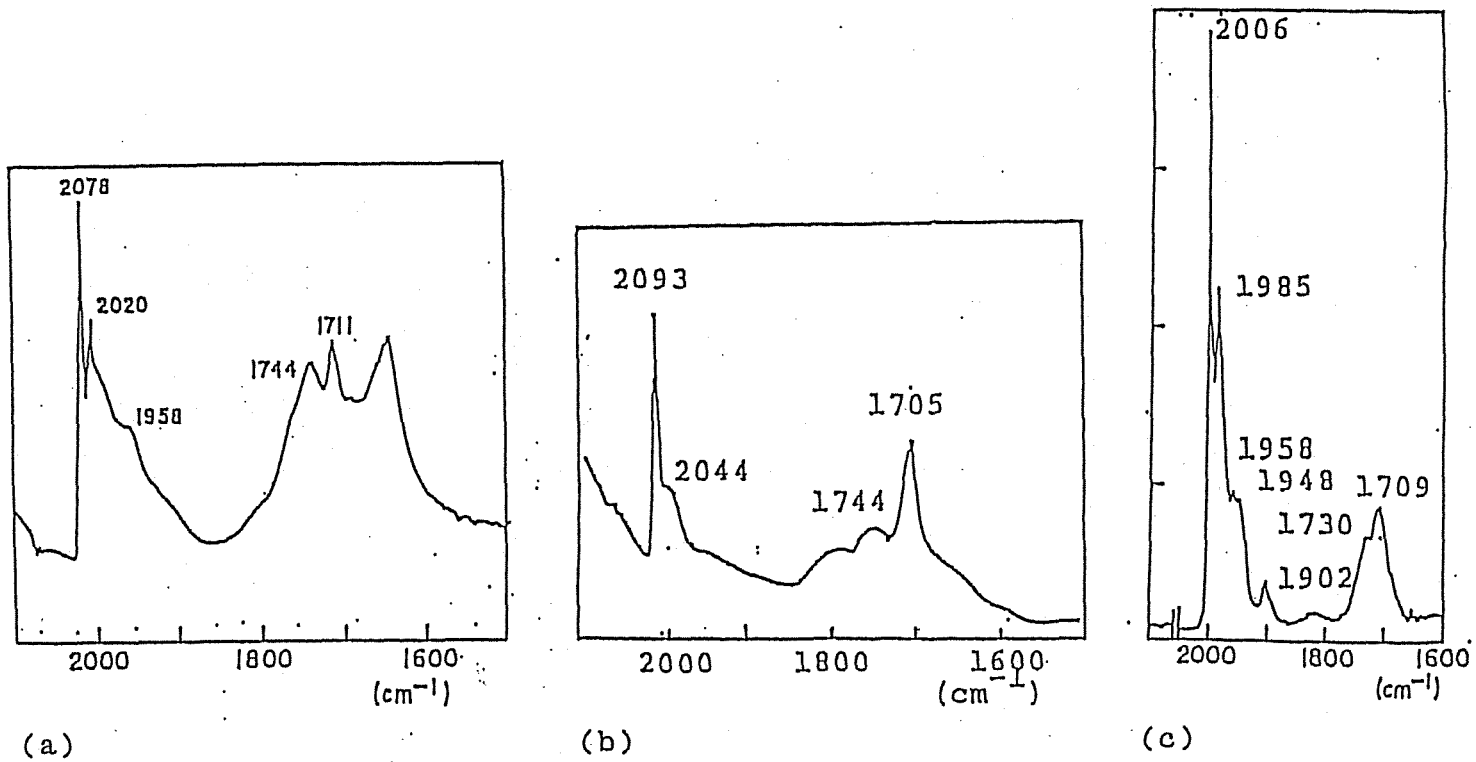

Figure 3. FTIR spectra of $Rh_xFe_y(CO)_z$/NaY (a), $[NMe_3(CH_2Ph)]_2[Fe_2Rh_4(CO)_{16}]$ deposited on NaY (b), and $[NMe_3(CH_2Ph)]_2[Fe_2Rh_4(CO)_{16}]$ in acetonitrile (c).

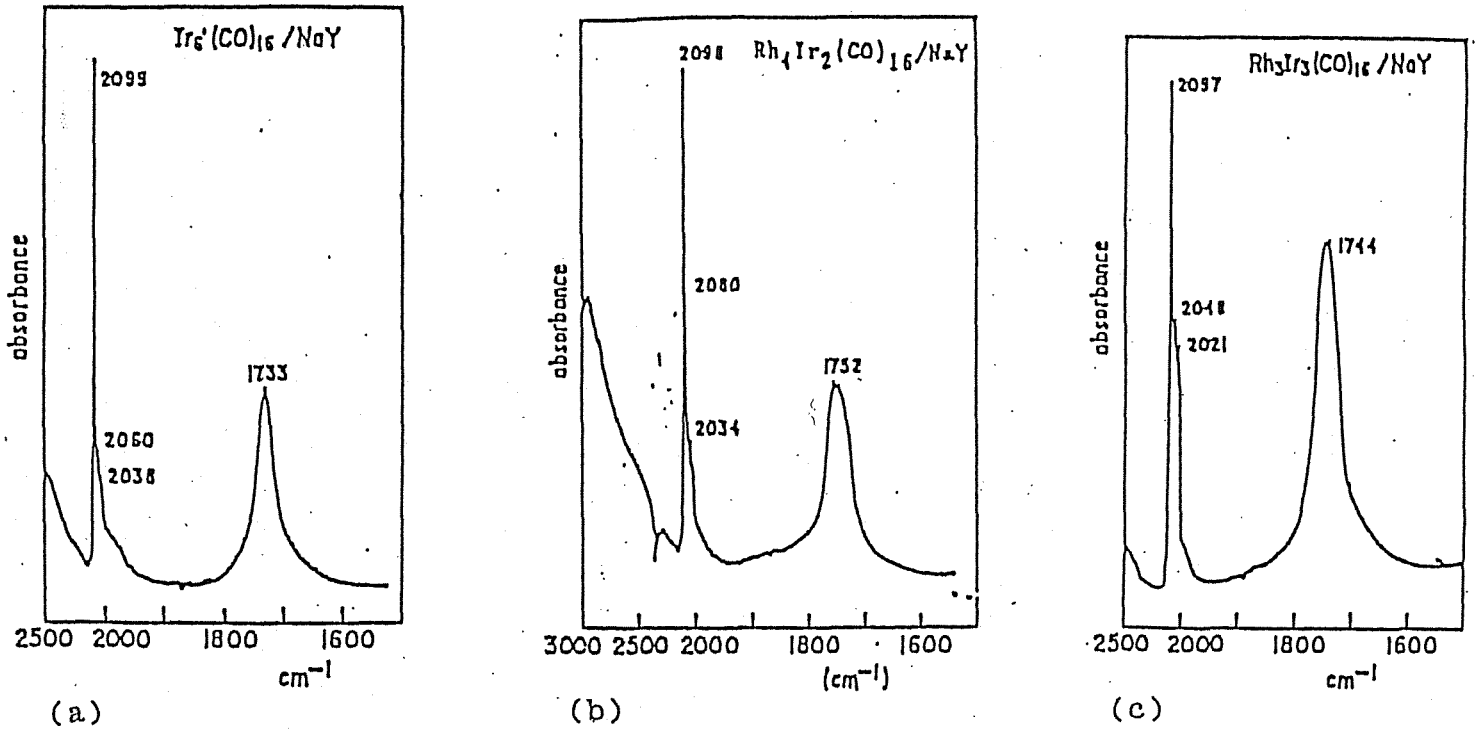

Figure 4. FTIR spectra of $Ir_6(CO)_{16}$/NaY (a), $Rh_4Ir_2(CO)_{16}$/NaY (b), and $Rh_3Ir_3(CO)_{16}$/NaY (c).

Table 3. Carbonyl Frequencies in cm^{-1} of $Rh_6(CO)_{16}$/NaY, $Rh_{6-x}Ir_x(CO)_{16}$/NaY, and $Ir_6(CO)_{16}$/NaY.

sample	terminal			edge bridging	face bridging	BWHH[a]
$Rh_6(CO)_{16}$/NaY	2098(s)	2060(w)			1760(m)	38
$Rh_5Ir(CO)_{16}$/NaY	2099(s)	2060(w)			1756(m)	42
$Rh_4Ir_2(CO)_{16}$/NaY	2098(s)	2062(w)	2036(w)		1752(m)	43
$Rh_3Ir_3(CO)_{16}$/NaY	2097(s)	2048(w)	2021(w)		1744(m)	45
$Ir_6(CO)_{16}$/NaY	2099(s)	2060(w)	2038(w)		1733(m)	41
$Rh_6(CO)_{16}$[b]	2105(w)	2070(s)	2047(sh)			
	2040(w)	2022(mw)	2020(mw)		1798(s)	
$Ir_6(CO)_{16}$[c] red isomer	2115(w)	2076(s)	2064(sh)			
	2036(mw)	2004(mw)			1765(s)	40
black isomer	2105(w)	2070(sh)	2058(s)	1850(m)		
	2040(m)	2012(m)	1995(mw)	1832(m)		

[a] Band width at half height of face-bridging CO.

[b] Nujol, *ref.*, L. Malatesta, G. Caglio, and M. Angoletta, *J. Chem. Soc., Chem. Commun.*, 532(1970).

[c] Nujol, *ref.*, L. Garlaschelli, S. Martinengo, P.L. Bellon, F. Demartin, M. Manassero, M.Y. Chiang, C. Wei, and R. Bau, *J. Am. Chem. Soc.*, 106, 6664(1984).

region of bridging carbonyls in the sample of $Rh^{3+}:Ir^{4+}$ = 3:3 is at 1744 cm^{-1}, intermediate between those of $Rh_6(CO)_{16}$/NaY (1760 cm^{-1}) and $Ir_6(CO)_{16}$/NaY (1733 cm^{-1}). On the other hand, the peak positions of terminal carbonyls were less sensitive to the metal compositions. Preliminary EXAFS study on this sample at Rh *K*-edge and Ir *L*-edge shows the substantial contribution of Rh-Ir bond (Table 4). From above FTIR and EXAFS study, $Rh_3Ir_3(CO)_{16}$ seems to be formed without the formation of a mixture of $Rh_6(CO)_{16}$ and $Ir_6(CO)_{16}$ in the zeolite.

Catalysis of Rh_6/NaY and Rh_xFe_y/NaY in CO Hydrogenation and Olefin Hydroformylation

The results of the CO hydrogenation by cluster/zeolite catalysts are shown in Table 5. Rh_6/NaY (2) gave higher activity for the formation of olefin-rich C_2-C_4 hydrocarbons at the CO conversion of 2-5 % than did the conventional Rh/SiO_2 derived from $RhCl_3 \cdot 3H_2O$. A small amount of acetaldehyde was also obtained. The CO conversion and the selectivity toward C_2-C_4 olefins were maintained for 40 h. The pattern of olefin and paraffin produced in C_1-C_5 range was not like a typical Schulz-Flory distribution. Products with chain lengths >C_4 were drastically diminished on (2), and there was a sharp maximum at C_3. The high selectivity toward C_2-C_4 olefins on (2) are proposed to be associated not only with controlling molecular-shape of the zeolite framework, but also with limiting the size of Rh particles less than 10 Å. We assume that the small Rh particles in the zeolite depress the hydrogenation activity,

Table 4. Results of the Curve-Fitting Analysis of $k^3\chi(k)$ of metal-metal bonding in $Rh_6(CO)_{16}$/NaY, $Ir_6(CO)_{16}$/NaY and $Rh_3Ir_3(CO)_{16}$/NaY.

	Rh *K*-edge				Ir *L*-edge			
	Rh-Rh		Rh-Ir		Ir-Ir		Ir-Rh	
Sample	C.N.	R (Å)	C.N.	R (Å)	C.N.	R (Å)	C.N.	R (Å)
$Rh_6(CO)_{16}$/NaY[a]	3.1	2.74						
$Ir_6(CO)_{16}$/NaY[b]					3.8	2.71		
$Ir_4(CO)_{12}$[c]					2.2	2.68		
$Ir_6(CO)_{16}$/NaY[c]					2.2	2.69		
$Rh_3Ir_3(CO)_{16}$/NaY[c]	0.8	2.72	0.2	2.74	1.4	2.73	0.8	2.81

[a] Empirical parameters derived from Rh foil are used.
[b] Empirical parameters derived from $Ir_4(CO)_{12}$ are used.
[c] Theoretical parameters presented by Teo and Lee are used. B.-K. Teo and P.A. Lee, *J. Am. Chem. Soc.*, 101, 2815(1979); 99, 3854(1977); 99, 3856(1977).

Table 5. CO hydrogenation on Rh_6/NaY, Rh_6+Fe_3/NaY, and Rh_xFe_y/NaY.[a]

catalyst[b]	Reaction temp.(°C)	CO conv. (%)	hydrocarbons specific rate of formation[c]					C_2-C_4 sel.(%)	C_3H_6/C_3H_8 ratio[d]	oxygenates specific rate of formation[c]			
			CH_4	C_2	C_3	C_4	C_5			MeOH	MeCHO	EtOH	PrOH
Rh_6/NaY	196	0.48	10.8	3.8	7.0	3.7	tr.	58.9	4.7	0	0.12	0	0
	225	2.0	40.0	11.9	21.1	11.9	tr.	52.9	4.0	0	2.11	0	0
	250	5.3	124	28.7	50.2	28.8	1.2	46.8	1.5	0	2.18	0	0
Rh_6+Fe_3/NaY	225	1.4	24.9	5.6	19.2	4.9	tr.	54.4	6.3	0	2.66	0.19	0
Rh_xFe_y/NaY	196	0.26	4.3	0.6	1.0	tr.	tr.	27.1	7.8	0.88	0.76	1.4	tr.
	225	0.83	18.7	4.0	4.6	1.2	tr.	34.4	3.8	0.54	1.4	3.0	tr.
Rh/SiO_2[e]	225	0.42	9.2	0.8	1.2	tr.	0	18.4	0.82	0	tr.	0	0
	250	2.3	51	2.6	4.1	tr.	0	11.8	0.42	0	tr.	tr.	0

[a]Reaction conditions: CO:H_2 = 1:1 (molar ratio), 1 atm, flow rate 20 ml/min.
[b]0.6 g, 2 wt% Rh.
[c]Specific rate of formation in mmol/$mmol_{Rh}$/min.
[d]Molar ratio of propylene to propane.
[e]$RhCl_3$ on SiO_2, H_2 reduction at 400 °C for 2 h.

because they chemisorb CO strongly but H_2 weakly: CO/Rh = 2.0 and H/Rh = 0.6 for Rh_6/NaY, CO/Rh = 0.32 and H/Rh = 0.43 for Rh/SiO_2. This is reflected in the high olefin/paraffin ratio of hydrocarbons produced. In this connection, it has been reported that Ru crystallites[43] derived from Ru carbonyls and Co (or Fe) particles[44] of size <12 Å in NaY gave a distribution of lower olefins centered on C_4 at low conversion (less than 1 %) in the CO hydrogenation.

Interestingly, Rh_xFe_y/NaY (6) prepared by the H_2-reduction of (5) gave high rates for oxygenates mainly consisting of ethanol and methanol in the CO hydrogenation. On the other hand, the rates for hydrocarbons on (6) are reduced compared with those on (2). To clarify the origin of promotion for alcohol formation on (6), a mixture of $Rh_6(CO)_{16}$ and $[HFe_3(CO)_{11}]^-$ were prepared by the reaction of pre-synthesized $Rh_6(CO)_{16}$/NaY with $Fe_2(CO)_9$, where $Rh_6(CO)_{16}$ and $[HFe_3(CO)_{11}]^-$ were located independently in the zeolite framework. The resulting sample (7) showed an IR spectrum apparently consisting of simple addition of peaks of $Rh_6(CO)_{16}$/NaY and $[HFe_3(CO)_{11}]^-$/NaY. The reduced catalyst Rh_6+Fe_3/NaY (8) derived from (7) preferentially gave olefin-rich C_2-C_4 hydrocarbons with a small amount of acetaldehyde and ethanol, and the product distribution was almost the same as that with (2). The results suggest that the improved formation of ethanol and methanol on (6) is related to the existence of adjacent Rh-Fe bimetallic sites in the NaY framework which activate CO insertion and successive hydrogenation to alcohols, as has been reported in the CO hydrogenation catalyzed on RhFe

cluster-derived catalysts on SiO_2.[22]

In order to ravel the promotion effect for alcohol production on Rh_xFe_y/NaY catalysts, hydroformylations of ethylene and propylene were performed as diagnostic reactions to evaluate CO insertion and successive hydrogenation in elementary steps of CO hydrogenation.

The results of hydroformylation of ethylene and propylene at atmospheric pressure are presented in Table 6. Activity and selectivity were measured after several hours, when the catalytic performance had reached a stationary state. Propanal was only obtained in ethylene hydroformylation on Rh_6/NaY (2). At higher temperatures, a small amount of 2-methyl-2-pentanal was formed, probably due to aldol condensation catalyzed by acidic zeolite surface. *In situ* FTIR study showed that Rh_6/NaY was converted to $Rh_6(CO)_{16}$/NaY under the conditions of ethylene hydroformylation at 150 °C. Rode *et al.*[32] have previously conducted the hydroformylation of propylene on the ion-exchanged Rh^{3+}/NaY at 1 atm and 150 °C, and found a formation of $Rh_6(CO)_{16}$ during the hydroformylation.

Interestingly, the bimetallic Rh_xFe_y/NaY catalysts (6) gave higher rates for aldehyde and alcohol than did Rh_6/NaY, while keeping the rates of simple hydrogenation of ethylene and propylene similar to rates on (2). Thus the selectivity toward oxygenates on (6) was increased compared with (2); 23 % on (6) and 52 % on (2) in ethylene hydroformylation. Notably, (6) effectively improved the selectivity toward alcohols as well as n/iso ratio; the selectivity toward normal-alcohol was improved

Table 6. Hydroformylation of Ethylene and Propylene on Rh_6/NaY and Rh_xFe_y/NaY catalysts.[a]

catalyst/NaY	olefin	reaction temp.	specific rates of formation,[b] min^{-1}				selectivity		
			C_2H_6	EtCHO + n-PrOH	C_3H_8	n,i-PrCHO[c] + n,i-BuOH[d]	oxygenates[e] mol %	aldehyde/alcohol % ratio[f]	n/iso ratio[g]
Rh_6	ethylene	150 °C	0.074	0.022			23	96/4	
Rh_6+Fe_3	ethylene	150 °C	0.081	0.029			26	97/3	
Rh_xFe_y	ethylene	150 °C	0.076	0.080			52	64/36	
Rh_6	propylene	175 °C			0.034	0.0038	10	92/8	1.3
Rh_6+Fe_3	propylene	175 °C			0.038	0.0057	13	89/11	1.3
Rh_xFe_y	propylene	175 °C			0.030	0.016	35	19/81	2.0

[a] Flow rate, olefin+CO+H_2 = 20+20+20 ml/min; total pressure, 1 atm.
[b] $mmol/mmol_{Rh}/min$.
[c] n-PrCHO = butanal, i-PrCHO = 2-methylpropanal.
[d] n-BuOH = 1-butanol, i-BuOH = 2-methylpropanol.
[e] (EtCHO + n-PrOH)/(C_2H_6 + EtCHO + n-PrOH) x 100 or (n,i-PrCHO + n,i-BuOH)/(C_3H_8 + n,i-PrCHO + n,i-BuOH) x 100.
[f] EtCHO/n-PrOH or n,i-PrCHO/n,i-BuOH, % molar ratio.
[g] (butanal + 1-butanol)/(2-methylpropanal + 2-methylpropanol), molar ratio.

on (6). By contrast, $[HFe_3(CO)_{11}]^-$/NaY was completely inactive for both hydroformylation and simple hydrogenation to paraffins under the reaction conditions. The mixture Rh_6+Fe_3/NaY (8) provided almost the same activity and selectivity as those on (2) in ethylene and propylene hydroformylation reactions.

These results imply that the RhFe bimetallic sites are essential for the promotion of hydroformylation activity and alcohol formation. Such Fe promotion could be explained in terms of the enhancement of CO insertion by C- and O-bonded CO activation. *In situ* FTIR spectrum of (6) in a flowing gas under the conditions of ethylene hydroformylation is shown in Figure 5, where the background spectrum of C_2H_4+CO+H_2 on NaY was subtracted. The new peak was observed at 1584 cm^{-1}, which was not obtained in the spectrum of $Rh_6(CO)_{16}$/NaY under the conditions of propylene hydroformylation (150 °C, 1 atm) reported by Rode *et al.*.[32] There are two possible species to assign this peak. One is η^2-acyl Rh-C(R)O-Fe formed *via* two-site activation on Rh-Fe bimetallic sites. Recently, Wolczanski *et al.* reported an A-frame type Rh-Zr complex with $\mu_2:\eta^2$-acetyl (ν_{CO} = 1490 cm^{-1}).[45] The other is carboxylates formed by the interaction of acyl intermediates with the cage oxide (or entrapped water).[46,47] In this case, the acyl formation through the CO insertion was improved on the Rh-Fe sites, and the acyl was stabilized on the cage wall in the form of carboxylates. It was proposed that the peaks at 1578 and 1419 cm^{-1} of Rh/NaX under the conditions of propylene hydroformylation were ascribed to carboxylates derived from the absorption of butanal on Al_2O_3 of

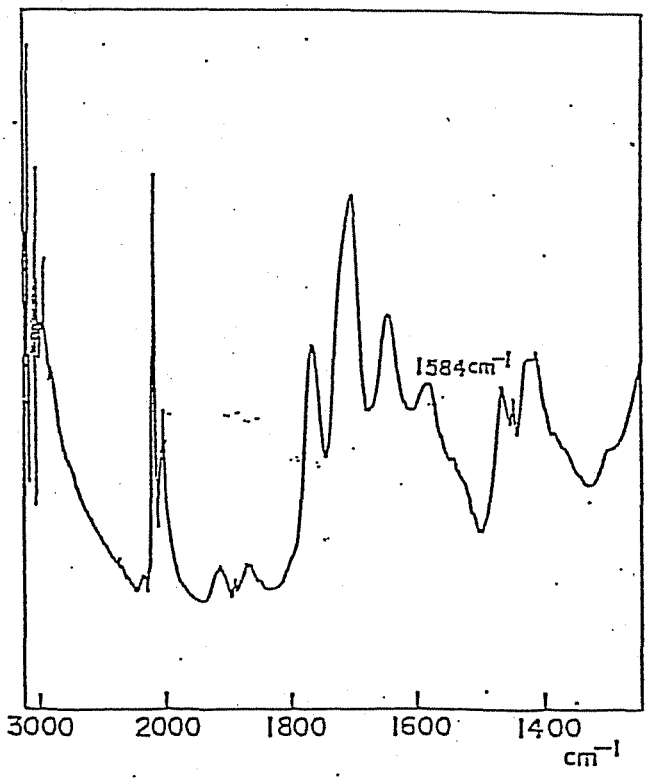

Figure 5. *In situ* FTIR spectrum of Rh_xFe_y/NaY under the conditions of ethylene hydroformylation: 150 °C; $C_2H_4+CO+H_2$ (1:1:1) gas, flow rate = 60 ml/min, 1 atm.

the cage wall.[32]

In propylene hydroformylation on (6), a high n/iso ratio of C_4-aldehydes and alcohols was achieved. Since such regioselectivity was not observed when SiO_2-supported RhFe bimetallic catalysts and $Rh_4(CO)_{12}/SiO_2$ are compared,[22] the promotion of Fe for the normal-alcohols in this instance would be explained by the geometric environment around the RhFe bimetallic sites in the NaY framework, favoring n-alkyl and n-acyl intermediates in the hydroformylation of propylene.

Conclusion

Rh, RhFe, Ir, and RhIr carbonyl clusters were prepared by "*ship-in-a-bottle*" synthesis in NaY framework. FTIR and EXAFS data strongly suggest the formation of $Rh_6(CO)_{16}$, $Rh_xFe_y(CO)_z$, $Ir_6(CO)_{16}$, and $Rh_{6-x}Ir_x(CO)_{16}$.

RhFe/NaY catalyst gave a high activity for C_1-C_2 alcohols from syngas and a high selectivity toward 1-butanol in propylene hydroformylation. Bimetallic RhFe sites generated in NaY activate CO insertion and successive hydrogenation to alcohols.

References

1 B.C. Gates, L. Guczi and H. Knözinger, eds., *"Metal Clusters in Catalysis"*, Elsevier, Amsterdam, 1986.

2 M. Ichikawa, in *"Tailored Metal Catalyst"*, Y. Iwasawa ed., D. Reidel Pub., Dordrecht, 1985, p.183

3 J.M. Basset, in *"Industrial Applications of Homogeneous Catalysis"*, A. Mortreux and F. Petit eds., D. Reidel Pub., Dortrecht, 1988, p. 293.

4 T. Yokoyama, H. Yamazaki, N. Kosugi, H. Kuroda, M. Ichikawa, and T. Fukushima, *J. Chem. Soc., Chem. Commun.*, 962(1984).

5 V.D. Alexiev, N. Binsted, J. Evans, G.N. Greaves, and R.J. Price, *J. Chem. Soc., Chem. Commun.*, 395(1987); N. Binsted, J. Evans, G.N. Greaves, and R.J. Price, *Organometallics*, **8**, 613(1989).

6 M. Deeba and B.C. Gates, *J. Catal.*, **67**, 303(1981).

7 A.K. Smith, B. Besson, J.M. Basset, R. Psaro, A. Fusi, and R. Ugo, *J. Organomet. Chem.*, **192**, C31(1980).

8 J.J. Venter and M.A. Vannice, *J. Am. Chem. Soc.*, **109**, 6204(1987); **111**, 2377(1989).

9 M. Ichikawa, K. Sekizawa, K. Shikakura, and M. Kawai, *J. Mol. Catal.*, **11**, 167(1981); M. Kawai, M. Uda, and M. Ichikawa, *J. Phys. Chem.*, **89**, 1654(1985).

10 B.G. Frederick, G. Apai, and T.N. Rhodin, *J. Am. Chem. Soc.*, **109**, 4797(1987).

11 S. Iijima and M. Ichikawa, *J. Catal.*, **94**, 313(1985).

12 A. Choplin, L. Huang, A. Theolier, P. Gallezot, J.M. Basset, U. Siriwardane, S.G. Shore, and R. Mathieu, *J. Am. Chem. Soc.*, **108**, 4224(1986).

13 J.R. Anderson and D.E. Mainwaring, *J. Catal.*, **35**, 162(1974).

14 M. Ichikawa, *J. Catal.*, **59**, 67(1979); *CHEMTECH*, 674(1982).

15 J.R. Shapley, S.J. Hardwick, D.S. Foose, G.D. Stucky, M.R. Churchill, C.Bueno, and J.P. Hutchinson, *J. Am. Chem. Soc.*,

103, 7383(1981).

16 L. Guczi, Z. Schay, K. Lazar, A. Vizi, and L. Marko, *Surf. Sci.*, **106**, 516(1981).

17 V.L. Kuznetsov, A.F. Danilynk, I.E. Kolosova, and Y.I. Yermakov, *React. Kinet. Catal. Lett.*, **21**, 249(1982).

18 A. Choplin, M. Leconte, J.M. Basset, S.G. Shore, and W.-L. Hsu, *J. Mol. Catal.*, **21**, 389(1983).

19 M. Kaminsky, K.J. Yoon, G.L. Geoffroy, and M.A. Vannice, *J. Catal.*, **91**, 338(1985).

20 J.P. Scott, J.R. Budge, A.L. Rheingold, and B.C. Gates, *J. Am. Chem. Soc.*, **109**, 7736(1987).

21 A. Fukuoka, M. Ichikawa, J.A. Hriljac, and D.F. Shriver, *Inorg. Chem.*, **26**, 3643(1987).

22 A. Fukuoka, T. Kimura, and M. Ichikawa, *J. Chem. Soc., Chem. Commun.*, 428(1988).

23 T. Kimura, A. Fukuoka, A. Fumagalli, and M. Ichikawa, *Catal. Lett.*, **2**, 227(1989).

24 D. Fraenkel and B.C. Gates, *J. Am. Chem. Soc.*, **102**, 2478(1980).

25 P.A. Jacobs and H.H. Nijs, *J. Catal.*, **65**, 328(1980).

26 D.W. Breck, *"Zeolite Molecular Sieves"*, Wiley, New York, 1974.

27 P. Zhou and B.C. Gates, *J. Chem. Soc., Chem. Commun.*, 347(1989).

28 L.L. Sheu, H. Knözinger, and W.M.H. Sachtler, *Catal. Lett.*, **2**, 129(1989).

29 R.D. Shannon, J.C. Vedrine, C. Naccache, and F. Lefebvre, *J.*

Catal., **88**, 431(1984).

30 E.J. Rode, M.E. Davis, and B.E. Hanson, *J. Catal.*, **96**, 563(1985).

31 N. Takahashi, A. Mijin, T. Ishikawa, K. Nebuka, and H. Suematsu, *J. Chem. Soc., Faraday Trans. 1*, **83**, 2605(1987).

32 E.J. Rode, M.E. Davis, and B.E. Hanson, *J. Catal.*, **96**, 574(1985).

33 M. Iwamoto, S. Nakamura, H. Kusano, and S. Kagawa, *J. Phys. Chem.*, **90**, 5244(1986).

34 F. Lefebvre, P. Gelin, C. Naccache, and Y. Ben Taarit, *Proc. 6th Intnl. Cong. Zeolite (Batterworth)*, 435(1985).

35 N. Kosugi and H. Kuroda, *Program EXAFS-1, EXAFS-2*, Research Center for Spectroscopy, the University of Tokyo, 1985.

36 L. Malatesta, G. Caglio, and M. Angoletta, *J. Chem. Soc., Chem. Commun.*, 532(1970).

37 L. Rao, X. Guo, T. Ito, A. Fukuoka, and M. Ichikawa, unpublished results.

38 G. Bergeret, P. Gallezot, P. Gelin, Y. Ben Taarit, F. Lefebvre, C. Naccache, and R.D. Shannon, *J. Catal.*, **104**, 279(1987).

39 A. Ceriotti, G. Longoni, R.D. Pergola, B.T. Heaton and D.O. Smith, *J. Chem. Soc., Dalton Trans.*, 1433(1983).

40 D. Ballivet-Tkatchenko, G. Coudurier, N.D. Chau, in *"Metal Microstructure in Zeolite"*, P.A. Jacobs, N.I. Jaeger, P. Jiru, and G. Ekloff eds., Elsevier, Amsterdam, 1982, p. 123.

41 S. Martinengo, P. Chini, V.G. Albano, F. Cariati, and S. Salvatori, *J. Organomet. Chem.*, **59**, 379(1973).

42 L. Garlaschelli, S. Martinengo, P.L. Bellon, F. Demartin, M. Manassero, M.Y. Chiang, C. Wei, and R. Bau, *J. Am. Chem. Soc.*, **106**, 6664(1984).

43 P.A. Jacobs and D. van Wouwe, *J. Mol. Catal.*, 17, 145(1982).

44 L.F. Nazar, G.A. Ozin, F. Hugues, J. Godber, and D. Rancourt, *J. Mol. Catal.*, 21, 313(1983).

45 G.S. Ferguson and P.T. Wolczanski, *J. Am. Chem. Soc.*, 108, 8293(1986).

46 T. Fukushima, H. Arakawa, and M. Ichikawa, *J. Chem. Soc., Chem. Commun.*, 729(1985).

47 C.H. Dai and S.D. Worley, *Langmuir*, 4, 326(1988).

LIST OF PUBLICATIONS

LIST OF PUBLICATIONS

CHAPTER 2

1 Homogeneous Multimetallic Catalysts Part 6. Hydroformylation and Hydroesterification of Olefins by Homogeneous Cobalt-Ruthenium Bimetallic Catalysts

M. Hidai, A. Fukuoka, Y. Koyasu, and Y. Uchida

J. Mol. Catal., **35**, 29-37(1986).

CHAPTER 3

2 Selective Olefin Hydroformylation on Carbon-supported Ru and Ru-Co Carbonyl Cluster-derived Catalysts

A. Fukuoka, H. Matsuzaka, M. Hidai, and M. Ichikawa

Chem. Lett., 941-944(1987).

CHAPTER 4

3 Promoter Effect of Iron on Olefin Hydroformylation catalyzed by SiO_2-supported Rhodium-Iron Carbonyl Clusters: Rh-Fe^{3+} Bimetallic Activation of Catalytic CO Insertion

A. Fukuoka, M. Ichikawa, J.A. Hriljac, and D.F. Shriver

Inorg. Chem., **26**, 3643-3645(1987).

4 Selective Hydrogenation of CO into C_1 and C_2 Alcohols by SiO_2-supported RhFe, PtFe, and PdFe Bimetallic Cluster-derived Catalysts

A. Fukuoka, T. Kimura, and M. Ichikawa

J. Chem. Soc., Chem. Commun., 428-430(1988).

5 Selective CO Hydrogenation to C_1-C_2 Alcohols Catalyzed on Fe-containing Rh, Pt, and Pd Bimetal Carbonyl Cluster-derived Catalysts

M. Ichikawa, A. Fukuoka, and T. Kimura

Proc. 9th Intnl. Cong. Catal.(Calgary), Vol II, 569-574(1988).

6 Fe-promoted Selective Methanol Synthesis in CO Hydrogenation Catalyzed on SiO_2-supported Ir_4Fe and Pd_6Fe_6 Bimetallic Cluster-derived Catalysts

T. Kimura, A. Fukuoka, A. Fumagalli, and M. Ichikawa

Catal. Lett., 2, 227-234(1989).

7 Bimetallic Promotion of Alcohol Production in CO Hydrogenation and Olefin Hydroformylation on RhFe, PtFe, PdFe, and IrFe Bimetallic Cluster-derived Catalysts

A. Fukuoka, T. Kimura, N. Kosugi, H. Kuroda, Y. Minai, Y. Sakai, T. Tominaga, and M. Ichikawa

J. Catal., submitted.

8 ^{13}C and ^{18}O Labelling FTIR Studies on C- and O-ended CO Chemisorption on Mn-promoted Rh Catalysts

M. Ichikawa, P.E. Hoffman, and A. Fukuoka

J. Chem. Soc., Chem. Commun., 1395-1396(1989).

CHAPTER 5

9 Selective Formation of Lower Alkenes and Alcohols in $CO+H_2$ Reaction Catalysed on NaY Zeolite-encapsulated Rh_6 and RhFe Bimetallic Cluster-derived Catalysts

L. Rao, A. Fukuoka, and M. Ichikawa

J. Chem. Soc., Chem. Commun., 458-460(1988).

10 Selective Hydroformylation of Ethylene and Propene Catalyzed on NaY Zeolite-entrapped Rh_6 and RhFe Clusters and Their Structural Characterization by EXAFS and FTIR

A. Fukuoka, L. Rao, N. Kosugi, H. Kuroda, and M. Ichikawa

Appl. Catal., 50, 295-301(1989).

11 Structural Characterization of Zeolite-entrapped Rh_6 and RhFe Bimetallic Clusters and Their Catalysis in CO Hydrogenation Reaction

A. Fukuoka, L. Rao, and M. Ichikawa

Nippon Kagaku Kaishi, 561-568(1989). (in Japanese)

12 Ensemble and Ligand Effects in Selective Alkane Hydrogenolysis Catalysed on Well-characterised RhIr and RhFe Bimetallic Cluster inside Zeolite

M. Ichikawa, L. Rao, T. Ito, and A. Fukuoka

Faraday Discuss. Chem. Soc., in press.

In addition, the author contributed to the following articles.

13 Hydroformyaltion of Cyclohexene Catalysed by Homogeneous Bimetallic Systems
M. Hidai, A. Fukuoka, Y. Koyasu, and Y. Uchida
J. Chem. Soc., Chem. Commun., 516-517(1984).

14 Hydrogenolysis of Acylcobalt Carbonyl with Metal Carbonyl Hydrides
Y. Koyasu, A. Fukuoka, Y. Uchida, and M. Hidai
Chem. Lett., 1083-1086(1985).

15 Preparation of Chemically Modified Electrodes by Attachment of Platinum Carbonyl Clusters and Their Efficient Electrocatalytic Action in Anodic Oxidation on Methanol
K. Machida, A. Fukuoka, M. Ichikawa, and M. Enyo
J. Chem. Soc., Chem. Commun., 1486-1487(1987).

16 Preparation of Platinum Cluster-impregnated Electrodes and Their Methanol Electrooxidation Characteristics
K. Machida, A. Fukuoka, M. Ichikawa, and M. Enyo
Nippon Kagaku Kaishi, 1426-1432(1988).

17 Scanning Tunnelling Microscopy of Rh_4 and Pt_{12} Carbonyl Clusters Adsorbed on Graphite
T. Fujimoto, A. Fukuoka, J. Nakamura, and M. Ichikawa
J. Chem. Soc., Chem. Commun., 845(1989).

Review Papers

18 Bimetallic Cluster Catalysts -Structure and Catalysis-

A. Fukuoka and M. Ichikawa

Surface Science (Hyomen Kagaku), 7, 157-167(1987). (in Japanese)

19 Grafting of Bimetallic Clusters on Surfaces -Their Structure and Catalysis-

A. Fukuoka and M. Ichikawa

Surface (Hyomen), 26, 435-449(1988). (in Japanese)

20 Chemistry of Cobalt-Ruthenium Mixed Metal Clusters and Mixed Metal Complexes

H. Matsuzaka, A. Fukuoka, Y. Koyasu, M. Ue, M. Orisaku, and M. Hidai

Nippon Kagaku Kaishi, 705-713(1988). (in Japanese)

21 Heteronuclear CO Activation in CO based Reactions Catalyzed by SiO_2-supported RhFe and PdFe Bimetallic Clusters

A. Fukuoka, T. Kimura, and M. Ichikawa

Catal. Today, in press.